# The Ecophysiology of Iron-Oxidizing Zetaproteobacteria: Microbe-Mineral Interactions, Transcriptomic Responses, and Biomineralization

# The ecophysiology of iron-oxidizing *Zetaproteobacteria*: microbe-mineral interactions, transcriptomic responses, and biomineralization

A dissertation presented

by

Jacob William Cohen

to

The Department of Organismic and Evolutionary Biology

in partial fulfillment of the requirements
for the degree of
Doctor of Philosophy
in the subject of
Biology

Harvard University
Cambridge, Massachusetts

December 2019

Dissertation advisor: Peter R. Girguis Jacob William Cohen

**The ecophysiology of iron-oxidizing *Zetaproteobacteria*: microbe-mineral interactions, transcriptomic responses, and biomineralization**

## Abstract

Neutrophilic microaerobic iron-oxidizing bacteria (FeOB) obtain energy by using reduced Fe(II) as an electron donor with oxygen as their electron acceptor. Much is still unknown about FeOB, however, despite their importance to the cycling of iron, a nutrient that is essential to life on Earth and limiting in many marine environments. In this dissertation I studied pure cultures of two marine hydrothermal vent iron-oxidizing *Zetaproteobacteria*, *Mariprofundus ferrooxydans* PV-1 and *Ghiorsea bivora* TAG-1, to further our understanding of FeOB physiology and the implications this has for their ecology. In Chapter 1 I use oxygen consumption measurements as a proxy for iron oxidation rates to show that, contrary to conventional wisdom, *M. ferrooxydans* PV-1 inhibits the dissolution of iron minerals it is growing on, while *G. bivora* TAG-1 is capable of both increasing and decreasing iron mineral dissolution rates. In Chapter 2, I explore how *G. bivora* TAG-1 contends with changes in environmental pH through examining its transcriptomic responses to both acute and chronic exposure to acidic and alkaline pH, representing increased proportions of hydrothermal vent fluid or seawater, respectively. I find that *G. bivora* TAG-1 is better suited to respond to a short-term decrease in pH, while increases in pH elicit a greater transcriptomic response as well as stress responses. I also show that responses to longer-term changes in pH are consistent with the differences in chemistry between seawater and vent fluid. Finally, in Chapter 3 I examine pH around individual *M. ferrooxydans* PV-1 cells and confirm that they establish low-pH microenvironments proximal to the cell. I then use geochemical modeling to show how this may

aid the cell in fixing carbon as well as in producing its twisted iron stalk. Altogether, the data presented here provide insights into the ecophysiology of a group of bacteria that are increasingly recognized as having a major role in iron cycling.

## Table of Contents

*To my parents Ann and Ken, my cat Audrey, and my wonderful partner Juna. Thank you all for so much love and support. I couldn't have done this without you.*

# Introduction

Iron is vital to all organisms on Earth, yet is limiting in much of Earth's oceans. This is because life evolved in ferruginous oceans; for billions of years Earth's oceans were at least in part replete with dissolved Fe(II) (1, 2). This changed with the evolution of oxygenic photosynthesis and the gradual oxygenation of the oceans. Fe(II) reacts rapidly with oxygen at neutral pH to form Fe(III), which is poorly soluble at neutral and alkaline pH (3). So as the oceans became more oxygenated, Fe(II) was gradually oxidized to Fe(III) and precipitated as iron oxyhydroxides (iron oxides) forming what we now know as banded iron formations (1, 4, 5). Thus, though life began in an environment where iron was plentiful and cells evolved to take advantage of its chemistry, bioavailable iron is relatively rare in modern oceans. The need for iron, however, remains as a remnant of its ubiquity.

In addition to catalysis and oxygen binding, many microbes have also evolved to use iron as a source of energy. One such group of microbes is the iron oxidizing bacteria, organisms that use reduced Fe(II) as an electron donor (3). This is a loose group based only on the use of Fe(II) as an electron donor, however, and these organisms are diverse phylogenetically, physiologically, and metabolically. The ability to oxidize Fe(II) for energy is widespread, particularly among the *Proteobacteria*, with representatives from the *Alpha-*, *Beta-*, *Gamma-* , and *Zetaproteobacteria*, classes, as well as the *Acidithiobacillia* class (1, 4, 6–8). These include anoxygenic phototrophs like the Alphaproteobacterium *Rhodopseudomonas palustris* that use light energy to excite relatively low-energy electrons from Fe(II) for photosynthesis and acidophilic aerobes like *Acidithiobacillus ferrooxidans*, a member of the *Acidithiobacillia*, which live at extremely low pH (9, 10). For both of these organisms, the reactivity of Fe(II) with oxygen at neutral pH does not present any particular problems because Fe(II) is stable at

circumneutral pH in the absence of oxygen (as for *R. palustris*) and in the presence of oxygen at low pH (as for *A. ferrooxidans*) (11–15).

The work presented in this thesis focuses on yet another group of iron oxidizers, the neutrophilic microaerobic iron oxidizing bacteria (FeOB). These organisms are mostly found within the *Beta-* and *Zetaproteobacteria*, though representatives from the *Gammaproteobacteria* have also been isolated (3, 16–19). Interestingly, freshwater FeOB are generally members of the *Betaproteobacteria* (e.g. *Gallionella* spp., *Sideroxydans* spp.) while marine FeOB and those found in terrestrial saltwater environments are usually *Zetaproteobacteria* (e.g. *Mariprofundus* spp., *Ghiorsea* spp.) (3, 17, 20–22). It should also be noted that all currently known *Zetaproteobacteria* are capable of oxidizing iron for energy and they are thus far only found in iron-rich environments. This and genomic evidence suggests that *Zetaproteobacteria* may therefore have evolved as specialists for iron oxidation (22).

FeOB live at circumneutral pH, obtaining energy by using Fe(II) as an electron donor with oxygen as their electron acceptor via the reaction $Fe^{2+} + 0.25\ O_2 + H^+ \rightarrow Fe^{3+} + 0.5\ H_2O$ (4, 8, 23, 24). The aforementioned reactivity of Fe(II) with oxygen has a number of implications for their physiology and ecology, however. First, oxygen and Fe(II) react quickly abiotically at neutral pH – the half life of Fe(II) in fully oxygenated water is around 12 to 15 minutes (25). FeOB circumvent this issue by living in environments with very low oxygen content, which keeps abiotic reaction rates slow and allows them to better compete with abiotic oxidation (26, 27). Indeed, at oxygen concentrations of ~10 μM FeOB have been shown to be responsible for upwards of 90% of iron oxidation (22, 23). FeOB are therefore usually found where anoxic ferruginous waters meet oxygenated water, where abiotic oxidation can remove much of the oxygen from the environment forming opposing gradients of $Fe^{2+}$ and $O_2$. Freshwater FeOB have

long been observed in terrestrial streams, iron seeps in wetlands, mines, and in association with plant roots (28–32). In marine environments, FeOB are present at areas of hydrothermal venting and on Fe(II)-containing basaltic minerals (33–38). Though habitats meeting the criteria FeOB require were thought to be relatively rare, recent research has shown that FeOB are far more widespread than was once believed, appearing on continental margins away from any hydrothermal influence, in coastal sediments, and in stratified pelagic environments (39–41). It is therefore believed that FeOB have a large influence on global iron cycling.

Another issue posed by oxidizing iron at circumneutral pH is that the waste product of this metabolism, Fe(III), is unstable at neutral pH and precipitates almost immediately as solid iron oxides via the reaction $Fe^{2+} + 0.25\ O_2 + 2.5\ H_2O \rightarrow Fe(OH)_3 + 2\ H^+$ (3). This necessitates that Fe(II) oxidation is carried out extracellularly, with cytochromes in the outer membrane accepting electrons from Fe(II) and passing them through the periplasm to the inner membrane where they are then passed to oxygen (42, 43). Furthermore, these iron oxides are autocatalytic for further iron oxidation, so FeOB must not only compete with the abiotic reaction of Fe(II) with $O_2$, but also with their waste products for both their electron donor and electron acceptor (27).

Even oxidizing iron on the outer membrane carries some risk for FeOB, namely that this would make it possible for them to become encrusted or even entombed in precipitated iron oxides, which could inhibit the acquisition of essential nutrients (16, 44). Though some FeOB do indeed encrust in iron oxides, many arrange their iron oxide waste products into highly ordered structures, for example twisted iron stalks, sheathes, and “dreads,” though some organisms simply produce amorphous iron oxides (39, 45, 46). Of these iron oxide structures, twisted stalks have been most extensively studied and there has been much research into how and why FeOB

make their stalks, as well as for the use of stalks as a biosignature for past iron oxidation (47, 48).

Stalk-forming FeOB are usually bean- or "C"-shaped cells that form stalks by attaching to a surface in suitable chemical conditions (i.e. low $pO_2$ with Fe(II) present) and beginning to oxidize iron (47). They produce acidic polysaccharides as they oxidize iron that bind Fe(III) before it precipitates as iron oxide in multiple fibrils, which make up the "ribbon" of the stalk (44). As the cell continues to oxidize iron, it continues to excrete its stalk, which pushes the cell away from the substrate the stalk is attached to. The cell rotates as it produces the stalk, resulting in its characteristic twisted ribbon morphology, though it is unclear what makes the cell turn during this process. Once the cell has moved far enough that the chemical conditions are no longer suitable, it produces flagella, detaches itself from the stalk, and swims off to start the process again, perhaps attaching to a previously produced stalk (45). As cells make stalks and other cells attach to these stalks and make their own in turn, stalk-forming FeOB can develop thick flocculent iron mats that can in some cases be meters thick and stretch for hundreds of square meters (3, 5, 49). Additionally, by affecting flow regimes these iron mats allow stalk-formers to act as "ecosystem engineers" that are able to modify the environment around them on much larger scales than that of bacterial cells (45).

Though FeOB are involved in the cycling of iron, a nutrient that is vital to life and limiting in much of the ocean, they remain relatively poorly understood. Iron oxidation has a low free energy yield ($\Delta G^\circ$ = -29 kj $mol^{-1}$ Fe(II), actual $\Delta G \approx$ -90 kj $mol^{-1}$ Fe(II) due to precipitation of waste products and low $pO_2$) and FeOB grow relatively slowly (*Mariprofundus ferrooxydans* PV-1 generation time ≈ 12 hr, *Ghiorsea bivora* TAG-1 generation time ≈ 22 hr when grown on $Fe^{2+}$), making the production of large amounts of biomass time consuming (3, 29, 37, 46). This is

in addition to the presence of large amounts of iron oxides that can interfere with standard molecular biology techniques (50). They are also currently unable to be grown as single colonies on solid media, making genetic manipulations difficult, and as of this time there are no genetically tractable representatives. To this end, this thesis furthers our understanding of FeOB physiology by using pure cultures to examine how FeOB affect iron oxidation rates in association with iron minerals (Chapter 1), how FeOB respond to changes in environmental pH (Chapter 2), and whether FeOB form pH microenvironments around their cells and the implications this has for biomineralization (Chapter 3).

The work comprising this thesis was done on two FeOB isolates, *Mariprofundus ferrooxydans* PV-1 and *Ghiorsea bivora* TAG-1. Both are members of the *Zetaproteobacteria* and both were isolated from deep-sea hydrothermal vents. There are some key differences between these bacteria, however, that allowed me to make comparisons to better understand FeOB physiology.

*M. ferrooxydans* PV-1 was isolated from Pele's Vents at Lō'ihi seamount off the coast of Hawai'i, a low-temperature (~30˚C) hydrothermal system with high iron content (up to ~1 mM) and little sulfide (up to 56 μM measured, but usually lower than 20 μM) in comparison to other vent systems (37, 51, 52). PV-1 was one of the first isolated *Zetaproteobacteria* and, as an obligate iron oxidizer, serves as a model organism for studying marine microaerobic iron oxidation. It is also a model for studying the twisted iron stalks, with multiple studies focused on the structure and production of its stalks (37, 47, 48, 53).

*Ghiorsea bivora* TAG-1, on the other hand, was isolated from the Trans-Atlantic Geotraverse (TAG) vent field in the Mid Atlantic Ridge, a high temperature (290-321˚C) hydrothermal system that also has very high iron content (1640 μM), though TAG-1 was isolated

from a diffuse flow with a temperature measured to be 5˚C (46, 54). Interestingly, TAG-1 does not make structured iron oxides. Instead it produces amorphous oxides, and these oxides are often covered in cells when viewed under a microscope. It is unclear why many FeOB produce highly ordered structures when some do not, though one hypothesis for why FeOB form stalks postulates that doing so helps prevent encrustation by iron oxides (47). It has been proposed that TAG-1 may produce a different exopolysaccharide instead of that used by stalk formers that it simply sheds when iron oxides precipitate on and bind to it. It should also be noted that TAG-1 is one of two known FeOB that can use $H_2$ as an electron donor in addition to Fe(II) (46).

There has been much interest in measuring rates of FeOB iron oxidation, as they act to prevent dissolved reduced iron from reaching the overlying water column. Previous studies have mostly been conducted over short time scales (minutes to hours) using voltammetric measurements of dissolved iron (23). In doing so investigators have demonstrated that FeOB do compete with abiotic reactions and oxidize iron more quickly than killed controls at low oxygen concentrations ($\leq$25 μM $O_2$) (22, 23). Though these studies have provided valuable insight to FeOB physiology, they do not take into account the fact that FeOB exist in their environments for much longer periods of time.

I address this in Chapter 1 by examining iron oxidation rates of *M. ferrooxydans* PV-1 and *G. bivora* TAG-1 over day to week time scales using oxygen measurements as a proxy for iron oxidation. I also explore how each strain affects iron mineral dissolution by using zero-valent iron (ZVI) and pyrrhotite ($Fe_{1-x}S$, x = 0 – 0.17) powders as solid iron sources, rather than dissolved Fe(II). I show that both strains are capable of decreasing net iron oxidation rates by inhibiting mineral dissolution when grown on ZVI. I also show that PV-1 is capable of

decreasing net iron oxidation rates when grown on pyrrhotite while TAG-1, in contrast, increases iron oxidation rates when using pyrrhotite as its iron source.

Interestingly, many marine FeOB preferentially grow at pH levels well below the average of seawater (~pH 8.1) (22, 36, 37, 46, 55). In fact, many will not grow at pH 8.0 or above, only surviving in the range of 5.5 to ~7.5. Hydrothermal vents are dynamic systems, though, with frequent changes in flow regimes and thus shifts in the proportion of a given cell's environment that is composed of acidic vent fluid (as low as pH 3) or of seawater (56, 57). In Chapter 2, I provide insights as to how FeOB that live at hydrothermal vents contend with changes in extracellular pH through studying the transcriptomic responses of TAG-1 and inferring what this means for its physiology. I test both short- and long-term exposure to acidic and alkaline pH in cultures grown on ZVI by extracting RNA from these cultures and sequencing the resulting transcriptomes. I find that TAG-1 seems to be better suited to short exposures to more acidic (and thus more vent-influenced) conditions, increasing the expression of genes related to translation, inorganic ion transport, and energy metabolism in comparison to the control. Acute exposure to more alkaline pH, however, elicits a stress response from TAG-1, where it decreases the expression of genes related to translation while increasing the expression of those related to signal transduction and motility, as well as integrases.

Chronic exposure to pH conditions outside its optimum, on the other hand, can be linked back to the challenges imposed by greater exposure to vent fluid or seawater. Under long-term exposure to a more acidic pH, TAG-1 increases expression of genes related to motility, as well as phosphate acquisition and heavy metal resistance when compared to the control. It also increases expression of many energy metabolism related genes. Long-term growth under alkaline conditions, however, revealed that TAG-1 decreases many of the same energy metabolism-

related genes that were higher in expression under acidic conditions. Similarly, genes related to phosphate acquisition and heavy metal resistance were also less expressed than the control. Integrases were still mostly expressed to a higher degree than in the control, indicating that alkaline conditions are still provoking a stress response even after multiple days of exposure (58).

pH also affects some important aspects of iron oxidation as a lifestyle; in particular the energy yield of iron oxidation decreases with decreasing pH and the $Fe^{3+}$ waste products of FeOB are more soluble at lower pH (1). It has been previously demonstrated that phototrophic iron oxidizers escape encrustation by the iron oxides they produce by generating a low pH microenvironment around their cells, but it was unknown whether FeOB were even capable of a similar phenotype (59). In Chapter 3, I use a pH sensitive fluorescent dye in combination with confocal microscopy to image "pH landscapes" around PV-1 cells and demonstrate that they do indeed actively mediate the establishment of an acidic microenvironment around themselves. Furthermore, I use geochemical modeling to show that in exchange for a modest loss in energetic yield for iron oxidation, PV-1 may benefit from increased availability of carbon dioxide. I also show that establishing a low pH microenvironment may aid PV-1 in the production of its twisted iron stalk.

The data presented in this thesis comprise significant advances in FeOB physiology. By taking advantage of a number of techniques, I was able to add to our understanding of this relatively understudied group of organisms that are involved in cycling one of the most important nutrients to life on Earth. Though the experiments I preformed were done with pure cultures, I also recognize and expound upon the importance of linking laboratory studies back to how these

organisms exist in nature. It is my hope that my work can be used further to examine more aspects of FeOB physiology and better study them.

**References**


1. **Ilbert M**, **Bonnefoy V**. 2013. Insight into the evolution of the iron oxidation pathways. Biochim Biophys Acta - Bioenerg **1827**:161–175.

2. **Anbar AD**. 2008. Oceans: Elements and evolution. Science (80- ) **322**:1481–1483.

3. **Emerson D**, **Fleming EJ**, **McBeth JM**. 2010. Iron-oxidizing bacteria: an environmental and genomic perspective. Annu Rev Microbiol **64**:561–583.

4. **Dubinina GA**, **Sorokina AYu**. 2014. Neutrophilic lithotrophic iron-oxidizing prokaryotes and their role in the biogeochemical processes of the iron cycle. Microbiology **83**:1–14.

5. **Chan CS**, **Emerson D**, **Luther GW**. 2016. The role of microaerophilic Fe-oxidizing micro-organisms in producing banded iron formations. Geobiology **14**:509–528.

6. **Hallbeck L**, **Pedersen K**. 1990. Culture parameters regulating stalk formation and growth rate of *Gallionella ferruginea*. J Gen Microbiol **136**:1675–1680.

7. **Bird LJ**, **Bonnefoy V**, **Newman DK**. 2011. Bioenergetic challenges of microbial iron metabolisms. Trends Microbiol **19**:330–340.

8. **Hedrich S**, **Schlömann M**, **Barrie Johnson D**. 2011. The iron-oxidizing proteobacteria. Microbiology **157**:1551–1564.

9. **Widdel F**, **Schnell S**, **Heising S**, **Ehrenreich A**, **Assmus B**, **Schink B**. 1993. Ferrous iron oxdation by anoxygenic phototrophic bacteria. Nature **362**:834–836.

10. **Weber K a**, **Achenbach L a**, **Coates JD**. 2006. Microorganisms pumping iron: anaerobic microbial iron oxidation and reduction. Nat Rev Microbiol **4**:752–764.

11. **Schädler S**, **Burkhardt C**, **Hegler F**, **Straub KL**, **Miot J**, **Benzerara K**, **Kappler A**. 2009. Formation of cell-iron-mineral aggregates by phototrophic and nitrate-reducing anaerobic Fe(II)-oxidizing bacteria. Geomicrobiol J **26**:93–103.

12. **Kappler A**, **Newman DK**. 2004. Formation of Fe(III)-minerals by Fe(II)-oxidizing photoautotrophic bacteria. Geochim Cosmochim Acta **68**:1217–1226.

13. **Miot J**, **Benzerara K**, **Morin G**, **Kappler A**, **Bernard S**, **Obst M**, **Férard C**, **Skouri-Panet F**, **Guigner JM**, **Posth N**, **Galvez M**, **Brown GE**, **Guyot F**. 2009. Iron biomineralization by anaerobic neutrophilic iron-oxidizing bacteria. Geochim Cosmochim Acta **73**:696–711.

14. **Moreno-Paz M**, **Gómez MJ**, **Arcas A**, **Parro V**. 2010. Environmental transcriptome analysis reveals physiological differences between biofilm and planktonic modes of life of

the iron oxidizing bacteria *Leptospirillum* spp. in their natural microbial community. BMC Genomics **11**:404.

15. **Bonnefoy V**, **Holmes DS**. 2012. Genomic insights into microbial iron oxidation and iron uptake strategies in extremely acidic environments. Environ Microbiol **14**:1597–1611.

16. **Emerson D**. 2012. Biogeochemistry and microbiology of microaerobic Fe(II) oxidation. Biochem Soc Trans **40**:1211–6.

17. **McAllister SM**, **Davis RE**, **McBeth JM**, **Tebo BM**, **Emerson D**, **Moyer CL**. 2011. Biodiversity and emerging biogeography of the neutrophilic iron-oxidizing *Zetaproteobacteria*. Appl Environ Microbiol **77**:5445–5457.

18. **Barco RA**, **Hoffman CL**, **Ramírez GA**, **Toner BM**, **Edwards KJ**, **Sylvan JB**. 2017. In-situ incubation of iron-sulfur mineral reveals a diverse chemolithoautotrophic community and a new biogeochemical role for *Thiomicrospira*. Environ Microbiol **19**:1322–1337.

19. **Emerson D**, **Field EK**, **Chertkov O**, **Davenport KW**, **Goodwin L**, **Munk C**, **Nolan M**, **Woyke T**. 2013. Comparative genomics of freshwater Fe-oxidizing bacteria: Implications for physiology, ecology, and systematics. Front Microbiol **4**:1–17.

20. **Emerson JB**, **Thomas BC**, **Alvarez W**, **Banfield JF**. 2016. Metagenomic analysis of a high carbon dioxide subsurface microbial community populated by chemolithoautotrophs and bacteria and archaea from candidate phyla. Environ Microbiol **18**:1686–1703.

21. **Colman DR**, **Garcia JR**, **Crossey LJ**, **Karlstrom K**, **Jackson-Weaver O**, **Takacs-Vesbach C**. 2014. An analysis of geothermal and carbonic springs in the western United States sustained by deep fluid inputs. Geobiology **12**:83–98.

22. **McAllister SM**, **Moore RM**, **Gartman A**, **Luther GW**, **Emerson D**, **Chan CS**. 2019. The Fe(II)-oxidizing *Zetaproteobacteria*: historical, ecological and genomic perspectives. FEMS Microbiol Ecol **95**:1–18.

23. **Druschel GK**, **Emerson D**, **Sutka R**, **Suchecki P**, **Luther GW**. 2008. Low-oxygen and chemical kinetic constraints on the geochemical niche of neutrophilic iron(II) oxidizing microorganisms. Geochim Cosmochim Acta **72**:3358–3370.

24. **Edwards KJ**, **Bach W**, **McCollom TM**, **Rogers DR**. 2004. Neutrophilic Iron-Oxidizing Bacteria in the Ocean: Their Habitats, Diversity, and Roles in Mineral Deposition, Rock Alteration, and Biomass Production in the Deep-Sea. Geomicrobiol J **21**:393–404.

25. **Emerson D**, **Revsbech NP**. 1994. Investigation of an iron-oxidizing microbial mat community located near Aarhus, Denmark: Field studies. Appl Environ Microbiol **60**:4022–4031.

26. **Glazer BT**, **Rouxel OJ**. 2009. Redox speciation and distribution within diverse Iron-dominated microbial habitats at Loihi Seamount. Geomicrobiol J **26**:606–622.

27. **Rentz J a.**, **Kraiya C**, **Luther GW**, **Emerson D**. 2007. Control of ferrous iron oxidation within circumneutral microbial iron mats by cellular activity and autocatalysis. Environ Sci Technol **41**:6084–6089.

28. **Emerson D**, **Weiss J V.**, **Megonigal JP**. 1999. Iron-oxidizing bacteria are associated with ferric hydroxide precipitates (Fe-plaque) on the roots of wetland plants. Appl Environ Microbiol **65**:2758–2761.

29. **Roden EE**, **Sobolev D**, **Glazer B**, **Luther GW**. 2004. Potential for microscale bacterial Fe redox cycling at the aerobic-anaerobic interface. Geomicrobiol J **21**:379–391.

30. **Sobolev D**, **Roden EE**. 2001. Suboxic Deposition of Ferric Iron by Bacteria in Opposing Gradients of Fe(II) and Oxygen at Circumneutral pH. Appl Environ Microbiol **67**:1328–1334.

31. **Sobolev D**, **Roden EE**. 2002. Evidence for rapid microscale bacterial redox cycling of iron in circumneutral environments. Antonie van Leeuwenhoek, Int J Gen Mol Microbiol **81**:587–597.

32. **James RE**, **Ferris FG**. 2004. Evidence for microbial-mediated iron oxidation at a neutrophilic groundwater spring. Chem Geol **212**:301–311.

33. **Henri PA**, **Rommevaux-Jestin C**, **Lesongeur F**, **Mumford A**, **Emerson D**, **Godfroy A**, **Ménez B**. 2016. Structural iron (II) of basaltic glass as an energy source for *Zetaproteobacteria* in an abyssal plain environment, offthe mid atlantic ridge. Front Microbiol **6**:1–18.

34. **Hoshino T**, **Kuratomi T**, **Morono Y**, **Hori T**, **Oiwane H**, **Kiyokawa S**, **Inagaki F**. 2016. Ecophysiology of *Zetaproteobacteria* associated with shallow hydrothermal iron-oxyhydroxide deposits in Nagahama Bay of Satsuma Iwo-Jima, Japan. Front Microbiol **6**:1–11.

35. **Makita H**, **Kikuchi S**, **Mitsunobu S**, **Takaki Y**, **Yamanaka T**, **Toki T**, **Noguchi T**, **Nakamura K**, **Abe M**, **Hirai M**, **Yamamoto M**, **Uematsu K**, **Miyazaki J**, **Nunoura T**, **Takahashi Y**, **Takai K**. 2016. Comparative Analysis of Microbial Communities in Iron-Dominated Flocculent Mats in Deep-Sea Hydrothermal Environments. Appl Environ Microbiol **82**:5741–5755.

36. **Makita H**, **Tanaka E**, **Mitsunobu S**, **Miyazaki M**, **Nunoura T**, **Uematsu K**, **Takaki Y**, **Nishi S**, **Shimamura S**, **Takai K**. 2017. *Mariprofundus micogutta* sp. nov., a novel iron-oxidizing zetaproteobacterium isolated from a deep-sea hydrothermal field at the Bayonnaise knoll of the Izu-Ogasawara arc, and a description of *Mariprofundales* ord. nov. and *Zetaproteobacteria* classis nov. Arch Microbiol **199**:335–346.

37. **Emerson D**, **Rentz JA**, **Lilburn TG**, **Davis RE**, **Aldrich H**, **Chan C**, **Moyer CL**. 2007. A novel lineage of proteobacteria involved in formation of marine Fe-oxidizing microbial mat communities. PLoS One **2**.

38. **Edwards KJ**, **Bach W**, **Rogers DR**. 2003. Geomicrobiology of the ocean crust: A role for chemoautotrophic Fe-bacteria. Biol Bull **204**:180–185.

39. **Chiu BK**, **Kato S**, **McAllister SM**, **Field EK**, **Chan CS**. 2017. Novel pelagic iron-oxidizing *Zetaproteobacteria* from the Chesapeake Bay oxic-anoxic transition zone. Front Microbiol **8**:1–16.

40. **Laufer K**, **Nordhoff M**, **Halama M**, **Martinez RE**, **Obst M**, **Nowak M**, **Stryhanyuk H**, **Richnow HH**, **Kappler A**. 2017. Microaerophilic Fe(II)-Oxidizing *Zetaproteobacteria* Isolated from Low-Fe Marine Coastal Sediments: Physiology and Composition of Their Twisted Stalks. Appl Environ Microbiol **83**:1–20.

41. **Rubin-Blum M**, **Antler G**, **Tsadok R**, **Shemesh E**, **Austin JA**, **Coleman DF**, **Goodman-Tchernov BN**, **Ben-Avraham Z**, **Tchernov D**. 2014. First evidence for the presence of iron oxidizing *Zetaproteobacteria* at the levantine continental margins. PLoS One **9**:1–10.

42. **Barco RA**, **Emerson D**, **Sylvan JB**, **Orcutt BN**, **Jacobson Meyers ME**, **Ramírez GA**, **Zhong JD**, **Edwards KJ**. 2015. New Insight into Microbial Iron Oxidation as Revealed by the Proteomic Profile of an Obligate Iron-Oxidizing Chemolithoautotroph. Appl Environ Microbiol **81**:5927–5937.

43. **Summers ZM**, **Gralnick JA**, **Bond DR**. 2013. Cultivation of an Obligate Fe (II)-Oxidizing Lithoautotrophic Bacterium Using Electrodes. MBio **4**:1–5.

44. **Chan CS**, **Fakra SC**, **Edwards DC**, **Emerson D**, **Banfield JF**. 2009. Iron oxyhydroxide mineralization on microbial extracellular polysaccharides. Geochim Cosmochim Acta **73**:3807–3818.

45. **Chan CS**, **McAllister SM**, **Leavitt AH**, **Glazer BT**, **Krepski ST**, **Emerson D**. 2016. The architecture of iron microbial mats reflects the adaptation of chemolithotrophic iron oxidation in freshwater and marine environments. Front Microbiol **7**.

46. **Mori JF**, **Scott JJ**, **Hager KW**, **Moyer CL**, **Küsel K**, **Emerson D**. 2017. Physiological and ecological implications of an iron- or hydrogen-oxidizing member of the *Zetaproteobacteria*, *Ghiorsea bivora*, gen. nov., sp. Nov. ISME J **11**:2624–2636.

47. **Chan CS**, **Fakra SC**, **Emerson D**, **Fleming EJ**, **Edwards KJ**. 2011. Lithotrophic iron-oxidizing bacteria produce organic stalks to control mineral growth: implications for biosignature formation. ISME J **5**:717–727.

48. **Krepski ST**, **Emerson D**, **Hredzak-Showalter PL**, **Luther GW**, **Chan CS**. 2013. Morphology of biogenic iron oxides records microbial physiology and environmental conditions: Toward interpreting iron microfossils. Geobiology **11**:457–471.

49. **Scott JJ**, **Glazer BT**, **Emerson D**. 2017. Bringing microbial diversity into focus: high-resolution analysis of iron mats from the Lō‘ihi Seamount. Environ Microbiol **19**:301–316.

50. **Barco R a.**, **Edwards KJ**. 2014. Interactions of proteins with biogenic iron oxyhydroxides and a new culturing technique to increase biomass yields of neutrophilic, iron-oxidizing bacteria. Front Microbiol **5**:1–11.

51. **Karl DM**, **McMurtry GM**, **Malahoff A**, **Garcia MO**. 1988. Loihi Seamount, Hawaii: a mid-plate volcano with a distinctive hydrothermal system. Nature.

52. **Sedwick P.**, **McMurtry G.**, **Macdougall J.** 1992. Chemistry of hydrothermal solutions from Pele's Vents, Loihi Seamount, Hawaii. Geochim Cosmochim Acta **56**:3643–3667.

53. **Comolli LR**, **Luef B**, **Chan CS**. 2011. High-resolution 2D and 3D cryo-TEM reveals structural adaptations of two stalk-forming bacteria to an Fe-oxidizing lifestyle. Environ Microbiol **13**:2915–2929.

54. **Campbell AC**, **Palmer MR**, **Klinkhammer GP**, **Bowers TS**, **Edmond JM**, **Lawrence JR**, **Casey JF**, **Thompson G**, **Humphris S**, **Rona P**, **Karson JA**. 1988. Chemistry of hot springs on the Mid-Atlantic Ridge. Nature **335**:514–519.

55. **Field EK**, **Kato S**, **Findlay AJ**, **MacDonald DJ**, **Chiu BK**, **Luther GW**, **Chan CS**. 2016. Planktonic marine iron oxidizers drive iron mineralization under low-oxygen conditions. Geobiology **14**:499–508.

56. **Johnson KS**, **Beehler CL**, **Sakamoto-Arnold CM**, **Childress JJ**. 1986. In situ measurements of chemical distributions in a deep-sea hydrothermal vent field. Science (80- ) **231**:1139–1141.

57. **Schultz A**, **Dickson P**, **Elderfield H**. 1996. Temporal variations in diffuse hydrothermal flow at TAG. Geophys Res Lett **23**:3471–3474.

58. **Guerin É**, **Cambray G**, **Sanchez-Alberola N**, **Campoy S**, **Erill I**, **Re S Da**, **Gonzalez-Zorn B**, **Barbé J**, **Ploy MC**, **Mazel D**. 2009. The SOS response controls integron recombination. Science (80- ) **324**:1034.

59. **Hegler F**, **Schmidt C**, **Schwarz H**, **Kappler A**. 2010. Does a low-pH microenvironment around phototrophic $Fe^{II}$-oxidizing bacteria prevent cell encrustation by $Fe^{III}$ minerals? FEMS Microbiol Ecol **74**:592–600.

# Chapter 1

Diverse iron-oxidizing *Zetaproteobacteria* exert differential controls on mineral dissolution

**Abstract**

Iron-oxidizing bacteria (FeOB) must compete with abiotic reactions for their electron donors and electron acceptors. Many studies have shown that FeOB catalyze Fe(II) oxidation faster than abiotic rates at low $pO_2$, thereby outcompeting these abiotic reactions. FeOB have also been implicated in increasing mineral dissolution rates. Here, we present evidence that neither of these is always the case. We used a non-invasive optical oxygen sensor to monitor oxygen consumption as a proxy for iron oxidation in incubations of two diverse FeOB, *Mariprofundus ferrooxydans* PV-1 and *Ghiorsea bivora* TAG-1, grown on solid iron sources over timescales of days to weeks. We show that both FeOB have the capacity to decrease net iron oxidation rates when grown on zero-valent iron powder, and *M. ferrooxydans* PV-1 is able to do the same when grown on pyrrhotite, a natural iron mineral. Furthermore, we show that this decrease in net iron oxidation rate is due to inhibition of mineral dissolution, likely as a result of cells and extracellular polysaccharide covering mineral grains. This effect remains even if the FeOB that produced this EPS are no longer metabolically active. Altogether, the data presented here have implications for how we understand iron cycling, as we can no longer assume that FeOB will invariably increase net iron oxidation and mineral dissolution rates.

**Introduction**

Iron-oxidizing bacteria (FeOB) are microorganisms that catalyze the oxidation of Fe(II) to Fe(III) for energy. FeOB are phylogenetically diverse, as with representatives within the α, ß, γ , and ζ classes of Proteobacteria, as well as the Firmicutes, Nitrospirae, and Actinobacteria (1–4). FeOB flourish in aqueous systems characterized generally by low $pO_2$ and elevated levels of $Fe^{2+}$ (5–8), such as freshwater aquifers, regions of acidic discharge, acidic natural and

anthropogenic estuarine sediments, and deep-ocean habitats, including hydrothermal vents and fractured basalts (9–12).

Notably, neutrophilic FeOB (i.e., those that live at circumneutral pH) must contend with the reactivity of $Fe^{2+}$ and $O_2$, which rapidly react to form iron oxyhydroxide precipitates, including ferrihydrite and trace amounts of lepidocrocite and goethite (1, 13). The resulting iron oxyhydroxides are also autocatalytic, further accelerating abiotic iron oxidation (4, 14–16). In addition to the presence and persistence of abiotically-formed oxyhyrdoxides, many FeOB organize their iron oxide waste products into structures including twisted stalks, sheaths, and "dreads." (17–19). These structures do not form abiotically, thus they are considered diagnostic features of neutrophilic FeOB (4, 17–20). Stalk-forming FeOB in particular are known to produce flocculent iron oxide mats, which can be meters thick and cover hundreds of square meters, as is the case at Lō'ihi Seamount (11, 17). Fe(II) and $O_2$ gradients have been shown to converge sharply near mat surfaces and the architecture of iron mats suggests that these mats change flow regimes around them (18, 21).

Neutrophilic FeOB experience constant competition for their electron donor from both their electron acceptor and the waste products of their metabolism. As such, neutrophilic FeOB in particular are most abundant in environments with opposing gradients of Fe(II) and $O_2$, such as the iron-rich vents at the Loihi seamounts, where $pO_2$ values are low enough for them to compete with abiotic reactions (12, 15, 16, 22, 23). While such environments were once thought to be relatively uncommon, recent studies have shown that FeOB are much more widespread than previously expected, having been found in coastal sediments and on continental margins (17, 24).

To examine the rates of biotic iron oxidation by neutrophilic FeOB, previous lab-based studies have generally documented biotic oxidation rates by measuring the changes in dissolved Fe(II) via A) cyclic voltammetry over short time periods (20-70 minutes;(16, 25)); or B) changes in the total iron content in live cultures vs controls over several days (19). In the voltammetric studies, the authors benefitted from measuring [$Fe^{2+}$] in real time, compensating for the confounding factors of abiotic oxidation and -more importantly- the rapid abiotic autocatalysis that occurs after the formation of oxyhyrdoxides. In longer-term studies with total iron sampling, the authors were able to look at net iron oxidation over time, but with limited ability to resolve biotic and abiotic oxidation rates.

However, FeOB live in dynamic environments, and of course flourish for more than a mere few hours. This begs the question as to how FeOB contend with the abiotic processes with which they compete over longer time scales. The null state would be that they do not, and if that is the case the abiotic autocatalytic iron oxidation may ultimately govern the density and distribution in natural settings. On the other hand, FeOB are recognized as ecosystem engineers that can modify the their environments (18), which poses the question of whether FeOB are able to influence their environment sufficiently to mitigate the abiotic processes.

In this study we examined the oxidation rates of two *Zetaproteobacteria* from two genera, *Mariprofundus ferrooxydans* PV-1 and *Gheorsia bivora* TAG-1 when grown on iron minerals over several days (with zero valent iron) to three weeks (with ($Fe_{1-x}S$, x = 0 – 0.17) ite). To that end, we designed an experimental setup that allowed us to conduct four parallel incubations in gastight microcosms. We employed an optical oxygen sensor, or optode, to continuously and non-invasively monitor oxygen concentrations in FeOB cultures over the course of the incubation. Solid phase, zero-valent iron (ZVI), which releases Fe(II) over time

through dissolution, as well as pyrrhotite ($Fe_{1-x}S$, x = 0 – 0.17), were used as sources of iron. These data reveal that FeOB grow and flourish over the times course of these experiments. Notably, reactors containing live FeOB exhibited net rates that were *slower* than the abiotic controls. Thus, FeOB are capable of moderating abiotic iron oxidation rates. Through another series of experiments, we tested how FeOB achieve this, with our data being most consistent with the hypothesis that FeOB inhibit the abiotic interaction of the solid-phase iron with dissolved oxygen. This phenotype can be present in both stalk- and non-stalk-forming FeOB, and can occur at both lower (e.g., ~25 μM) and higher (e.g., ~110 μM) oxygen concentrations. Dissolution inhibition also appears to be dependent on the mineral being colonized. While both FeOB used in this study decreased dissolution rates of ZVI and *M. ferrooxydans* PV-1 also decreased dissolution of pyrrhotite, *G. bivora* TAG-1 was able to increase the iron oxidation rate of pyrrhotite. The results and discussion below elaborate on these observations, and present a model of how FeOB have the capacity to manage their environment to favor their metabolic activity in lieu of the autocatalytic abiotic iron oxidation.

## Methods

### Culturing

Two strains of *Zetaproteobacteria, Mariprofundus ferrooxydans* PV-1 *and Ghiorsea bivora* TAG-1, were cultured in artificial seawater-zero valent iron (ASW-ZVI) plates as previously described in the National Center for Marine Algae and Microbiota culturing guidelines for *Mariprofundus ferrooxydans* PV-1. Specifically, petri dishes were filled with 20 ml of artificial seawater (pH ~6.4), to which approximately 100 mg of -200 mesh zero valent iron (ZVI, Alfa Aesar Inc.) was added as a source of Fe(II). To reduce the risk of contamination,

the ZVI was sterilized prior to use by exposure to 24 hours of gamma irradiation from a $^{137}Cs$ source at 200 rad•min$^{-1}$. Next, plates were placed in sealed gas-tight jars designed for anaerobic culture, which were equipped with valves allowing the air inside to be removed via vacuum and replaced with a gas mix of 8% $O_2$/10% $CO_2$/82% $N_2$. Jars were incubated at laboratory temperature (~24° C). Separate jars were used for each strain.

**Cell counts**

Cells were quantified by direct count as in Emerson and Moyer 2002 (11). Slides inscribed with 1 cm diameter circles (Electron Microscopy Sciences) were coated in 1% agarose, and 10 µl of sample to be counted was spread evenly within each circle. Slides were air dried and then stained with 10 µl of 1 mM SYTO 13 nucleic acid dye (Thermo Fisher Inc.). Fluorescent cells were counted on an Axio Scope.a1 microscope (Zeiss) equipped with a counting grid of area 0.01 mm$^2$ at 1000x magnification, as well as a 470 nm LED and FITC filter set. Fifteen grids were counted per circle and three circles per sample. Cell concentrations were calculated using the formula:

$$Cell\ concentration(cells \bullet ml^{-1}) = (Average\ total\ cells\ counted\ for\ sample \div 15\ fields) \times (Area\ of\ circle \div area\ of\ grid) \times 100 \times dilution\ factor.$$

**Measurements of rates of oxygen consumption by PV-1 and TAG-1**

*Cell suspension preparation*: Because iron oxides are autocatalytic for further iron oxidation (16), which could contribute significantly to abiotic oxygen consumption early on in the treatments and confound our determination of biological oxygen consumption, we removed

the majority of the iron oxides present in FeOB cultures prior to inoculation. This was done by using serological pipettes to gently mix then harvest 12 ml of cell culture from ASW-ZVI plates. This aliquot was transferred to a 15 ml tube (VWR), then vortexed vigorously to dislodge cells from stalks and other iron oxide aggregates. *M. ferrooxydans* PV-1 tubes were then centrifuged at 19xG in a Sorvall Legend RT centrifuge (Thermo Fisher Inc.) for 1 min. As the iron oxide particles produced by TAG-1 are smaller than those produced by PV-1, TAG-1 tubes were centrifuged at 215xG for 1 minute to achieve comparable results as determined by cell counts. In both cases, a 6 ml aliquot of supernatant was then transferred to a new tube and cell concentrations were determined as described above. An 0.5 ml aliquot of supernatant was also removed and placed on a heat block at 100˚C for 5 minutes to serve as a killed control.

*Oxygen concentration measurements:* Oxygen concentrations over time were recorded using a non-invasive optical oxygen probe (optode). The optode uses fiber optic cables to read light reflected from oxygen sensor spots inside sealed containers. The amount of light reflected changes based on the concentration of oxygen around the spot, allowing the optode to determine the oxygen concentration inside sealed vessels.

Pst3 optode sensor spots (PreSens Precision Sensing GmbH) were affixed to the inner walls of 100 ml glass serum vials (Wheaton) with silicone adhesive. After the adhesive set, sensor spots were calibrated using air-saturated water and 100% $N_2$ gas according to the manufacturer's instructions. Vials were washed with 3% oxalic acid to remove any iron residue and sterilized in a bath of 10% HCl and rinsed with ultrapure water prior to use.

For these experiments, four glass vials with sensor spots were filled with 6 ml ASW. Oxygen concentrations were measured in the headspace, so it was left large in relation to the

amount of media added in order to minimize the effects of diffusion of oxygen in water. 30 mg ZVI, pre-sterilized via 24 hours of gamma irradiation from a $^{137}Cs$ source at 200 rad•$min^{-1}$, was added to each vial. Three vials were inoculated from prepared cell suspension aliquots to a final cell concentration of approximately $3.5 \bullet 10^5$ cells•$ml^{-1}$. The remaining vial was inoculated with an equivalent volume of heat-killed cell suspension. This was done to help differentiate between biological iron oxidation and abiotic iron oxidation catalyzed by the added iron oxides and dead bacterial cells acting as nucleating agents. Vials were then sealed with butyl rubber stoppers and their headspaces were replaced with gas mixes of either 8% $O_2$/10% $CO_2$/82% $N_2$ ("8% $O_2$" experiments) or 2% $O_2$/10% $CO_2$/88% $N_2$ ("2% $O_2$" experiments) to ambient pressure. The gas mix for 2% $O_2$ experiments was mixed using mass flow controllers (Omega Technologies) and stock gas tanks of 10% $O_2$/90% N, 100% $CO_2$, and 100% $N_2$.

An optode fiber optic cable was then attached to each vial and vials were incubated in a temperature-controlled room at 20˚C on a rocker, again to minimize the effects of diffusion. The oxygen concentration inside the vials was read every 5 minutes by an OXY-4 SMA optode (PreSens Precision Sensing GmbH). After 3 days (for 8% $O_2$ experiments) or 5 days (for 2% $O_2$ experiments) the headspace was again replaced with the original gas mix and oxygen concentrations were read every 5 minutes for an additional 3 days.

*Sampling:* Vials were removed, vortexed vigorously to dislodge the iron mats that were formed, and decanted into 15 ml tubes. 1 ml aliquots were taken from each tube and immediately used to determine final ferrous iron concentrations by ferrozine assay (26). 0.5 ml aliquots were removed for cell counts and fixed by mixing 1:1 with a 5% glutaraldehyde in ASW solution

(2.5% final glutaraldehyde concentration). Samples were fixed overnight at 4˚C and final cell concentrations were determined by direct count as described above.

**Measurements of rates of oxygen consumption by PV-1 and TAG-1 at 5˚C**

Oxygen consumption rates at 5˚C were conducted using an optode to measure headspace oxygen concentrations as the experiments using the 8% $O_2$/10% $CO_2$/82% $N_2$ gas mix detailed above, except these experiments were conducted in a temperature controlled room set to 5˚C.

**Iron concentration measurements**

All Fe(II) concentrations were measured using the ferrozine assay. 1 ml aliquots were centrifuged at 13000 rpm and 20 µl sample supernatant added to 980 µl ferrozine solution (2 mM ferrozine in 50 mM HEPES, pH 7.0) in a 1 ml cuvette and vortexed to mix. Absorbances were read at 562 nm on a Cary 100 UV-Vis Spectrophotometer (Agilent Technologies) and all measurements were done in triplicate.

**Oxygen consumption rate measurements with $HgCl_2$ addition**

Oxygen measurement experiments including $HgCl_2$ were initially set up the same way as 8% $O_2$ experiments. After 3 days, however, the media in the vials was removed via pipetting and replaced with ASW containing 1 mM $HgCl_2$. This was done carefully to not disturb the iron mat that had formed over the ZVI, allowing the demonstration of the effects of the mat on ZVI dissolution without living cells present. The $Fe^{2+}$ concentration of the removed ASW was determined by ferrozine assay.

Headspaces were then replaced with 8% $O_2$/10% $CO_2$/82% $N_2$, optode cables were reattached, and the oxygen concentration was measured every 5 minutes for 3 days. Fe(II) concentrations were then checked daily by ferrozine assay.

**Imaging of iron mat formation**

To observe mat formation for the duration of the experiments detailed above, cells were cultured for confocal microscopy in 60 mm petri dishes. These plates were used as they are approximately the same diameter as the 100 ml serum vials used for oxygen consumption experiments. Six plates were prepared for each strain and each plate contained 6 ml ASW and 30 mg gamma-sterilized ZVI and was inoculated to a final cell concentration of 3.5• x $10^5$ cells•$ml^{-1}$. These plates were placed in gas-tight jars, the jars were filled with a gas mix of 8% $O_2$/10% $CO_2$/82% $N_2$ and placed on a rocker in a temperature controlled room set to 20˚C.

One plate per strain was removed for imaging each day and jars were refilled with the same gas mix. Cells were visualized by staining with 1 µl/ml SYTO 13 nucleic acid dye (Thermo-Fischer). Polysaccharides were visualized by staining with 1 µl/ml rhodamine-conjugated *Ricinus communis* agglutinin 1 (RCA1, Vector Laboratories). Plates were incubated in the dark for 20 minutes after stain additions. Plates were then imaged on a Zeiss LSM 880 confocal microscope equipped with a dipping objective. Each stain was imaged using appropriate laser excitation wavelengths and ZVI particles were imaged using reflected light. Image stacks were made into 3D projections using Fiji (27).

**Oxygen consumption rate measurements of FeOB grown on pyrrhotite**

Experiments using pyrrhotite as an iron source were initially set up in the same manner as other oxygen consumption experiments, except instead of ZVI, 200 mg gamma-sterilized pyrrhotite powder was used as an iron source. This powder was made of commercially available pyrrhotite ($Fe_{(1-x)}2$, x = 0 to 0.2; Ward's Science) which was milled using a disk mill and sieved to -200 mesh (<74 μm, the same size as the ZVI powder used in other experiments). Vials were sealed with butyl rubber stoppers and their headspaces were replaced with 8% $O_2$/10% $CO_2$/82% $N_2$. Vials were then placed on a rocker at 20˚C and optode fiber optic cables were attached. Oxygen concentrations were measured every 5 minutes.

After two weeks, vials were removed and their headspaces were refreshed with the starting gas mix. They were placed back on the rocker and optode and their oxygen concentrations were again measured every 5 minutes for an additional week. Vials were then taken down and sampled for Fe(II) concentration via ferrozine assay.

**Results**

**Biotic and Abiotic Oxygen and Iron consumption during FeOB Incubations on Fe(0)**

When grown on ZVI at 20˚C, *M. ferrooxydans* PV-1 consistently consumed oxygen more slowly than heat-killed controls. Slower oxygen consumption was apparent after just 24 hours and persisted after vial headspaces were refreshed with the same gas mix. This was true for oxygen concentrations of both 2% and 8%. (Fig. 1.1)

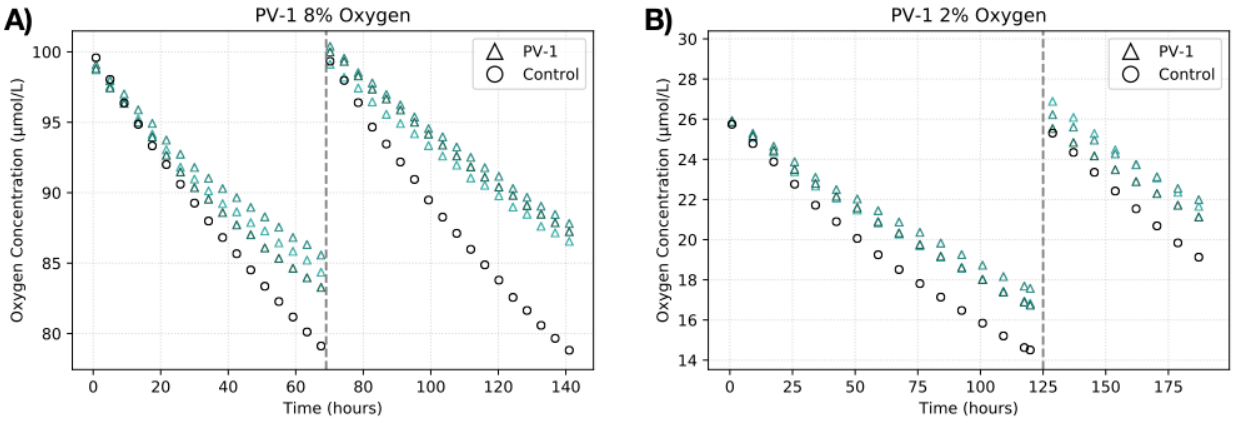


**Figure 1.1) Oxygen consumption over time by *M. ferrooxydans* PV-1 in sealed vials**. A) Vials containing 8% $O_2$ headspace, growth media and zero-valent Iron were inoculated (control was inoculated with heat-killed culture including oxides) and oxygen was monitored non-invasively for three days. Dashed line represents where headspace was replenished. B) Same treatment, except for the use of 2% $O_2$ in the headspace.

*G. bivora* TAG-1, on the other hand, initially consumed oxygen more quickly than controls. Oxygen consumption began to slow after 2 (for 8% $O_2$) or 3 (for 2% $O_2$) days, however, and after vial headspaces were refreshed TAG-1 clearly consumed oxygen more slowly than controls. This occurred at both oxygen concentrations tested, but was more apparent at 8% $O_2$. Some 2% $O_2$ vials consumed oxygen at nearly the same rate as controls after the headspace refresh, but this was still slower than their oxygen consumption rates 24 hours post-inoculation. (Fig. 1.2)

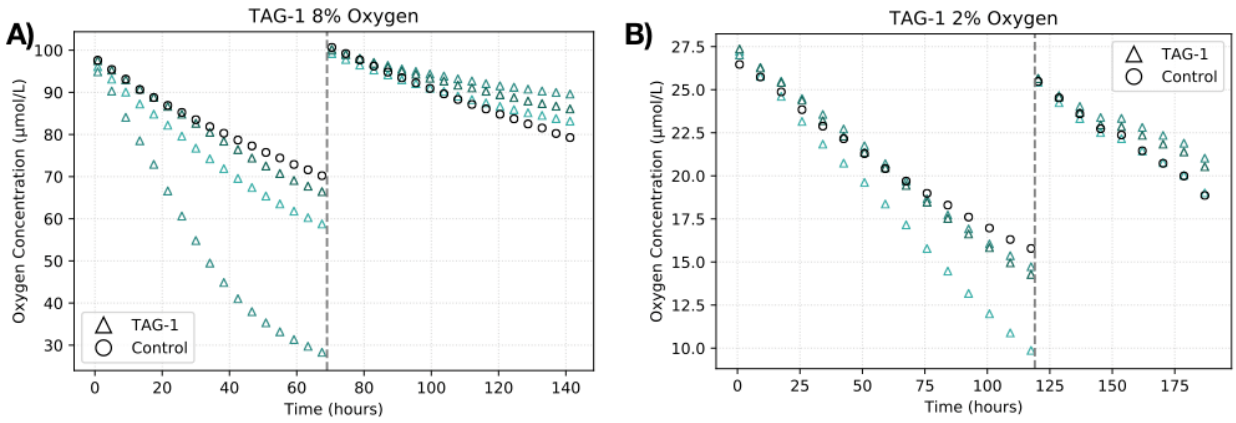


**Figure 1.2) Oxygen consumption over time by *G. bivora* TAG-1 in sealed vials.** A) Vials containing 8% $O_2$ headspace, growth media and zero-valent iron were inoculated (control was inoculated with heat-killed culture including oxides) and oxygen was monitored non-invasively for three days. Dashed line represents where headspace was replenished. B) Same treatment, except for the use of 2% $O_2$ in the headspace.

When grown on ZVI at 5˚C and 8% $O_2$, PV-1 did not show a consistent pattern, with different vials consuming both less and more oxygen than the control both before and after their headspaces were refreshed. TAG-1, however, initially consumed oxygen more slowly than the control. This rate increased after headspaces were refreshed, and TAG-1 then consumed oxygen at approximately the same rate as the control. (Fig. 1.3A & 1.3B)

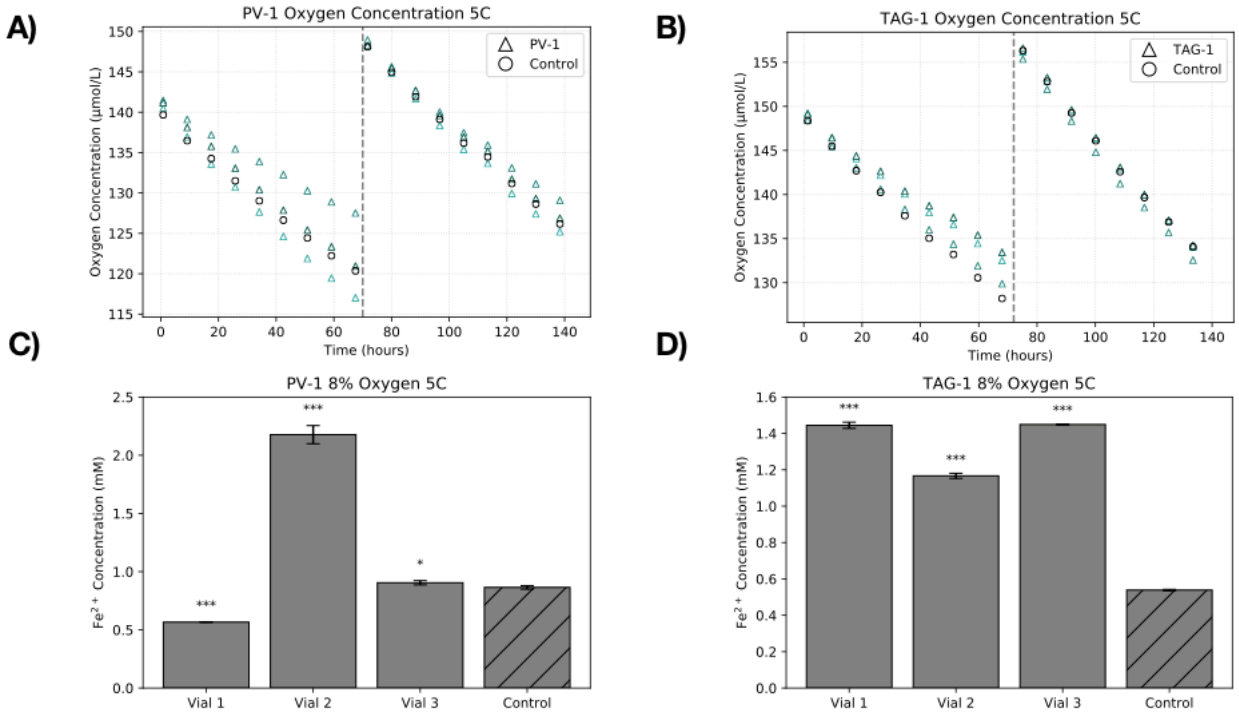


**Figure 1.3) Oxygen concentration measurements over time and end of experiment ferrous iron concentrations for incubations done at 5˚C.** A) and B) are oxygen concentration measurements over time for PV-1 and TAG-1 cultures, respectively. Dashed lines mark when vial headspace were refreshed with starting gas mix. C) and D) are concentrations of ferrous iron in each vial at the end of the experiment for PV-1 and TAG-1 respectively. (* = P<0.05, *** = P<0.001)

In incubations at 20˚C, vials with live cells consistently had far lower Fe(II) concentrations at the end of each experiment than heat-killed controls. At 2% $O_2$, both PV-1 and TAG-1 live vials had <250 µM Fe(II), while controls contained close to 1 mM Fe(II). For incubations done at 8% $O_2$, Fe(II) concentrations in life cells were close to 0 and often undetectable. As in the 2% $O_2$ experiments, controls at 8% $O_2$ had far higher Fe(II) concentrations at approximately 500 µM. (Fig. 1.4)

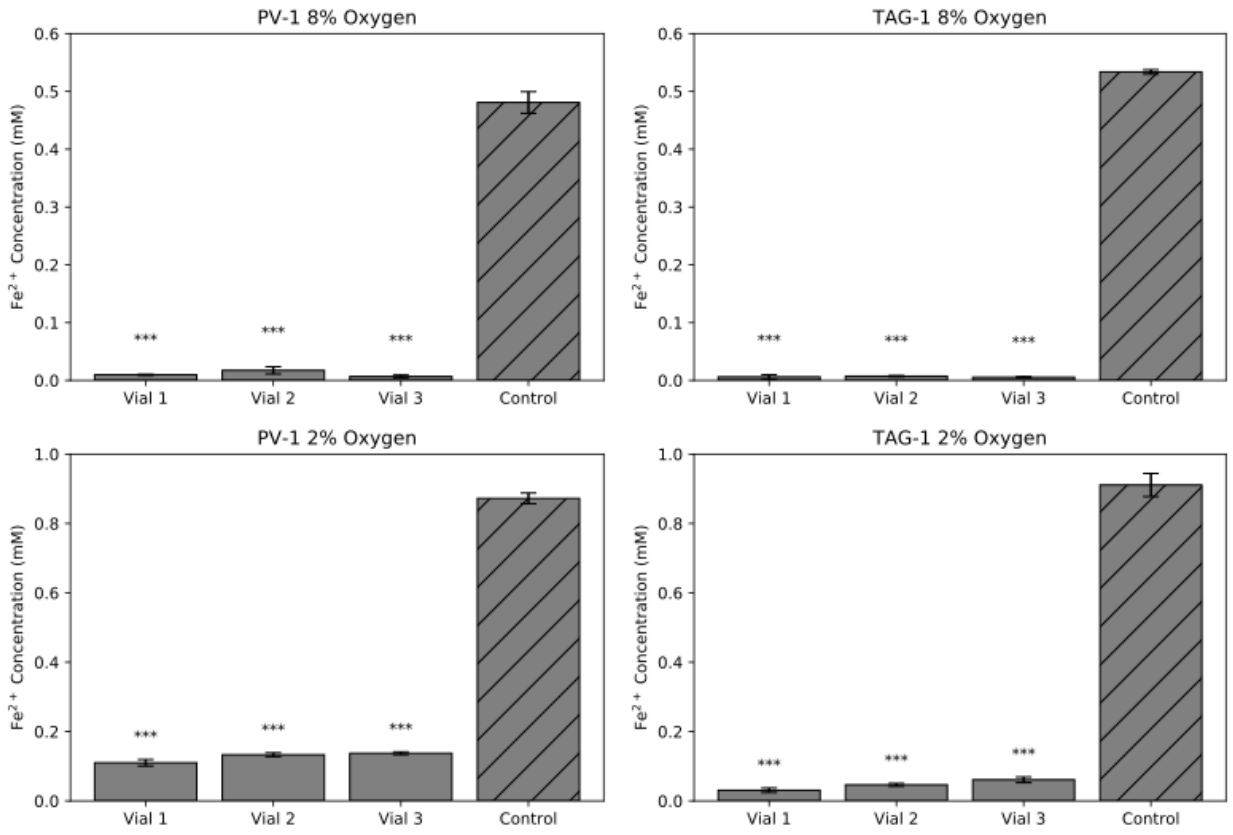


**Figure 1.4) Final ferrous iron concentrations measured in two strains of aerobic iron oxidizing bacterial cultures.** PV-1 and TAG-1 were grown on zero-valent iron in gastight vials. After six days, aliquots were recovered for ferrous iron quantification in vials with living cells, as well as those with dead cells. (*** = P<0.001)

This pattern did not hold true for incubations done at 5˚C, however. At lower temperatures, PV-1 Fe(II) concentrations ranged from ~566 µM to ~2.18 mM in live vials and was ~865 µM in the killed control. TAG-1 Fe(II) were similarly high in live vials, in the range of 1.26 - 1.54mM. Here the killed control actually had lower a Fe(II) concentration of 539µM. (Fig. 1.3C & 1.3D)

**Biotic and Abiotic Oxygen and Iron consumption during FeOB Incubations on Pyrrhotite**

When grown at 20˚C with pyrrhotite as their iron source, *M. ferrooxydans* PV-1 initially appeared to consume oxygen at the same rate as the killed control. The oxygen consumption rate

then increased and PV-1 cultures consumed oxygen more quickly than the control, starting at around 72 hours. After about 300 hours the oxygen consumption rate began to slow. Vials with live cells then consumed oxygen at approximately the same rate as the control after headspaces were refreshed. (Fig. 1.5A)

*G. bivora* TAG-1, on the other hand, always consumed oxygen more quickly than the killed control. This rate also slowed over the course of the experiment, but oxygen consumption rates in live vials were still faster than the control even after vial headspaces were refreshed. (Fig. 1.5B)

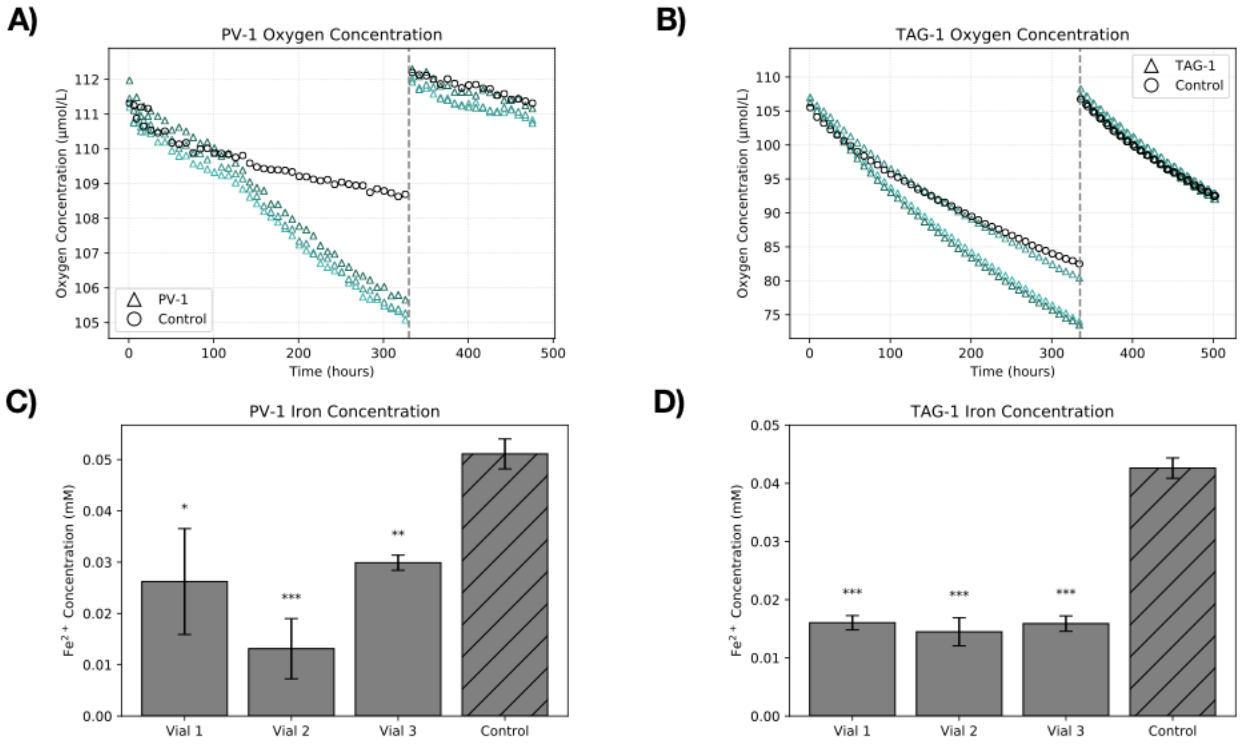


**Figure 1.5) Oxygen concentration measurements over time and end of experiment ferrous iron concentrations for incubations with pyrrhotite as iron source**. A and B) Oxygen concentration measurements over time for PV-1 and TAG-1 respectively. Dashed lines mark when vial headspace were refreshed with starting gas mix. C and D) Ferrous iron concentrations in each vial at the end of the experiment for PV-1 and TAG-1 respectively. Note the Y-axis is much smaller than other similar figures presented in this chapter. (* = P<0.05, ** = P<0.01, *** = P<0.001)

Vials with live PV-1 cells had low but detectable levels of Fe(II) at the conclusion of the experiment, in the range of ~13 μM – ~30 μM Fe(II). The killed control had significantly more dissolved iron at ~50 μM Fe(II) ($P<0.05$), likely the result of pyrrhotite dissolving more slowly than ZVI. (Fig. 1.5C)

Vials with live TAG-1 cells similarly had low levels of Fe(II) that were still within detection range. Fe(II) concentrations in these vials varied less than those of PV-1 vials, ending the experiment at ~15 μM. The control again had significantly more dissolved iron at ~40 μM ($P<0.05$). (Fig. 1.5D)

**Biotic and Abiotic Oxygen consumption in FeOB Incubations poisoned with $HgCl_2$**

As in the initial oxygen consumption experiments, *M. ferrooxydans* PV-1 consumed oxygen more slowly than the control. After culture media was replaced with fresh ASW containing $HgCl_2$ and headspaces were refreshed, vials that had live cells in them continued to consume oxygen more slowly than the control. Notably the rate of oxygen consumption in the control began to slow as well towards the end of the experiment. We think that this is an effect of the $HgCl_2$ addition and its interactions with oxygen. (Fig. 1.6A)

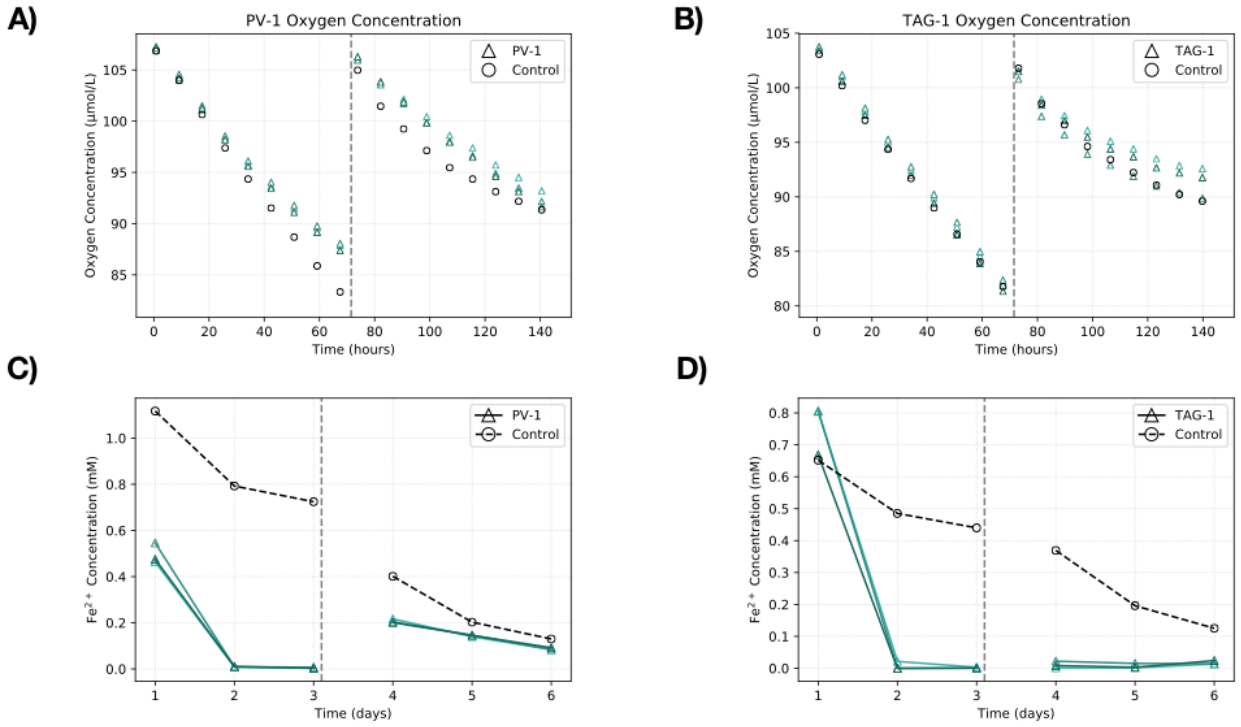


**Figure 1.6) Oxygen and ferrous iron time courses for FeOB incubations killed with $HgCl_2$.** A) and B) are oxygen measurements over time for *M. ferrooxydans* PV-1 and *G. bivora* TAG-1 respectively. C) and D) are ferrous iron concentrations over time *M. ferrooxydans* PV-1 and *G. bivora* TAG-1 respectively, determined by ferrozine assay. Dashed lines indicate where culture media was replaced by new media containing $HgCl_2$ and vial headspaces were refreshed with the starting gas mix.

Daily measurements of Fe(II) concentrations showed that vials with live PV-1 cells have lower Fe(II) concentrations than the control after just 24 hours (~600 µM vs 1.2 mM). Both decreased after 48 hours to approximately 800 µM in the control and nearly undetectable levels in vials with live cells. After the media exchange and headspace refresh, vials that had live cells increased in Fe(II) concentration to ~350 µM, while the control increased to ~500 µM. These values continued to decrease, until the Fe(II) concentration in the control was only slightly higher than in vials that had live cells (both ~225 µM; Fig. 1.6C).

*Ghiorsea bivora* TAG-1 consumed oxygen at approximately the same rate as the control at the start of the experiment. After media was replaced with ASW containing $HgCl_2$ and the headspaces were refreshed, vials with live TAG-1 cells consumed oxygen slightly more slowly

than controls, with one vial consuming oxygen at approximately the same rate as the control. Again the oxygen consumption rate of the control slowed towards the end of the experiment due to the addition of the $HgCl_2$. (Fig. 1.6B)

After 24 hours, Fe(II) concentrations were approximately the same between vials with live TAG-1 cells and the control, with two of three live vials actually having more dissolved iron. Live vials again had undetectable amounts of Fe(II) after 48 hours, while the control decreased to ~500 μM. This remained the case until the media and headspaces were exchanged. After the addition of ASW containing $HgCl_2$, Fe(II) concentrations remained extremely low in vials that had live TAG-1 cells. There was, however, a slight increase in dissolved iron 72 hours after the media was exchanged. Fe(II) in the control remained high 24 hours post-media exchange, at about 400 μM, decreasing slowly over time to about 150 μM at the conclusion of the experiment. (Fig. 1.6D)

**Confocal microscopy time course of active FeOB mats**

Confocal microscopy showed that after 1 day *M. ferrooxydans* PV-1 cells began to attach to ZVI granules and produce stalks, visible as aggregates of polysaccharide (Fig 1.7). After 2 days, attached cells are more numerous and by 3 days post-inoculation many ZVI granules are almost completely covered by cells. Additionally, stalk production had covered many ZVI granules. By day 4 few ZVI granules were visible, as they were mostly covered by stalks with cells interspersed throughout. After day 5 the iron mat had increased in thickness, and flocs covered all ZVI granules, leaving none visible. By day 6 these mats were up to 300 μM thick in some areas.

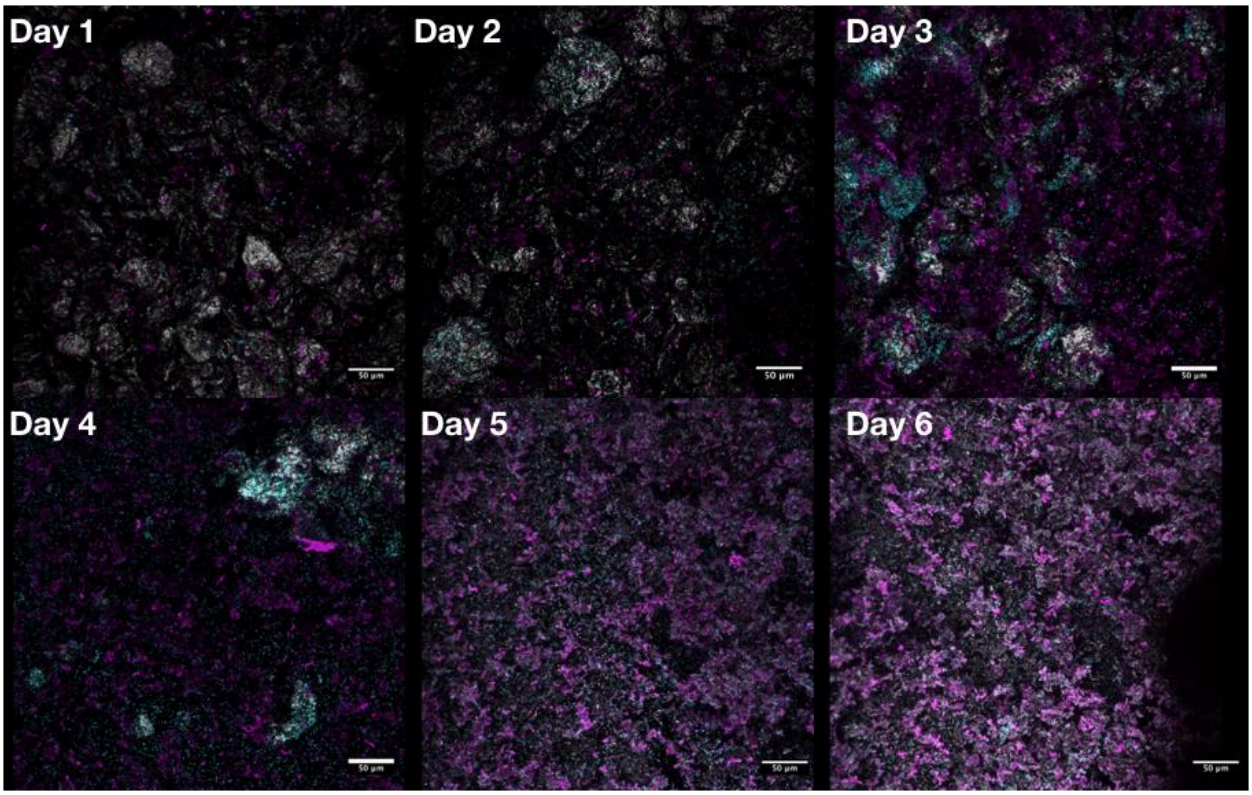


**Figure 1.7) Visualization of *M. ferrooxydans* PV-1 growth on zero-valent iron over time.** Cyan: cells stained with SYTO 13 DNA stain, magenta: polysaccharide stained with rhodamine-conjugated *Ricinus communis* agglutinin, and white: reflected light.

*G. bivora* TAG-1 cells had also begun to attach to ZVI granules after 1 day with some polysaccharide production (Fig 1.8). By day 2, there were already large clumps of cells in some areas. By day 3 cells covered the majority of ZVI granules, though with less polysaccharide present than in PV-1 cultures. This remained the case for the remainder of the experiment. Though much of the ZVI was covered by polysaccharide, most ZVI was covered only by cells. There were still ZVI particles visible by day 6, however. This is in contrast to PV-1 cultures, which completely covered the ZVI by day 5. TAG-1 mats also thickened over the course of the experiment, generally to about 100 μM by day 6.

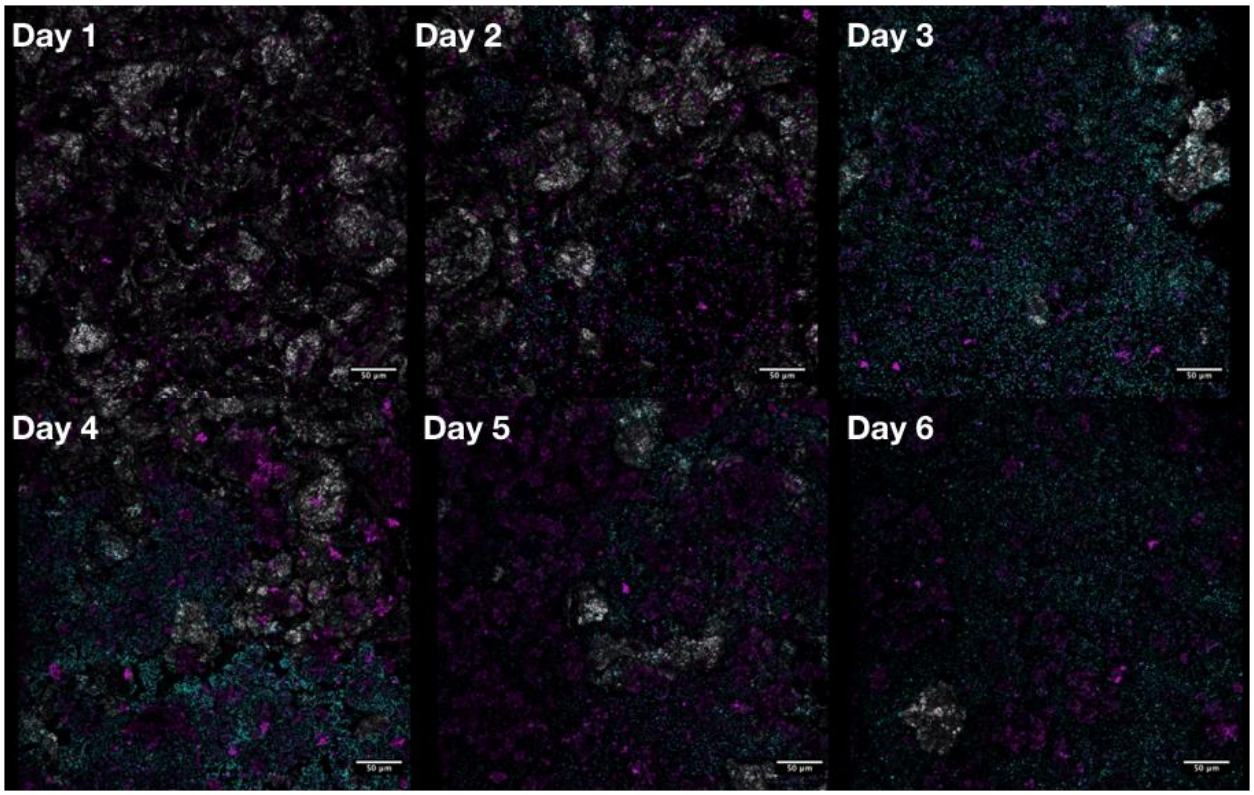


**Figure 1.8) Visualization of growth of *G. bivora* TAG-1 on zero-valent iron over time.** Cyan: cells stained with SYTO 13 DNA stain, magenta: polysaccharide stained with rhodamine-conjugated *Ricinus communis* agglutinin, and white: reflected light.

## Discussion

### FeOB consume oxygen more slowly than killed controls when grown on solid zero-valent iron

In this study, we show that iron-oxidizing bacteria are capable of decreasing iron oxidation rates when grown on iron minerals at 20˚C. In addition, vials in which live cells grew have very low final dissolved Fe(II) concentrations in comparison to killed controls. If this were simply a matter of the FeOB keeping Fe(II) levels low by consuming it more quickly than it could be replenished through dissolution of ZVI, we would expect to see an increase in oxygen consumption rates. On the other hand, if FeOB were slowing oxygen consumption rates by

decreasing the oxidation of dissolved Fe(II) (e.g., by reducing the autocatalytic capacity of the iron oxides they generate), we would expect higher Fe(II) concentrations in controls. Taken together, these data therefore point towards a decrease in mineral dissolution.

This is in contrast to previous studies where FeOB have only been implicated in increasing weathering rates (28, 29). This observation made sense in the past, as one can usually safely assume that microbially catalyzed reactions will proceed at an increased rate relative to abiotic systems. Indeed, this is even true for FeOB when they are provided with dissolved $Fe^{2+}$ (12, 15, 16, 25). When given a solid iron source, however, it seems that the story is not so simple. Indeed, even the two FeOB studied here behaved differently from one another, with PV-1 slowing oxygen consumption rates both before and after vial headspaces were refreshed while TAG-1 only appeared to reduce oxygen consumption rates after vial headspaces were refreshed. This may be related to the fact that PV-1 is a stalk forming FeOB, which allows them to form very thick iron mats compared to sheath- and amorphous oxide-forming organisms (11, 17, 18, 30). It is well known that microbial mats are able to influence the chemistry of their surroundings, and the iron mats of FeOB are no exception (18, 31). We hypothesize that these mats slow diffusion around minerals, preventing contact with fresh seawater and thereby inhibiting dissolution.

It is important to note that this affects the *net* iron oxidation rate. FeOB must still compete with abiotic Fe(II) oxidation for their electron donors and acceptors (15, 16, 25). Both PV-1 and TAG-1 are most likely oxidizing iron faster than the abiotic rate in the microenvironment around the ZVI on which they are growing. However, this is probably slower than the abiotic rate of oxidation around the ZVI in vials that never had live cells.

These patterns do not hold true, however, at temperatures that are more representative of the majority of the seafloor, here represented by incubations conducted at 5˚C. In fact, there was no discernable pattern for PV-1 when it was grown at this temperature, with different vials consuming oxygen both faster and slower than the control. Final dissolved iron concentrations also are also difficult to interpret, as of the three vials inoculated with live PV-1, one had a higher Fe(II) concentration than the control, one lower, and one only slightly higher.

TAG-1 also showed different results than at 20˚C. Here vials inoculated with live cells consumed slightly less oxygen than the control before their headspaces were refreshed. After the refresh, however, all vials consumed oxygen at approximately the same rate. Additionally, all three vials inoculated with live TAG-1 cells had much higher final Fe(II) concentrations compared with the control.

We hypothesize that in these experiments, FeOB growth was slow to non-existent. This is consistent with both strains being found in warmer waters around hydrothermal vents and having optimal growth temperatures of 30˚C (PV-1) and 20˚C (TAG-1) (2, 32). We were also unable to observe cells or stalks (in the case of PV-1) via microscopy post-incubation. It is therefore likely that variations in oxygen consumption and final Fe(II) concentrations were due to heterogeneity in the way that the ZVI lay in the vials (i.e. some ZVI powder may have been more clumped than in other vials, leading to less contact with media and therefore less dissolution).

**FeOB are also capable of affecting dissolution rates of natural iron sulfide minerals**

To demonstrate how FeOB affect dissolution of naturally occurring minerals, we incubated both strains with pyrrhotite, a known iron source for FeOB (33). Because pyrrhotite does not dissolve as readily as ZVI it was necessary to use more of it for each culture and

incubate these cultures for a longer duration. The resulting changes in oxygen concentration were not as large. However, there were still clear differences between strains and between each strain and their respective controls.

*Mariprofundus ferrooxydans* PV-1 initially consumed oxygen more quickly than the control. This is in contrast to experiments where it was grown on ZVI, where it started to slow oxygen consumption almost immediately. When grown on pyrrhotite, oxygen consumption did not begin to slow until approximately 275 hours. After the headspace in each vial was refreshed, the oxygen consumption rate had slowed to be approximately the same as the control. Additionally, at the end of the experiment there was significantly more dissolved Fe(II) in the control. This indicates that, although it seems to increase dissolution rates initially, PV-1 is likely to affect pyrrhotite in the same way as it does ZVI over longer time periods. We think that this is due to the much slower dissolution rate of pyrrhotite compared to ZVI making these growth conditions less favorable for PV-1, increasing the amount of time needed for PV-1 to grow to cover mineral grains and thus inhibit mineral dissolution.

*Ghiorsea bivora* TAG-1, on the other hand, consumed oxygen more quickly than the control for the entire length of the experiment, including after headspaces had been refreshed. The control also had a significantly higher dissolved iron concentration at the end of the experiment than vials that contained live cells. The difference in phenotypes between when TAG-1 is grown on ZVI and when it is grown on pyrrhotite could again be due to the differences in dissolution rates between ZVI and pyrrhotite. It may be that TAG-1 is only able to decrease iron mineral dissolution when the mineral it is growing on dissolves quickly. This would allow for faster growth and the ability to cover more of each mineral grain. It should also be noted that ZVI oxidation can evolve hydrogen, which TAG-1 can use as an electron donor (32).

Additionally, ZVI must first be oxidized to $Fe^{2+}$ before FeOB can utilize it. Pyrrhotite already contains $Fe^{2+}$, so TAG-1 could be able to oxidize it directly without an initial oxidation step, increasing dissolution rates.

Alternatively, different FeOB may inhibit mineral dissolution rates in different ways. In this case PV-1 could use a strategy that works on more mineral types than TAG-1. It is unclear whether this phenomenon is an adaptation to growing on iron minerals or simply an emergent property of forming a thick iron mat. Because FeOB must compete with abiotic reactions for their electron donors and acceptors, mat production might be conducive to growth on minerals. It could allow more dissolved $Fe^{2+}$ to reach stalked cells that have grown away from their iron source by inhibiting diffusion of oxygen towards the iron mineral substrate thereby reducing abiotic oxidation reaction rates. If this is the case, FeOB that do not form thick iron mats like TAG-1 would be less able to slow these abiotic rates and could simply have to outcompete them.

**Minerals exposed to FeOB continue to dissolve more slowly after FeOB are killed**

We have demonstrated that FeOB are able to inhibit the dissolution of iron minerals, but it was unclear whether this was due to an alteration of the minerals themselves or if FeOB simply change the environment around the minerals they grow on. For example, do live cells simply consume $O_2$ to such low levels that it slows the dissolution of ZVI, which requires $O_2$ to dissolve at an appreciable rate? We examined which was the case by growing FeOB on ZVI powder for before replacing their growth media with fresh ASW containing $HgCl_2$, which would kill any live cells.

Oxygen concentrations for the first 72 hours of each incubation were as expected, with *M. ferrooxydans* PV-1 consuming oxygen more slowly than the control and *G. bivora* TAG-1

consuming oxygen at approximately the same rate. After the media was replaced with $HgCl_2$-containing ASW and vial headspaces had been refreshed, however, both strains consumed oxygen more slowly than the control despite the cells being killed.

In addition, vials with live cells always had lower dissolved Fe(II) concentrations than the control, which were mostly around the detection limit for the ferrozine assay. Even after the media in each vial was replaced, vials that had live cells had lower Fe(II) concentrations than vials which never had live cells growing in them. Because the new media did not contain any Fe(II) to start with, this means that the ZVI in vials that had living cells dissolved more slowly than in the control despite those cells now being dead.

These data suggest that FeOB do not have to be present after they have inhibited the dissolution of iron minerals for inhibition to continue. They may be altering the surface structure or inhibiting diffusion around the mineral surface and thereby reducing dissolution rates. FeOB have in the past been recognized as "ecological engineers," and this is another example of how they could modify their environment to suit their needs (18). Additionally, the fact that TAG-1 inhibited new dissolution to a much greater degree than PV-1 also suggests that there may be different mechanisms for dissolution inhibition among diverse FeOB.

**Iron mats grow to cover mineral grains**

We examined how each FeOB strain grows on ZVI over time using confocal microscopy. This revealed that though both strains grew over the ZVI, they did so in different ways. PV-1 grew in thick mats, covering ZVI particles in cells at first, but also with a large amount of polysaccharide. In most places, we were unable to find exposed ZVI – it was entirely obscured by the formation of iron mats, around 300 μm thick at times. TAG-1, in contrast, had far greater

amounts of cells visible. Though it did produce polysaccharide, most of what could be seen obscuring the ZVI particles were large numbers of cells. TAG-1 also made a much thinner mat, around 100 μm in thickness, leaving some ZVI exposed even after six days.

Again, this suggests that there may be different strategies used by FeOB to inhibit mineral dissolution. It should also be noted that after 48 hours, when dissolved Fe(II) levels should be extremely low, there is still ZVI left exposed. Additionally, cell numbers continue to increase after this, indicating that dissolved iron is still available to growing cells despite there being very little present in the bulk media.

**Conclusion**

The data presented here clearly demonstrate that FeOB have the capacity to reduce, as well as increase, the dissolution of iron minerals. This has far-reaching implications for our understanding of iron cycling in Earth's oceans. Much of the oceanic crust is composed of iron-rich basalt as well as iron sulfides near regions of hydrothermal venting, both of which have been shown to be potential iron sources for the growth of FeOB (28, 33–35). Until now it was assumed that the presence of FeOB or FeOB biosignatures like twisted iron stalks meant that these organisms would be increasing the dissolution rates of these iron minerals. This study shows that this assumption is not always correct. Indeed, the effects of mineral colonization by FeOB should be assessed on a more case-by-case basis, as different FeOB are capable of affecting mineral dissolution rates in different ways.

## References


1. **Chan CS**, **Fakra SC**, **Emerson D**, **Fleming EJ**, **Edwards KJ**. 2011. Lithotrophic iron-oxidizing bacteria produce organic stalks to control mineral growth: implications for biosignature formation. ISME J **5**:717–727.

2. **Emerson D**, **Rentz JA**, **Lilburn TG**, **Davis RE**, **Aldrich H**, **Chan C**, **Moyer CL**. 2007. A novel lineage of proteobacteria involved in formation of marine Fe-oxidizing microbial mat communities. PLoS One **2**.

3. **Weber K a**, **Achenbach L a**, **Coates JD**. 2006. Microorganisms pumping iron: anaerobic microbial iron oxidation and reduction. Nat Rev Microbiol **4**:752–764.

4. **Chan CS**, **Emerson D**, **Luther GW**. 2016. The role of microaerophilic Fe-oxidizing micro-organisms in producing banded iron formations. Geobiology **14**:509–528.

5. **Anderson CR**, **James RE**, **Fru EC**, **Kennedy CB**, **Pedersen K**. 2006. In situ ecological development of a bacteriogenic iron oxide-producing microbial community from a subsurface granitic rock environment. Geobiology **4**:29–42.

6. **James RE**, **Ferris FG**. 2004. Evidence for microbial-mediated iron oxidation at a neutrophilic groundwater spring. Chem Geol **212**:301–311.

7. **Sobolev D**, **Roden EE**. 2001. Suboxic Deposition of Ferric Iron by Bacteria in Opposing Gradients of Fe(II) and Oxygen at Circumneutral pH. Appl Environ Microbiol **67**:1328–1334.

8. **Søgaard EG**, **Aruna R**, **Abraham-Peskir J**, **Bender Koch C**. 2001. Conditions for biological precipitation of iron by Gallionella ferruginea in a slightly polluted ground water. Appl Geochemistry **16**:1129–1137.

9. **Hallbeck L**, **Pedersen K**. 1991. Autotrophic and mixotrophic growth of Gallionella ferruginea. J Gen Microbiol **137**:2657–2661.

10. **Sobolev D**, **Roden EE**. 2002. Evidence for rapid microscale bacterial redox cycling of iron in circumneutral environments. Antonie van Leeuwenhoek, Int J Gen Mol Microbiol **81**:587–597.

11. **Emerson D**, **Moyer CL**. 2002. Neutrophilic Fe-oxidizing bacteria are abundant at the Loihi Seamount hydrothermal vents and play a major role in Fe oxide deposition. Appl Environ Microbiol **68**:3085–3093.

12. **Emerson D**, **Revsbech NP**. 1994. Investigation of an iron-oxidizing microbial mat community located near Aarhus, Denmark: Field studies. Appl Environ Microbiol **60**:4022–4031.

13. **Gault AG**, **Ibrahim A**, **Langley S**, **Renaud R**, **Takahashi Y**, **Boothman C**, **Lloyd JR**, **Clark ID**, **Ferris FG**, **Fortin D**. 2011. Microbial and geochemical features suggest iron

redox cycling within bacteriogenic iron oxide-rich sediments. Chem Geol **281**:41–51.

14. **Krepski ST**, **Emerson D**, **Hredzak-Showalter PL**, **Luther GW**, **Chan CS**. 2013. Morphology of biogenic iron oxides records microbial physiology and environmental conditions: Toward interpreting iron microfossils. Geobiology **11**:457–471.

15. **Lueder U**, **Druschel G**, **Emerson D**, **Kappler A**, **Schmidt C**. 2018. Quantitative analysis of O2 and Fe2+ profiles in gradient tubes for cultivation of microaerophilic Iron(II)-oxidizing bacteria. FEMS Microbiol Ecol **94**:1–15.

16. **Rentz J a.**, **Kraiya C**, **Luther GW**, **Emerson D**. 2007. Control of ferrous iron oxidation within circumneutral microbial iron mats by cellular activity and autocatalysis. Environ Sci Technol **41**:6084–6089.

17. **Emerson D**, **Fleming EJ**, **McBeth JM**. 2010. Iron-oxidizing bacteria: an environmental and genomic perspective. Annu Rev Microbiol **64**:561–583.

18. **Chan CS**, **Mcallister SM**, **Leavitt AH**, **Glazer BT**, **Krepski ST**, **Emerson D**, **Chan CS**. 2016. The Architecture of Iron Microbial Mats Reflects the Adaptation of Chemolithotrophic Iron Oxidation in Freshwater and Marine Environments **7**:1–18.

19. **Chiu BK**, **Kato S**, **McAllister SM**, **Field EK**, **Chan CS**. 2017. Novel pelagic iron-oxidizing Zetaproteobacteria from the Chesapeake Bay oxic-anoxic transition zone. Front Microbiol **8**:1–16.

20. **Picard A**, **Kappler A**, **Schmid G**, **Quaroni L**, **Obst M**. 2015. Experimental diagenesis of organo-mineral structures formed by microaerophilic Fe(II)-oxidizing bacteria. Nat Commun **6**:1–8.

21. **Glazer BT**, **Rouxel OJ**. 2009. Redox speciation and distribution within diverse Iron-dominated microbial habitats at Loihi Seamount. Geomicrobiol J **26**:606–622.

22. **Neubauer SC**, **Emerson D**, **Megonigal JP**. 2002. Life at the energetic edge: Kinetics of circumneutral iron oxidation by lithotrophic iron-oxidizing bacteria isolated from the wetland-plant rhizosphere. Appl Environ Microbiol **68**:3988–3995.

23. **Roden EE**, **Sobolev D**, **Glazer B**, **Luther GW**. 2004. Potential for microscale bacterial Fe redox cycling at the aerobic-anaerobic interface. Geomicrobiol J **21**:379–391.

24. **Rubin-Blum M**, **Antler G**, **Tsadok R**, **Shemesh E**, **Austin JA**, **Coleman DF**, **Goodman-Tchernov BN**, **Ben-Avraham Z**, **Tchernov D**. 2014. First evidence for the presence of iron oxidizing zetaproteobacteria at the levantine continental margins. PLoS One **9**:1–10.

25. **Druschel GK**, **Emerson D**, **Sutka R**, **Suchecki P**, **Luther GW**. 2008. Low-oxygen and chemical kinetic constraints on the geochemical niche of neutrophilic iron(II) oxidizing microorganisms. Geochim Cosmochim Acta **72**:3358–3370.

26. **Stookey LL**. 1970. Ferrozine-A New Spectrophotometric Reagent for Iron. Anal Chem **42**:779–781.

27. **Schindelin J**, **Arganda-Carreras I**, **Frise E**, **Kaynig V**, **Longair M**, **Pietzsch T**, **Preibisch S**, **Rueden C**, **Saalfeld S**, **Schmid B**, **Tinevez JY**, **White DJ**, **Hartenstein V**, **Eliceiri K**, **Tomancak P**, **Cardona A**. 2012. Fiji: An open-source platform for biological-image analysis. Nat Methods **9**:676–682.

28. **Edwards KJ**, **Rogers DR**, **Wirsen CO**, **McCollom TM**. 2003. Isolation and characterization of novel psychrophilic, neutrophilic, Fe-oxidizing, chemolithoautotrophic alpha- and gamma-proteobacteria from the deep sea. Appl Environ Microbiol **69**:2906–2913.

29. **Edwards KJ**, **Bach W**, **McCollom TM**, **Rogers DR**. 2004. Neutrophilic Iron-Oxidizing Bacteria in the Ocean: Their Habitats, Diversity, and Roles in Mineral Deposition, Rock Alteration, and Biomass Production in the Deep-Sea. Geomicrobiol J **21**:393–404.

30. **Toner BM**, **Berquó TS**, **Michel FM**, **Sorensen J V.**, **Templeton AS**, **Edwards KJ**. 2012. Mineralogy of iron microbial mats from Loihi Seamount. Front Microbiol **3**:1–18.

31. **Hoehler TM**, **Bebout BM**, **Marais DJ Des**. 2001. The role of microbial mats in the production of reduced gases on the early Earth **412**:324–327.

32. **Mori JF**, **Scott JJ**, **Hager KW**, **Moyer CL**, **Küsel K**, **Emerson D**. 2017. Physiological and ecological implications of an iron- or hydrogen-oxidizing member of the Zetaproteobacteria, Ghiorsea bivora, gen. nov., sp. Nov. ISME J **11**:2624–2636.

33. **Barco RA**, **Hoffman CL**, **Ramírez GA**, **Toner BM**, **Edwards KJ**, **Sylvan JB**. 2017. In-situ incubation of iron-sulfur mineral reveals a diverse chemolithoautotrophic community and a new biogeochemical role for Thiomicrospira. Environ Microbiol **19**:1322–1337.

34. **Henri PA**, **Rommevaux-Jestin C**, **Lesongeur F**, **Mumford A**, **Emerson D**, **Godfroy A**, **Ménez B**. 2016. Structural iron (II) of basaltic glass as an energy source for zetaproteobacteria in an abyssal plain environment, offthe mid atlantic ridge. Front Microbiol **6**:1–18.

35. **Edwards KJ**, **Bach W**, **Rogers DR**. 2003. Geomicrobiology of the ocean crust: A role for chemoautotrophic Fe-bacteria. Biol Bull **204**:180–185.

# Chapter 2

Transcriptomic response of the iron oxidizing bacterium *Ghiorsea bivora* TAG-1 to acute and chronic changes in pH reveals how it survives in hydrothermal vent environments

**Abstract**

Iron oxidizing bacteria (FeOB) are often found in hydrothermal vent habitats, where they must contend with rapid changes in extracellular chemistry due to turbulent mixing of cold, alkaline seawater with hot, acidic vent fluid. This presents a number of issues for any microbe residing in such an environment, but FeOB in particular will experience shifts in electron donor and acceptor availability with changes in pH. We studied how one such organism, *Ghiorsea bivora* TAG-1, responds to both acute and chronic exposure to pH outside its optimum by examining its transcriptional response as a proxy for physiological change. We show that acute exposure to a more acidic environmental (pH = 5.5) results in differential expression of genes, including those related to translation under acute exposure, motility under chronic exposure, and inorganic ion transport in both. We also demonstrate that subjecting TAG-1 to more alkaline environment (pH = 7.5) induces a greater transcriptional response, including greatly increased expression of motility and signal transduction related genes during acute exposure and decreases in expression of genes related to energy metabolism and inorganic ion transport after chronic exposure. The data presented here are among the first to explore how FeOB contend with changes in environmental pH, and provide insight as to how they might survive at hydrothermal vents.

**Introduction**

Deep-sea hydrothermal vents are dynamic ecosystems due to the mixing of two chemically distinct endmember fluids: seawater and vent fluid. Seawater at the ocean floor is cold (typically around 2-4˚C), alkaline (pH ~8), has low metal content (≤0.001 μM iron), and has high concentrations of oxygen (~100 mM around vent fields) and sulfate (~28 mM) (1, 2). Vent fluid, in contrast, is hot (reaching up to 400˚C), acidic (as low as pH ~3), rich in heavy metals,

and chemically reducing with concentrations of sulfide, hydrogen, and ferrous iron in the hundreds of micromolar to millimolar range (1–4). Microorganisms in vent fields often take advantage of these differences in chemical concentrations, living along steep gradients generated by this mixing, with electron donors plentiful in reduced vent fluid and electron acceptors abundant in seawater (5). These gradients are spatially and temporally variable, however, and organisms that reside in such dynamic environments must be able to contend with sudden changes in the chemical conditions of their habitat (6, 7).

Neutrophilic iron-oxidizing bacteria (FeOB) are chemolithoautotrophs that use reduced iron ($Fe^{2+}$) as an electron donor and oxygen as their electron acceptor (8–10). At circumneutral pH, however, oxygen and $Fe^{2+}$ rapidly react to form $Fe^{3+}$, which then precipitates as iron oxyhydroxides (11, 12). For this reason, FeOB generally live in opposing gradients of oxygen and $Fe^{2+}$ where abiotic reactions are slower and FeOB can better compete with abiotic oxidation for their electron donors (9, 10, 13). The chemical gradients established by hydrothermal venting provide an ideal environment for this metabolism, where ferruginous vent fluid comes into contact with oxygenated seawater, establishing zones of low oxygen and high $Fe^{2+}$, which is replenished by rapid mixing due to advective flow from vents (9, 14–18). Interestingly, pH also affects the stability of dissolved iron, with abiotic oxidation of $Fe^{2+}$ proceeding more slowly at lower pH (19). Environments that are more acidic, therefore, tend to have more iron available for oxidation by FeOB. As most FeOB isolates tested to date grow best at pH around 6.5, it is likely that iron oxidation as a lifestyle is facilitated by the increased $Fe^{2+}$ stability afforded by lower pH (20). Vent fluid in combination with the oxygen provided by seawater may therefore provide an ideal environment for FeOB.

*Ghiorsea bivora* TAG-1, one such FeOB, is a member of the *Zetaproteobacteria*, a bacterial clade comprised exclusively of FeOB (17, 20, 21). Originally isolated from an iron-rich mat at the Trans-Atlantic Geotraverse vent site in the Mid Atlantic Ridge, TAG-1 is capable of oxidizing both $Fe^{2+}$ and $H_2$ found in vent fluid, with $O_2$ as its sole electron acceptor (17). Like many vent organisms, TAG-1 grows best at intermediate conditions between vent fluid and seawater. As such, it prefers mesophilic temperatures (~20˚C), low concentrations of $O_2$, and a circumneutral, albeit slightly acidic pH of around 6.5 (17, 20).

The gradients within which TAG-1 thrives can shift over short time scales due to the turbulent mixing of seawater and vent fluid (6). One environmental factor that these microbes likely experience are changes in pH. Extracellular pH is a major factor governing physiology and biochemistry of bacteria in many environments, and in most environments – especially at hydrothermal vents – pH changes are necessarily coupled with other changes in ambient chemistry (22–24). For example, a decrease in pH resulting from greater vent fluid influence is accompanied by an increase in availability of reduced electron donors as well as more heavy metals such as cadmium, cobalt, copper, and lead, which may be poisonous to bacteria (1, 2). This includes iron, which at sufficiently high concentrations is toxic even to FeOB (19). In contrast, an increase in pH from an influx of seawater brings with it an increase in $O_2$, less bioavailability of many metals that form insoluble oxides, and greater oxidative stress (1, 4).

At the diffuse hydrothermal vent flows within which TAG-1 is found, it is likely not always residing in its pH optimum. In these environments, acidic vent fluids mix with more alkaline seawater in a turbulent manner and this venting is not constant. Flow regimes can be altered on short time scales, increasing or decreasing the proportion of vent fluid making up the environment with a corresponding change in the proportion of seawater present (4, 5). This may

be especially relevant to FeOB because of their metabolism. While greater hydrothermal influence increases availability of $Fe^{2+}$, it also increases the stability of $Fe^{3+}$, decreasing its precipitation rate and slowing the removal of one of the reaction end products, thereby decreasing the energetic yield of iron oxidation (12, 25). Additionally, an increase in seawater influence would have a compounding effect on iron availability by decreasing the total amount of dissolved iron present, decreasing the stability of $Fe^{2+}$, and increasing $pO_2$ leading to further oxidation.

TAG-1 lives in a mixture of these two endmember fluids, and must contend with these temporal changes in conditions that will result in a variety of challenges. These challenges include episodic scarcity of electron acceptors (when their surroundings are more hydrothermal fluid dominated), episodic scarcity of electron donors (when their surrounding are more seawater-dominant), potential metal toxicity, potential oxidative stress, and even intercellular acid-base regulatory stress. Indeed, the chemical differences between hydrothermal vent fluid and seawater pose a number of challenges for microbes living in vent environments, but the physiological responses of FeOB in general, and TAG-1 specifically, remain unknown.

In this study, we explored how TAG-1 responds to vent system dynamics, using transcriptional abundance analysis as a proxy for its physiological response to changing pH. We conducted a series of treatments examining TAG-1's response to acute changes in pH (pH 5.5 and 7.5, which are near the extremes of its pH tolerance). We also conducted a series of treatments examining its response to chronic exposure to pH 5.5 and 7.5. We then compared its responses to the transcriptional state of TAG-1 grown at pH 6.5, which has been shown to be its pH growth optimum, and is a pH typical of diffuse vents (17, 20, 26, 27). We also tested TAG-1's acute response to a pH of 8.0, to represent exposure to pure seawater (1). Interestingly, TAG-

1 cannot grow at pH 8.0, raising the question of how an organism that lives in the ocean but cannot grow at seawater pH reacts to an influx of pure seawater (17, 20).

We found that TAG-1 is likely better able to contend with acute exposure to acidic conditions than to alkaline pH. We saw relatively small transcriptomic changes under acute exposure to pH 5.5 with, for instance, some genes related to translation being found in higher abundance relative to controls grown at pH 6.5. This was in contrast to TAG-1's acute response to alkaline conditions, where many more genes related to translation were much less expressed, with multiple ribosomal and tRNA-related genes affected. Motility-related genes, however, were greatly more expressed under alkaline conditions, including many genes related to flagellar structure and the flagellar motor.

When allowed to acclimate to its pH extremes, we found that TAG-1 differentially expressed a number of genes that can be related to the chemical differences between vent fluid and seawater. This included many genes related to inorganic ion transport and metabolism, including genes involved in phosphate transport and heavy metal resistance, the genes for which were more highly expressed under low pH conditions compared to the control and less expressed under alkaline conditions. We also observed differences in genes related to energy metabolism, particularly genes related to hydrogen metabolism, which were slightly more highly expressed at pH 5.5, but much less expressed under chronic exposure to pH 7.5.

## Methods

### Cultivation conditions

*Ghiorsea bivora* TAG-1 was cultured in artificial seawater-ZVI plates, according to the National Center for Marine Algae and Microbiota culturing guidelines for cultivating marine

iron-oxidizing bacteria. Petri dishes were filled with 20 ml artificial seawater (ASW, pH ~6.4), with 100 mg –200 mesh zero-valent iron (ZVI) powder (Alfa Aesar Inc.), sterilized via gamma irradiation, added as an Fe(II) source. Plates were incubated in gas-tight jars with valves that allowed the jar headspace to be replaced with a gas mix of 8% $O_2$/10% $CO_2$/82% $N_2$. Jars were incubated at ambient temperature (~24˚C).

**Growth conditions under differing pH regimes for transcriptome analysis**

*Growth conditions for acute pH exposure*

*G. bivora* TAG-1 was inoculated to a concentration of $5 \bullet 10^5$ cells$\bullet$ml$^{-1}$ in 12 ASW-ZVI plates as described above. Plates were incubated in a gas mix of 8% $O_2$/10% $CO_2$/82% $N_2$ at 20˚C. When cells had grown to late log phase, determined to be after 4 days by direct cell count after Emerson and Moyer 2002, plates were removed and amended with buffers to bring them to the pH levels of interest (16). This was done by adding 1 ml 1M stock of MES (pH 5.5, Amresco Inc.), PIPES (pH 6.5, Sigma-Aldrich), HEPES (pH 7.5, EMD Millipore), or Tris-HCl (pH 8.0, Corning Inc.) to bring the final buffer concentration in each plate to 50 mM. A total of 3 plates were amended for each pH. Plates were then incubated again at 20˚C with the original gas mix headspace for 30 min prior to RNA extraction.

*Growth conditions for chronic pH exposure*

*G. bivora* TAG-1 was again inoculated to a concentration of $5 \bullet 10^5$ cells$\bullet$ml$^{-1}$ in 9 ASW-ZVI plates as described above with the exception that these plates contained 19 ml ASW and 1 ml 1M buffer stock of MES (pH 5.5), PIPES (pH 6.5), or HEPES (pH 7.5), yielding a final concentration of 50 mM buffer, with 3 plates amended to each pH. Cells used for inoculating chronic exposure plates were cultivated at their respective pH using the appropriate buffer

previous to inoculation to reduce any lag in growth due to acclimation. Plates were also prepared at pH 8.0 buffered with Tris-HCl, but TAG-1 was unable to grow at pH 8.0.

In addition, 3 "dummy" plates were made for pH 7.5, again with 50 mM HEPES. This was done because the pH of the plates to be extracted did not remain at 7.5 over time, with pH slowly decreasing, presumably due to iron oxidation. To account for this, a dummy plate was removed from the jar each day and its pH measured. Then the volume of 1 M sterile filtered NaOH required to bring the pH back to 7.5 was determined. An equal volume of sterile 1 M NaOH was added to all pH 7.5 plates, which were then gently mixed and returned to the jar for further incubation. All plates were harvested for RNA extraction when cells were in late log phase at 4 days based on previous cell growth rate measurements.

**RNA extraction, concentration, and sequencing**

Each late log phase plate was mixed by pipetting, then its contents were transferred to a 50 ml tube (VWR). Tubes were then centrifuged at 2500xG in a Sorvall Legend RT centrifuge (Thermo Fisher Inc.) for 10 min. The liquid supernatant was discarded and the pellet was resuspended in 2.5 ml PowerBead Solution from the RNeasy PowerSoil Total RNA Kit (QIAGEN). This was then transferred to a PowerBead Tube and the RNeasy PowerSoil protocol was followed to manufacturer specification, with the exception of step 17, where RNA was allowed to precipitate at -20˚C for 45 minutes instead of 10 minutes, as this was found to increase RNA yields.

Purified RNA was then concentrated using an RNA Clean and Concentrator kite (Zymo Research) and quantified using a Qubit fluorometer (Thermo Fisher Inc.). RNA samples were then diluted to 33 $ng \bullet \mu l^{-1}$ in a 96-well plate and 1 µl SUPERase-IN RNase inhibitor (Thermo

Fisher Inc.) was added to each sample. The 96-well plate was then sealed and sent to the Broad Institute Microbial 'Omics Core for library preparation and sequencing via NovaSeq (Illumina).

**Analysis of NovaSeq sequencing data**

NovaSeq FASTQ files were first quality checked using FastQC (https://www.bioinformatics.babraham.ac.uk/projects/fastqc/). Any overrepresented reads were then removed with a custom Python script provided by the Harvard FAS Informatics and Scientific Applications Group. Remaining adapter sequences were removed using Trim Galore! (http://www.bioinformatics.babraham.ac.uk/projects/trim_galore/) and again quality checked using FastQC.

Quality checked reads were aligned to a reference transcriptome for *G. bivora* TAG-1 and quantified to transcripts per million (TPM) using kallisto (28). Kallisto results were then analyzed for differential expression using the sleuth R package (29). Briefly, acute pH exposures at pH 5.5, 7.5, and 8.0 were compared to acute exposure pH 6.5 as a control. This allowed us to obtain beta values (biased estimates for fold change) for each transcript and determine which were significantly differentially expressed. The same process was then done for chronic pH exposures (i.e., chronic pH 5.5 and 7.5 reads were compared to chronic pH 6.5 as a control). COG (Collections of Orthologous Groups) functional group identifiers were then assigned to each transcript using eggNOG-mapper (30, 31).

## Results

### Gene expression changes after acute exposure to pH 5.5

After TAG-1 was exposed to pH 5.5 for 30 minutes, 146 genes were significantly differentially expressed, the lowest number of any treatment (n = 3). Of these, 77 were more highly expressed when compared to cells grown at pH 6.5 and then exposed to added buffer at pH 6.5 (the control, which represents TAG-1's growth under optimum pH conditions). Moreover, 69 genes were lower in expression when compared to cells grown at pH 6.5 (Figure 2.1).

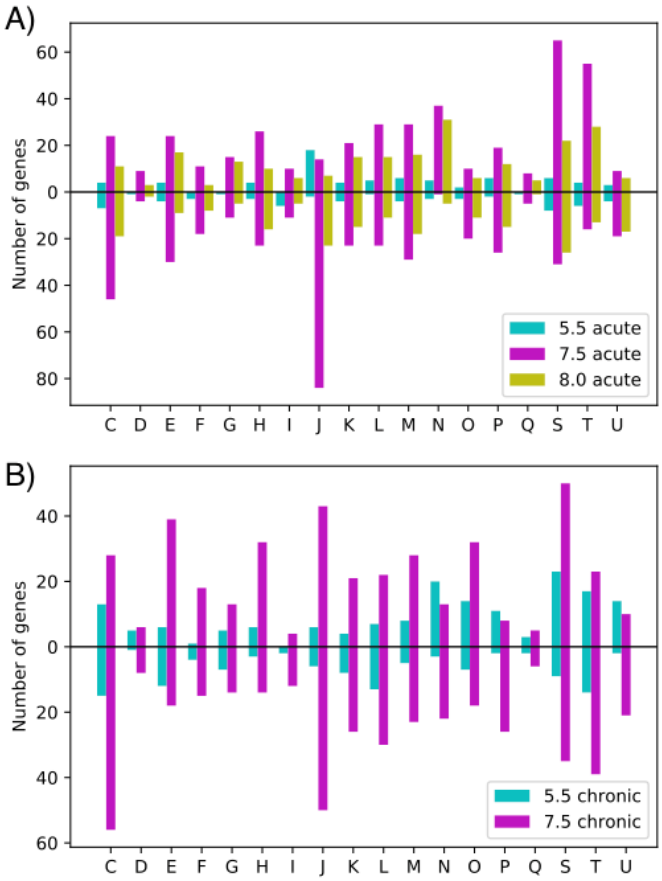


**Figure 2.9) Number of genes differentially expressed in each COG functional category.** Bars above zero indicate how many genes were greater in abundance than pH 6.5 controls while bars below zero indicate how many genes were lesser in abundance for A) acute pH treatments and B) chronic pH treatments. COG functional category designations are as follows: C) Energy production and conversion, D) Cell cycle control and mitosis, E)Amino Acid metabolism and transport, F)Nucleotide metabolism and transport, G) Carbohydrate metabolism and transport, H) Coenzyme metabolism, I) Lipid metabolism, J) Translation, K) Transcription, L) Replication and repair, M) Cell wall/membrane/envelop biogenesis, N) Cell motility, O)Post-translational modification, protein turnover, chaperone functions, P) Inorganic ion transport and metabolism, Q) Secondary Structure, S)Function Unknown, T) Signal Transduction, U) Intracellular trafficking and secretion.

In terms of COG functional groups, the strongest response was in translation, where 18 genes were more highly expressed while only 2 were expressed at a lower level compared to pH 6.5. Genes that were more highly expressed in this category are mainly related to ribosomal structure, for example 50S ribosomal proteins L23, L5, and L2 (Table 2.1) and 30S ribosomal proteins S17, S3, and S8.

**Table 2.1 Selected genes that were found to be differentially expressed under acute exposure to pH 5.5 compared to pH 6.5 controls**

| Gene Description | Accession | $\beta$ Value[†] |
|---|---|---|
| *Translation* | | |
| 50S ribosomal protein L23 | WP_038248598.1 | 0.38 |
| 50S ribosomal protein L5 | WP_038248618.1 | 0.34 |
| 50S ribosomal protein L2 | WP_038248600.1 | 0.32 |
| 30S ribosomal protein S17 | WP_038248609.1 | 0.33 |
| 30S ribosomal protein S3 | WP_038248603.1 | 0.31 |
| 30S ribosomal protein S8 | WP_038248623.1 | 0.29 |
| *Inorganic ion transport and metabolism* | | |
| Phosphate transport system regulatory protein PhoU | WP_038248274.1 | 0.29 |
| Phosphate ABC transporter ATP-binding protein | WP_038248272.1 | 0.26 |
| *Energy production and conversion* | | |
| Cytochrome b | WP_038250724.1 | 0.76 |
| Cytochrome c | WP_038247745.1 | -0.50 |

[†] $\beta$ values are a biased estimate of $\log_2$ fold change.

Inorganic ion transport and metabolism also had a relatively strong response, with 6 genes more highly expressed and 2 lower in expression compared to cells grown at pH 6.5. Interestingly, 2 of the 6 more highly expressed genes were related to phosphate acquisition. These were the phosphate transport system regulatory protein PhoU and phosphate ABC transporter ATP-binding protein (32, 33).

It should also be noted that 2 of the top 10 differentially expressed genes were cytochromes. A *b*-type cytochrome was more highly expressed while a *c*-type cytochrome was lower in expression. Overall, however, there was not a strong signal for energy production and conversion, with 4 genes in this functional group being lower in expression compared to pH 6.5 and 7 higher in expression.

**Gene expression changes after acute exposure to pH 7.5**

After acute exposure to pH 7.5, 930 genes were differentially expressed when compared to the pH 6.5 control, the most of any treatment. Overall, 468 genes were more highly expressed in the when compared to pH 6.5, whereas 462 genes were lower in expression (n= 3; Figure 2.1).

Among COG functional groups with known functions, signal transduction had the most genes that were higher in expression at 55, as well as 16 genes that were lower in expression. Here many of the more highly expressed genes are related to the signaling molecule cyclic-di-GMP (34, 35). This includes a diguanylate cyclase response regulator and multiple GGDEF-domain containing proteins which act to synthesize cyclic-di-GMP (Table 2.2) (36, 37). Under these conditions, however, some of the genes that experienced the most decrease in expression belong to this functional group such as RNA polymerase-binding protein DksA.

**Table 2.2 Selected genes that were found to be differentially expressed under acute exposure to pH 7.5 compared to pH 6.5 controls**

| Gene Description | Accession/ Locus Tag[††] | $\beta$ Value |
|---|---|---|
| *Signal transduction* | | |
| Diguanylate cyclase response regulator | WP_051938008.1 | 0.54 |
| GGDEF domain-containing protein | WP_051938033.1 | 0.49 |
| GGDEF domain-containing protein | WP_051938303.1 | 0.45 |
| RNA polymerase-binding protein DksA | WP_038250478.1 | -0.78 |
| *Motility* | | |
| Flagellar protein | WP_038246668.1 | 0.69 |
| Flagellar protein | WP_038249280.1 | 0.65 |
| Flagellar hook-length control protein FliK | WP_038249484.1 | 0.59 |
| Flagellar hook-associated protein | WP_038249282.1 | 0.58 |
| Flagellar hook-basal body protein | WP_038248753.1 | 0.56 |
| Flagellar motor protein | WP_038247009.1 | 0.23 |
| *Translation* | | |
| 50S ribosomal protein L25 | WP_038250792.1 | -0.99 |
| 50S ribosomal protein L36 | WP_081881118.1 | -0.92 |
| 50S ribosomal protein L13 | WP_038250764.1 | -0.90 |
| 30S ribosomal protein S12 | WP_038246681.1 | -0.90 |
| 30S ribosomal protein S16 | WP_038250342.1 | -0.72 |
| 30S ribosomal protein S10 | WP_038248590.1 | -0.71 |
| 16S rRNA processing protein RimM | WP_038250340.1 | -0.82 |
| Aminoacyl-tRNA hydrolase | WP_038250789.1 | -0.73 |
| Threonine--tRNA ligase | WP_038246478.1 | -0.65 |
| *Other genes of interest* | | |
| Integron integrase | WP_081881045.1 | 0.79 |
| Integrase | DM09_RS01235 | 0.42 |
| Integrase | WP_038246874.1 | 0.18 |

[††]Locus tags are listed for genes that do not have an assigned accession number.

The COG functional group with the next most genes that were higher in expression is motility. Here, 37 genes were more highly expressed, with only 1 lower in expression. This includes many flagellar proteins, flegellar hook associated proteins, and proteins related to the flagellar motor.

Translation, on the other hand, had many genes lower in expression after acute exposure to pH 7.5, with only 14 genes more highly expressed and 84 expressed at lower levels than the pH 6.5 control. In contrast to acute exposure to pH 5.5, here many of the most differentially expressed genes are ribosome related. This includes 50S ribosomal proteins L25, L36, and L13, 30S ribosomal proteins S12, S16, and S10, and 16S rRNA processing protein RimM. Genes related to protein and tRNA synthesis are also included in this category, such as aminoacyl-tRNA hydrolase and threonine-tRNA ligase.

Additionally, an integron integrase is among the most highly expressed genes compared to the pH 6.5 control. A putative integrase and another integrase are also significantly more highly expressed at this pH.

**Gene expression changes after acute exposure to pH 8.0**

A total of 483 genes were significantly differentially expressed when TAG-1 under pH 8.0 acute response conditions, with 246 more highly expressed and 237 expressed less than in the pH 6.5 control (n = 3). Overall, pH 8.0 acute response was very similar to that of pH 7.5 acute, though fewer genes were affected (Figure 2.1). Here the greatest number of genes that were more highly expressed compared to pH 6.5 was in motility, with 31 genes expressed at greater abundance than the pH 6.5 control and 5 expressed at lower levels. As in pH 7.5 acute response,

many of the same flagellar and flagellar hook proteins were more highly expressed, though flagellar motor proteins were not. In fact the most highly expressed motility gene was flagellar basal-body rod protein FlgG (Table 2.3).

**Table 2.3 Selected genes that were found to be differentially expressed under acute exposure to pH 8.0 compared to pH 6.5 controls**

| Gene Description | Accession | $\beta$ Value |
|---|---|---|
| *Motility* | | |
| Flagellar basal-body rod protein FlgG | WP_038248751.1 | 0.74 |
| Flagellar protein | WP_038246668.1 | 0.46 |
| Flagellar protein | WP_038249280.1 | 0.59 |
| Flagellar hook-length control protein FliK | WP_038249484.1 | 0.39 |
| Flagellar hook-associated protein | WP_038249282.1 | 0.39 |
| Flagellar hook-basal body protein | WP_038248753.1 | 0.59 |
| Flagellar motor protein | WP_038247009.1 | 0.46 |
| *Signal transduction* | | |
| Diguanylate cyclase response regulator | WP_051938008.1 | 0.71 |
| HDOD domain-containing protein | WP_051938358.1 | 0.83 |
| GGDEF domain-containing protein | WP_051938033.1 | 0.30 |
| RNA polymerase-binding protein DksA | WP_038250478.1 | -1.18 |
| *Translation* | | |
| Ribonuclease P protein component | WP_051937888.1 | -1.07 |
| 50S ribosomal protein L25 | WP_038250792.1 | -0.62 |
| 30S ribosomal protein S12 | WP_038246681.1 | -0.67 |
| Aminoacyl-tRNA hydrolase | WP_038250789.1 | -0.45 |
| Threonine--tRNA ligase | WP_038246478.1 | -0.40 |
| *Other genes of interest* | | |
| Integrase | WP_038246874.1 | 1.95 |
| Integron integrase | WP_081881045.1 | 0.80 |

The next highest number of genes expressed at greater abundance than the control were in signal transduction (28 more highly expressed and 13 lower in expression). The same diguanylate cyclase response regulator that was higher in expression at pH 7.5 was also higher in expression at pH 8.0, as well as one GGDEF-domain containing protein and RNA polymerase-

binding protein DksA. An HDOD-domain containing protein was also more highly expressed. Proteins with this domain have been shown to be involved with c-di-GMP signaling as well as control of flagellar synthesis (38).

As in pH 7.5 acute, translation was generally lower in expression, with 7 genes more highly expressed and 23 expressed at lower levels than the pH 6.5 control. Again this included ribosomal proteins as well as tRNA-related proteins. Here the gene that was lowest in abundance compared to the control was a ribonuclease P protein component (WP_051937888.1).

Notably, the second most differentially expressed gene at pH 8.0 was an integrase (WP_038246874.1), which was very highly expressed at $\beta = 1.95$. This integrase was also higher in expression at pH 7.5, though not nearly as much ($\beta = 0.18$). The same integrase that was higher in expression at pH 7.5 (WP_081881045.1) than the control was also higher in expression to approximately the same degree at pH 8.0 with $\beta = 0.80$.

**Gene expression changes after chronic exposure to pH 5.5**

When grown at a constant pH of 5.5, TAG-1 differentially expressed 309 genes, with 194 more highly expressed compared to cultures grown at pH 6.5 and 115 expressed at a lower level ($n = 3$; Figure 2.1). Interestingly, the COG functional group with the highest number of genes that were expressed at a higher level than at pH 6.5 that are of a known function was motility. Here 20 genes were more highly expressed while only 3 were lower in abundance. This is in contrast to the pH 5.5 acute response where fewer motility related genes were as highly expressed. In fact the most highly expressed gene at this treatment was a flagellar protein (Table 2.4), though this is listed in the transcriptome as a pseudogene. Other more highly expressed motility related genes are also flagellar proteins. Genes related to twitching motility are also

higher in abundance at this pH than at pH 6.5, with type IV pili twitching motility protein PilT and twitching motility protein PilT among the most highly expressed genes. (Table 2.4)

**Table 2.4 Selected genes that were found to be differentially expressed under chronic exposure to pH 5.5 compared to pH 6.5 controls**

| Gene Description | Accession/ Locus Tag | $\beta$ Value |
|---|---|---|
| *Motility* | | |
| Flagellar protein | DM09_RS09225 | 5.08 |
| Flagellar hook protein FlgE | WP_038249488.1 | 0.64 |
| Flagellar hook-length control protein FliK | WP_038249484.1 | 0.54 |
| Flagellar hook-basal body protein | WP_038248753.1 | 0.40 |
| Type IV pili twitching motility protein PilT | WP_038250446.1 | 0.73 |
| Twitching motility protein PilT | WP_038250445.1 | 0.63 |
| *Inorganic ion transport and metabolism* | | |
| Iron permease | WP_038247652.1 | -0.98 |
| Phosphate-binding protein | WP_038248266.1 | 0.97 |
| Phosphate transport system regulatory protein PhoU | WP_038248274.1 | 0.48 |
| Phosphate ABC transporter, permease protein PstA | WP_038248270.1 | 0.44 |
| Phosphate ABC transporter ATP-binding protein | WP_038248272.1 | 0.33 |
| Copper-translocating P-type ATPase | WP_038247225.1 | 0.57 |
| CusA/CzcA family heavy metal efflux RND transporter | WP_051937923.1 | 0.52 |
| CusA/CzcA family heavy metal efflux RND transporter | WP_038247213.1 | 0.31 |
| *Energy production and conversion* | | |
| FMN-binding domain-containing protein | WP_038249330.1 | -0.96 |
| Alcohol dehydrogenase | WP_038247650.1 | -0.92 |
| Cytochrome c | WP_038249325.1 | 0.80 |
| Cytochrome c | WP_051937832.1 | 0.51 |
| Cytochrome cbb3 | WP_038247221.1 | 0.58 |
| Uptake hydrogenase small subunit | WP_038247362.1 | 0.38 |
| Nickel-dependent hydrogenase large subunit | WP_038246869.1 | 0.29 |

Response of inorganic ion transport genes, on the other hand, was similar to pH 5.5 acute response, with 11 genes more highly expressed and 2 expressed at lower levels than the pH 6.5 control. The 9$^{th}$ most differentially expressed gene was one of these less expressed genes, an iron

permease. Also as in pH 5.5 acute response, many phosphate acquisition genes were more highly expressed. These include a phosphate-binding protein (WP_038248266.1), phosphate transport system regulatory protein PhoU, and two phosphate ABC transporter proteins. Interestingly, other genes in this functional group seem to be related to heavy metal transport. A copper-translocating P-type ATPase and two CusA/CzcA family heavy metal efflux RND transporters were all more highly expressed than at pH 6.5.

There were also changes to energy production and conversion, with 13 genes expressed at greater abundance and 15 expressed at lower levels than the control. In the top 20 differentially expressed genes, both an FMN-binding domain-containing protein and an alcohol dehydrogenase were expressed at much lower levels. Many of the other genes in this category are cytochrome related. Two *c*-type cytochromes as well as a *cbb3*-type cytochrome were all more highly expressed. It should also be noted that hydrogenase related genes were slightly more highly expressed as well, for example an uptake hydrogenase small subunit gene and a nickel-dependent hydrogenase large subunit gene.

**Gene expression changes after chronic exposure to pH 7.5**

When TAG-1 was grown at a constant pH of 7.5, it differentially expressed 870 genes, with 401 expressed more highly and 469 less expressed compared to pH 6.5 controls (n = 2; Figure 2.1). Here genes related to energy production and conversion are mostly lower in abundance, with 56 genes less expressed and 28 more highly expressed compared to when TAG-1 is grown at pH 6.5. In fact, 14 of the top 20 differentially expressed genes belong to this functional group and all are expressed at lower levels than the control. In contrast to pH 5.5 chronic response, the two most differentially expressed genes expressed at lower levels are a

Ni/Fe-hydrogenase, b-type cytochrome subunit and a nickel-dependent hydrogenase large subunit (Table 2.5). An uptake hydrogenase small subunit, as well as the [NiFe]-hydrogenase assembly, chaperone, HybE were also expressed much less than in the pH 6.5 control. Subunits I and II of a *cbb3*-type cytochrome-*c* oxidase were expressed at lower levels as well. Additionally, multiple F0F1 ATP synthase related genes were lower in abundance and in the top 20 most differentially expressed genes. (Table 2.5)

**Table 2.5 Selected genes that were found to be differentially expressed under chronic exposure to pH 7.5 compared to pH 6.5 controls**

| Gene Description | Accession/ Locus Tag | $\beta$ Value |
|---|---|---|
| *Energy production and conversion* | | |
| Ni/Fe-hydrogenase, b-type cytochrome subunit | WP_051937872.1 | -2.58 |
| Nickel-dependent hydrogenase large subunit | WP_038246869.1 | -2.31 |
| Uptake hydrogenase small subunit | WP_038247362.1 | -1.73 |
| [NiFe]-hydrogenase assembly, chaperone, HybE | WP_051937869.1 | -1.70 |
| Cytochrome-c oxidase, cbb3-type subunit I | WP_038249038.1 | -2.19 |
| Cytochrome-c oxidase, cbb3-type subunit II | WP_038249221.1 | -2.13 |
| F0F1 ATP synthase subunit gamma | WP_038248672.1 | -1.97 |
| F0F1 ATP synthase subunit beta | WP_038248675.1 | -1.89 |
| F0F1 ATP synthase subunit epsilon | WP_038248679.1 | -1.81 |
| F0F1 ATP synthase subunit alpha | WP_038248670.1 | -1.75 |
| F0F1 ATP synthase subunit B | WP_038248666.1 | -1.70 |
| *Motility* | | |
| Flagellar protein | WP_038246668.1 | -0.29 |
| Flagellar hook-associated protein | WP_038249282.1 | -0.60 |
| Flagellar motor protein | WP_038247009.1 | 0.49 |
| *Inorganic ion transport and metabolism* | | |
| Iron permease | WP_038247652.1 | 0.98 |
| Phosphate-binding protein | WP_038248266.1 | -1.26 |
| Phosphate transport system regulatory protein PhoU | WP_051938184.1 | -0.57 |
| Copper-translocating P-type ATPase | WP_038247225.1 | -0.54 |
| Copper-translocating P-type ATPase | WP_038249028.1 | -0.24 |
| Copper resistance protein B | WP_038247227.1 | -0.68 |
| CusA/CzcA family heavy metal efflux RND transporter | WP_051937923.1 | 0.44 |
| CusA/CzcA family heavy metal efflux RND transporter | WP_038247213.1 | -0.35 |
| *Other genes of interest* | | |
| Integrase | DM09_RS01235 | 0.59 |
| Integron integrase | WP_081881045.1 | 0.35 |
| Integrase | WP_038246874.1 | -0.81 |

Inorganic ion transport and metabolism related genes were also mostly lower in expression compared to the control, with 8 genes more highly expressed and 26 expressed at lower levels. The same iron permease that was less expressed under chronic pH 5.5 conditions

was expressed at higher levels here. In contrast to pH 5.5 chronic, many phosphate acquisition genes were expressed to a lesser degree as well (e.g., a phosphate-binding protein and phosphate transport system regulatory protein PhoU). Metal resistance genes also show opposite patterns from pH 5.5 chronic response, with lower expression levels of 2 copper-translocating P-type ATPase genes and a copper resistance protein B gene in comparison to the pH 6.5 control. Interestingly, of the two CusA/CzcA family heavy metal efflux RND transporters that were more highly expressed under chronic pH 5.5 conditions, one was still more highly expressed at pH 7.5 but one was lower in expression levels.

In contrast to acute alkaline response, motility expression under chronic pH 7.5 conditions had no clear pattern. Here 13 genes were more highly expressed and 22 were lower in abundance. Many of the genes that were higher in expression when TAG-1 was exposed to pH 7.5 for only a short time were not significantly differently expressed when it was grown at pH 7.5. Furthermore, of those that were significantly differentially expressed, not all of them were higher in expression. Multiple flagellar proteins were instead less expressed, while a flagellar motor protein was still more highly expressed than the control.

As in both acute alkaline responses, multiple integrases were higher in expression under chronic exposure to pH 7.5. The third integrase that was more highly expressed under acute alkaline conditions was less expressed here, however.

## Discussion

The experiments presented herein describe the transcriptional responses of the FeOB *G. bivora* TAG-1 to acute and chronic pH changes it would likely be exposed to in a hydrothermal vent environment. It is important to note that TAG-1 was isolated from diffuse hydrothermal vents along the Mid-Atlantic ridge (17). Such diffuse vents are an admixture of vent effluent and ambient seawater, and are characterized by their spatial and temporal variability, in particular rapid temporal changes in temperature, pH, oxygen, and dissolved metals including iron. Typically, diffuse vents at the Mid-Atlantic ridge exhibit a pH of 6.5, though pH can swing from 5 to greater than 7 over short time scales (minutes to hours) (7, 26, 27, 39). Also, as a vent field ages, its pH typically becomes more alkaline, until there is a cessation of vent flow. We designed these experiments to better understand how TAG-1 responds to changes in environmental pH that result when the proportion of vent and ambient seawater changes: more acidic conditions arise when there is a greater proportion of vent effluent, and more alkaline conditions arise when there is a greater proportion of seawater. Here, we present global transcriptional changes in TAG-1 cultures as they contend with short-lived exposure to changes in pH (i.e. the "acute" treatments), as well as how it might acclimate to prolonged exposure to said changes in pH (i.e. the "chronic" treatments).

### Response to acute changes in environmental pH

*G. bivora* TAG-1's response to short term exposure to acidic pH was the least pronounced of any treatment, with fewer genes differentially expressed compared to other experiments. It is plausible that this modest response in gene expression change (relative to the control pH of 6.5, which has been experimentally verified to be TAG-1's pH growth optimum)

(17, 20) implies that TAG-1 is well poised to contend with short-lived decreases in pH, requiring only small adjustments in protein synthesis. Here we present evidence that supports the hypothesis that TAG-1 is physiologically poised to cope with short-term decreases in environmental pH, while short term increases in environmental pH require a greater physiological response.

First, acute exposure to pH 5.5 was the only treatment where more genes related to translation were more highly expressed than were lower in expression compared to pH 6.5 controls. The fact that ribosomal protein genes were expressed at higher levels in this treatment implies an increase in the potential for TAG-1 to produce new proteins. We infer that this indicates that TAG-1 is poised to cope with more acidic pH levels by constitutively expressing genes involved in pH response even when growing at pH 6.5 and regulating this response primarily at the translational level.

This is in contrast to TAG-1's response to acute exposure to pH 7.5 and pH 8.0, where 6.4-fold and 3.3-fold more genes were differentially expressed compared to pH 5.5 acute exposure, respectively. Indeed, genes related to translation were found at much lower abundance in both acute alkaline pH treatments. This may be a strategy to conserve energy in response to lower availability of reduced electron donors present in an environment with a greater proportion of seawater (40). Protein synthesis is energetically expensive and cells often respond to stress by reducing expression of translation related genes, shunting the energy saved to other systems, as has been demonstrated previously in *Shewanella oneidensis* (22).

Interestingly, while all acute responses included changes in the expression of genes related to translation, there was no clear expression pattern in genes related to transcription. In all three treatments there were approximately as many genes that increased in expression level as

decreased, despite the close link between transcription and translation. While we assume this to be a real result, we do not know why this would occur and cannot rule out the possibility that differences in mRNA decay rates are responsible for this discrepancy. It has been shown that different mRNAs decay at different rates depending on a number of factors (41–43). It may be that these differences in decay rate are responsible for there appearing to be no pattern in genes related to transcription while, for example, there are a large number of translation related transcripts that were lower in abundance under alkaline conditions compared to the control.

Acute exposure to pH 5.5 also resulted in the least differential expression of motility-related genes of any treatment, with only 5 genes more highly expressed than the control and 3 less expressed. This suggests that motility is not an important response to short-term exposure to low pH. TAG-1 is therefore unlikely to be trying to "escape" environments that experience a sudden drop in pH and return to more optimal conditions. This again supports our hypothesis that TAG-1 contends well with acute exposure to acidic conditions.

Many motility-related genes were more highly expressed at both pH 7.5 and 8.0, on the other hand, indicating that motility is an important factor in contending with increases in environmental pH. This would require both the production of flagella and the powering of the flagellar motor, and genes involved in both of these processes are found in much higher abundance than the control in both acute pH 7.5 and pH 8.0 treatments. This suggests that TAG-1 does attempt to return to more acidic surroundings when it encounters a more alkaline environment.

Expression of genes related to signal transduction also supports our hypothesis of TAG-1 being better poised to respond to acidic pH than alkaline. Few of these genes are differentially expressed under acute exposure to pH 5.5 (4 of higher abundance and 6 of lower abundance). At

alkaline pH, though, many more are expressed at a higher level compared to the pH 6.5 control than are less expressed. This includes many genes related to cyclic di-GMP synthesis and response. Cyclic di-GMP is an important signaling molecule in many diverse bacteria and has been shown to increase in concentration in response to various stressors (34, 35). Interestingly, RNA polymerase-binding protein DksA, a transcription factor that is partially responsible for initiating the stress response in *E. coli*, is found at much lower abundance at alkaline pH. Canonically, this transcription factor is responsible for inhibiting expression of rRNA (44). Given that RNA related proteins are far less expressed at higher pH, it seems likely that TAG-1 would reduce expression of rRNA as well, and so may be doing so through a different stress response than that found in *E. coli*.

Integrases, too, are more highly expressed at both pH 7.5 and 8.0. Integrases catalyze gene cassette insertion through recombination, and similar integrase expression patterns have been observed in a number of bacteria during the SOS response (45, 46). Though this has usually been reported on as a response to antimicrobial agents, it is possible that TAG-1 initiates integrase expression to recombine with genetic material present in seawater in efforts to survive at higher pH. This further supports the hypothesis that TAG-1 much prefers more vent-influenced environments than seawater-influenced, as incorporating random pieces of genetic material is likely to produce detrimental effects but TAG-1 is still attempting to do so when exposed to pH levels similar to seawater.

Inorganic ion transport and metabolism at pH 5.5, on the other hand, reflects a response to an environment more influenced by hydrothermal venting. Multiple phosphate-acquisition genes in this functional group are expressed more highly than in the pH 6.5 control. The proteins these genes encode for are involved in active transport of phosphate from the environment.

Notably, hydrothermal vent fluid is generally low in phosphate, which has been scavenged by water-rock interactions (47). Expression patterns at low pH are consistent with phosphate scarcity resulting from this scavenging, as TAG-1 would require more and/or higher affinity phosphate transporters to cope with decreased concentrations of phosphate in a more vent fluid influenced environment.

Patterns in genes related to energy metabolism at pH 5.5 are consistent with TAG-1 making only slight adjustments to its physiology as well, with only 4 genes higher in expression than the pH 6.5 control and 7 less expressed. We think these genes are likely involved in metabolizing iron. Notably, two of the genes with the largest $\beta$-values at pH 5.5 are cytochromes, though one is more highly expressed (a *b*-type cytochrome) and the other less expressed (a *c*-type cytochrome). We hypothesize this to be TAG-1 responding to the potential of the $Fe^{2+}/Fe^{3+}$ couple as the midpoint potential of this reaction changes with pH (19, 48). Additionally, the midpoint potentials of bacterial cytochromes are known to change with pH (49). Because the energetic yield of iron oxidation decreases with decreasing pH and it is already a rather low energy metabolism (12), TAG-1 likely must change between cytochromes to maintain energy reserves at acidic pH.

Meanwhile far more energy metabolism related genes are lower in abundance at both pH 7.5 and 8.0 indicating more substantive changes in attempts to deal with alkaline pH. At high pH, TAG-1 likely relies on energy stores to provide it the energy it needs to power motility to return to a more optimum pH since, as previously mentioned, a greater seawater influence has a compounding effect on available electron donors for TAG-1, decreasing both the concentration of $Fe^{2+}$ and $H_2$ as well as the stability of $Fe^{2+}$ due to increased pH. Other *Zetaproteobacteria* are

known to produce polyphosphate granules for energy storage (50), so this seems a likely candidate for energy storage and could be looked for more closely in TAG-1 in future studies.

**Acclimation to pH outside of TAG-1's optimum**

Transcriptomic response of TAG-1 acclimated to pH conditions at the limits of its range for growth corresponds well with the chemical conditions of the endmember fluids that those pH extremes represent. This is perhaps most apparent in gene expression related to energy metabolism as at pH 5.5, TAG-1 increases the expression of cytochrome- and hydrogenase-related genes. This is likely a response to higher concentrations of reduced electron donors (i.e., $Fe^{2+}$ and $H_2$) that would result from a more vent fluid influenced environment. Vent fluid is often rich in both iron and hydrogen (1, 2), so we hypothesize that TAG-1 tries to take advantage of that by increasing its ability to metabolize both. It is unclear what exactly the function of the FMN-domain containing transcript that was so much less abundant is, but the alcohol dehydrogenase likely aids in fermenting stored carbohydrates when energy sources are scarce (51). Therefore it makes sense that it would be expressed to a lesser degree when TAG-1 has an ample supply of electron donors from vent fluid, as well as $CO_2$, and thus would not need to regenerate more $NAD(P)^+$.

Energy metabolism expression at pH 7.5, however, represents increased exposure to seawater, which is poor in both dissolved $Fe^{2+}$ and hydrogen (1). TAG-1 responds to this by reducing expression of a large number of genes related to energy conservation. The same hydrogenase subunit genes that were found at higher abundance at pH 5.5 are among the most differentially expressed at pH 7.5 and all were less expressed than the pH 6.5 control. Additional hydrogenase genes, as well as cytochrome *c*-oxidase and ATPase genes are much less expressed

as well. Though these genes are still expressed at some level, it seems that TAG-1 would conserve energy at a lower rate at high pH, consistent with there being very low concentrations of electron donors in seawater.

Acclimation to pH as a response to vent fluid or seawater is also apparent in inorganic ion transport and metabolism. Vent fluid is rich in dissolved metals, including iron and copper, and while $Fe^{2+}$ serves as an electron donor for TAG-1, it still requires iron as a cofactor in many enzymes (e.g., NiFe-hydrogenase and Fe-S clusters) (1, 2, 17). As a consequence, when grown at pH 5.5 we hypothesize that TAG-1 decreases expression of an iron permease as high availability of iron makes iron uptake easier. Copper and other heavy metals, however, are toxic to bacteria, and thus TAG-1 increased expression of genes related to heavy metal efflux, in particular those involved in copper efflux make sense (23, 52). Similar to acute exposure to low pH, phosphate acquisition genes are also more highly expressed at chronic pH 5.5 conditions. Again, this is likely a response to phosphate scarcity in vent fluid due to water-rock interactions scavenging phosphate (47).

Expression patterns related to inorganic ions are nearly opposite when TAG-1 is grown at pH 7.5. Low dissolved metal content in seawater necessitates increased effort dedicated to iron uptake, hence the same iron permease that was less expressed at pH 5.5 is at higher abundance at pH 7.5 than at pH 6.5 (1). Copper and other heavy metal efflux genes are also consequently found at lower expression levels at high pH, though one heavy metal efflux pump is still more highly expressed than the control, but not to the same degree as at pH 5.5 ($\beta = 0.44$ vs $\beta = 0.52$). Genes related to phosphate uptake are less abundant at pH 7.5 as well, though phosphate is still only present at low concentrations in seawater (53, 54). This may be a response to TAG-1

anticipating low amounts of electron donors and thus a low growth rate and demand for phosphate.

A number of genes related to motility are found at higher abundance than the control when TAG-1 has acclimated to pH 5.5, including a flagellar protein that was the most differentially expressed gene out of any treatment in this study. We hypothesize this to be a response to plentiful $Fe^{2+}$ and $H_2$ providing ample energy, which would allow TAG-1 to search for more optimal conditions via chemotaxis. That is to say, TAG-1 would still be under added stress (e.g., from heavy metals) in an environment with greater hydrothermal vent fluid influence than is ideal. It may therefore use the extra energy afforded by ample amounts of electron donors to try to return to a more suitable mix of vent fluid and seawater. Twitching motility also seems to be important at low pH, given the higher expression levels of a number of PilT genes, which are involved in twitching motility over surfaces as well as biofilm formation in *Pseudomonas aeruginosa* (55–58). TAG-1 may therefore increase biofilm formation at low pH. One explanation for this behavior may be increased flow rates closer to sites of hydrothermal venting necessitate better attachment to remain in contact with electron donor rich vent fluid.

Motility related gene expression patterns are less clear under chronic high pH conditions. In contrast to acute exposure to high pH, some flagellar genes are more highly expressed than the pH 6.5 control when TAG-1 is grown at pH 7.5 while others are expressed at lower levels. This may be due to trade offs between saving energy and attempting to move to a more suitable environment. In seawater, TAG-1 would not have access to much of the electron donors it requires and thus would not be able to conserve as much energy. It would, however, likely still be beneficial to the cell to get closer to vent fluid, bringing it back to a more suitable pH and

making nutrients more available. So some genes may be more highly expressed and some less expressed in a balancing act to deal with these two opposing issues.

Interestingly, two of the three integrases that are more highly expressed under acute alkaline conditions are also found at higher abundance than the control under chronic alkaline growth. The third, however, is less abundant. This indicates that TAG-1 cells are still under stress despite being acclimated to a high pH environment.

**Conclusion**

It has long been questioned how bacteria are able to persist in their environment and contend with changes in their extracellular chemistry. This study provides some of the first experimental glimpses into how an iron-oxidizing bacterial strain - *Ghiorsea bivora* TAG-1- responds to environmentally relevant changes in pH. Many of the observed changes in gene expression, such as increases in signal transduction and integrase expression, are commonly observed among a diversity of bacteria that are subject to changes in pH (22, 23). Heavy metal efflux pumps, too, have been observed to increase in expression in other bacteria, though this is especially relevant to TAG-1. In other studies of e.g., soil bacteria, acidic conditions trigger an increase in gene expression related to resistance of metals such as cadmium, zinc, and cobalt, which has been attributed to an increase in metal solubility at low pH (23). A decrease in pH for TAG-1, however, would be due to increased vent fluid influence and would coincide with a dramatic increase in metal concentrations (1, 2, 39). This would explain why metal resistance genes that increase in expression in TAG-1 at more acidic conditions seem to mostly be related to copper resistance.

In addition to these differences in expression that one might expect to occur in response to changes in pH, TAG-1 also displays some that were unexpected. In particular, increased expression of motility-related genes under acute exposure to alkaline pH is contrary to the response of other *Proteobacteria*, which have been observed to increase motility in response to more acidic pH and become less motile under more acidic conditions (24). TAG-1's expression patterns, however, are consistent with the hypothesis that alkaline pH poses physiological problems for FeOB. This is further evident from TAG-1's response to acute exposure to pH 8.0, where, likely due to physiological dysfunction, we saw similar responses in all COG functional categories to acute exposure to pH 7.5, but lower in magnitude in nearly all cases. In nature these challenges to TAG-1's survival include lower availability of electron donors and increased oxidative stress from higher oxygen concentrations, in addition to the more canonical issues that many other microbes would experience from changes in pH. In fact, it seems that these stressors may be too great for TAG-1 to overcome, as it is unable to grow at seawater pH (17, 20).

## References


1. **Von Damm KL**, **Edmond JM**, **Grant B**, **Measures CI**. 1985. Chemistry of submarine hydrothermal solutions at 21°N, East Pacific Rise. Geochim Cosmochim Acta **49**:2197–2220.

2. **German CR**, **Von Damm KL**. 2003. Hydrothermal Processes. Treatise on Geochemistry **6**–**9**:181–222.

3. **Tivey MK**, **Delaney JR**. 1986. Growth of large sulfide structures on the endeavour segment of the Juan de Fuca ridge. Earth Planet Sci Lett **77**:303–317.

4. **Johnson KS**, **Beehler CL**, **Sakamoto-Arnold CM**, **Childress JJ**. 1986. In situ measurements of chemical distributions in a deep-sea hydrothermal vent field. Science (80- ) **231**:1139–1141.

5. **Jannasch HW**, **Mottl MJ**. 1985. Geomicrobiology of Deep-Sea Hydrothermal Vents. Science (80- ) **229**:717–725.

6. **Johnson KS**, **Childress JJ**, **Beehler CL**. 1988. Short-term temperature variability in the Rose Garden hydrothermal vent field: an unstable deep-sea environment. Deep Sea Res **35**:1711–1721.

7. **Schultz A**, **Dickson P**, **Elderfield H**. 1996. Temporal variations in diffuse hydrothermal flow at TAG. Geophys Res Lett **23**:3471–3474.

8. **Emerson D**, **Revsbech NP**. 1994. Investigation of an iron-oxidizing microbial mat community located near Aarhus, Denmark: Field studies. Appl Environ Microbiol **60**:4022–4031.

9. **Emerson D**, **Moyer C**. 1997. Isolation and characterization of novel iron-oxidizing bacteria that grow at circumneutral pH. Appl Environ Microbiol **63**:4784–4792.

10. **Sobolev D**, **Roden EE**. 2001. Suboxic Deposition of Ferric Iron by Bacteria in Opposing Gradients of Fe(II) and Oxygen at Circumneutral pH. Appl Environ Microbiol **67**:1328–1334.

11. **Sobolev D**, **Roden EE**. 2002. Evidence for rapid microscale bacterial redox cycling of iron in circumneutral environments. Antonie van Leeuwenhoek, Int J Gen Mol Microbiol **81**:587–597.

12. **Emerson D**, **Fleming EJ**, **McBeth JM**. 2010. Iron-oxidizing bacteria: an environmental and genomic perspective. Annu Rev Microbiol **64**:561–583.

13. **Emerson D**, **Floyd MM**. 2005. Enrichment and isolation of iron-oxidizing bacteria at neutral pH. Methods Enzymol **397**:112–123.

14. **Makita H**, **Tanaka E**, **Mitsunobu S**, **Miyazaki M**, **Nunoura T**, **Uematsu K**, **Takaki Y**,

**Nishi S**, **Shimamura S**, **Takai K**. 2017. Mariprofundus micogutta sp. nov., a novel iron-oxidizing zetaproteobacterium isolated from a deep-sea hydrothermal field at the Bayonnaise knoll of the Izu-Ogasawara arc, and a description of Mariprofundales ord. nov. and Zetaproteobacteria classis nov. Arch Microbiol **199**:335–346.

15. **Toner BM**, **Santelli CM**, **Marcus M a.**, **Wirth R**, **Chan CS**, **McCollom T**, **Bach W**, **Edwards KJ**. 2009. Biogenic iron oxyhydroxide formation at mid-ocean ridge hydrothermal vents: Juan de Fuca Ridge. Geochim Cosmochim Acta **73**:388–403.

16. **Emerson D**, **Moyer CL**. 2002. Neutrophilic Fe-oxidizing bacteria are abundant at the Loihi Seamount hydrothermal vents and play a major role in Fe oxide deposition. Appl Environ Microbiol **68**:3085–3093.

17. **Mori JF**, **Scott JJ**, **Hager KW**, **Moyer CL**, **Küsel K**, **Emerson D**. 2017. Physiological and ecological implications of an iron- or hydrogen-oxidizing member of the Zetaproteobacteria, Ghiorsea bivora, gen. nov., sp. Nov. ISME J **11**:2624–2636.

18. **Emerson D**, **Rentz JA**, **Lilburn TG**, **Davis RE**, **Aldrich H**, **Chan C**, **Moyer CL**. 2007. A novel lineage of proteobacteria involved in formation of marine Fe-oxidizing microbial mat communities. PLoS One **2**.

19. **Bonnefoy V**, **Holmes DS**. 2012. Genomic insights into microbial iron oxidation and iron uptake strategies in extremely acidic environments. Environ Microbiol **14**:1597–1611.

20. **McAllister SM**, **Moore RM**, **Gartman A**, **Luther GW**, **Emerson D**, **Chan CS**. 2019. The Fe(II)-oxidizing Zetaproteobacteria: historical, ecological and genomic perspectives. FEMS Microbiol Ecol **95**:1–18.

21. **McAllister SM**, **Davis RE**, **McBeth JM**, **Tebo BM**, **Emerson D**, **Moyer CL**. 2011. Biodiversity and emerging biogeography of the neutrophilic iron-oxidizing Zetaproteobacteria. Appl Environ Microbiol **77**:5445–5457.

22. **Leaphart AB**, **Thompson DK**, **Huang K**, **Alm E**, **Wan XF**, **Arkin A**, **Brown SD**, **Wu L**, **Yan T**, **Liu X**, **Wickham GS**, **Zhou J**. 2006. Transcriptome profiling of Shewanella oneidensis gene expression following exposure to acidic and alkaline pH. J Bacteriol **188**:1633–1642.

23. **Wilks JC**, **Kitko RD**, **Cleeton SH**, **Lee GE**, **Ugwu CS**, **Jones BD**, **Bondurant SS**, **Slonczewski JL**. 2009. Acid and base stress and transcriptomic responses in Bacillus subtilis. Appl Environ Microbiol **75**:981–990.

24. **Maurer LM**, **Yohannes E**, **Bondurant SS**, **Radmacher M**, **Slonczewski JL**. 2005. pH regulates genes for flagellar motility, catabolism, and oxidative stress in Escherichia coli K-12. J Bacteriol **187**:304–319.

25. **Hegler F**, **Schmidt C**, **Schwarz H**, **Kappler A**. 2010. Does a low-pH microenvironment around phototrophic FeII-oxidizing bacteria prevent cell encrustation by FeIII minerals? FEMS Microbiol Ecol **74**:592–600.

26. **Perner M**, **Bach W**, **Hentscher M**, **Koschinsky A**, **Garbe-Schönberg D**, **Streit WR**, **Strauss H**. 2009. Short-term microbial and physico-chemical variability in low-temperature hydrothermal fluids near 5°S on the Mid-Atlantic Ridge. Environ Microbiol **11**:2526–2541.

27. **Sarradin PM**, **Caprais JC**, **Riso R**, **Kerouel R**, **Aminot A**. 1999. Chemical environment of the hydrothermal mussel communities in the Lucky Strike and Menez Gwen vent fields, Mid Atlantic Ridge. Cah Biol Mar **40**:93–104.

28. **Bray NL**, **Pimentel H**, **Melsted P**, **Pachter L**. 2016. Near-optimal probabilistic RNA-seq quantification. Nat Biotechnol **34**:525–527.

29. **Pimentel H**, **Bray NL**, **Puente S**, **Melsted P**, **Pachter L**. 2017. Differential analysis of RNA-seq incorporating quantification uncertainty. Nat Methods **14**:687–690.

30. **Huerta-Cepas J**, **Forslund K**, **Coelho LP**, **Szklarczyk D**, **Jensen LJ**, **Von Mering C**, **Bork P**. 2017. Fast genome-wide functional annotation through orthology assignment by eggNOG-mapper. Mol Biol Evol **34**:2115–2122.

31. **Huerta-Cepas J**, **Szklarczyk D**, **Heller D**, **Hernández-Plaza A**, **Forslund SK**, **Cook H**, **Mende DR**, **Letunic I**, **Rattei T**, **Jensen LJ**, **Von Mering C**, **Bork P**. 2019. EggNOG 5.0: A hierarchical, functionally and phylogenetically annotated orthology resource based on 5090 organisms and 2502 viruses. Nucleic Acids Res **47**:D309–D314.

32. **Muda M**, **Rao NN**, **Torriani A**. 1992. Role of PhoU in phosphate transport and alkaline phosphatase regulation. J Bacteriol **174**:8057–8064.

33. **Hollenstein K**, **Dawson RJP**, **Locher KP**. 2007. Structure and mechanism of ABC transporter proteins. Curr Opin Struct Biol 412–418.

34. **Chua SL**, **Sivakumar K**, **Rybtke M**, **Yuan M**, **Andersen JB**, **Nielsen TE**, **Givskov M**, **Tolker-Nielsen T**, **Cao B**, **Kjelleberg S**, **Yang L**. 2015. C-di-GMP regulates Pseudomonas aeruginosa stress response to tellurite during both planktonic and biofilm modes of growth. Sci Rep **5**:1–13.

35. **Hu Q**, **Zhang J**, **Chen Y**, **Hu L**, **Li W**, **He Z-G**. 2019. Cyclic di-GMP co-activates the two-component transcriptional regulator DevR in Mycobacterium smegmatis in response to oxidative stress . J Biol Chem **294**:12729–12742.

36. **Paul R**, **Weiser S**, **Amiot NC**, **Chan C**, **Schirmer T**, **Giese B**, **Jenal U**. 2004. Cell cycle-dependent dynamic localization of a bacterial response regulator with a novel di-guanylate cyclase output domain. Genes Dev **18**:715–727.

37. **Ryjenkov DA**, **Tarutina M**, **Moskvin O V.**, **Gomelsky M**. 2005. Cyclic diguanylate is a ubiquitous signaling molecule in bacteria: Insights into biochemistry of the GGDEF protein domain. J Bacteriol **187**:1792–1798.

38. **Liu YF**, **Liao CT**, **Song WL**, **Hsu PC**, **Du SC**, **Lo HH**, **Hsiao YM**. 2013. GsmR, a

response regulator with an HD-related output domain in Xanthomonas campestris, is positively controlled by Clp and is involved in the expression of genes responsible for flagellum synthesis. FEBS J **280**:199–213.

39. **Tivey M**. 2007. Generation of Seafloor Hydrothermal Vent Fluids and Associated Mineral Deposits. Oceanography **20**:50–65.

40. **Picard F**, **Loubière P**, **Girbal L**, **Cocaign-Bousquet M**. 2013. The significance of translation regulation in the stress response. BMC Genomics **14**.

41. **Geisberg J V.**, **Moqtaderi Z**, **Fan X**, **Ozsolak F**, **Struhl K**. 2014. Global analysis of mRNA isoform half-lives reveals stabilizing and destabilizing elements in yeast. Cell **156**:812–824.

42. **Andersson AF**, **Lundgren M**, **Eriksson S**, **Rosenlund M**, **Bernander R**, **Nilsson P**. 2006. Global analysis of mRNA stability in the archaeon Sulfolobus. Genome Biol **7**.

43. **Lugowski A**, **Nicholson B**, **Rissland OS**. 2018. Determining mRNA half-lives on a transcriptome-wide scale. Methods **137**:90–98.

44. **Girard ME**, **Gopalkrishnan S**, **Grace ED**, **Halliday JA**, **Gourse RL**, **Herman C**. 2018. DksA and ppGpp regulate the σ S stress response by activating promoters for the small RNA DsrA and the anti-adapter protein IraP. J Bacteriol **200**:1–12.

45. **Guerin É**, **Cambray G**, **Sanchez-Alberola N**, **Campoy S**, **Erill I**, **Re S Da**, **Gonzalez-Zorn B**, **Barbé J**, **Ploy MC**, **Mazel D**. 2009. The SOS response controls integron recombination. Science (80- ) **324**:1034.

46. **Strugeon E**, **Tilloy V**, **Ploy M**, **Da Re S**. 2016. The Stringent Response Promotes Antibiotic Resistance Dissemination by Regulating Integron Integrase Expression in Biofilms. MBio **7**:1–9.

47. **Wheat CG**, **Feely RA**, **Mottl MJ**. 1996. Phosphate removal by oceanic hydrothermal processes: An update of the phosphorus budget in the oceans. Geochim Cosmochim Acta **60**:3593–3608.

48. **Bird LJ**, **Bonnefoy V**, **Newman DK**. 2011. Bioenergetic challenges of microbial iron metabolisms. Trends Microbiol **19**:330–340.

49. **Moore GR**, **Pettigrew GW**, **Pitt RC**, **Williams RJP**. 1980. pH dependence of the redox potential of Pseudomonas aeruginosa cytochrome c-551. BBA - Bioenerg **590**:261–271.

50. **Hoshino T**, **Kuratomi T**, **Morono Y**, **Hori T**, **Oiwane H**, **Kiyokawa S**, **Inagaki F**. 2016. Ecophysiology of Zetaproteobacteria associated with shallow hydrothermal iron-oxyhydroxide deposits in Nagahama Bay of Satsuma Iwo-Jima, Japan. Front Microbiol **6**:1–11.

51. **Conway T**, **Sewell GW**, **Osman YA**, **Ingram LO**. 1987. Cloning and sequencing of the

alcohol dehydrogenase II gene from Zymomonas mobilis. J Bacteriol **169**:2591–2597.

52. **Rensing C**, **Fan B**, **Sharma R**, **Mitra B**, **Rosen BP**. 2000. CopA: An Escherichia coli Cu(I)-translocating P-type ATPase. Proc Natl Acad Sci U S A **97**:652–656.

53. **Patey MD**, **Rijkenberg MJA**, **Statham PJ**, **Stinchcombe MC**, **Achterberg EP**, **Mowlem M**. 2008. Determination of nitrate and phosphate in seawater at nanomolar concentrations. TrAC - Trends Anal Chem **27**:169–182.

54. **Wu J**, **Sunda W**, **Boyle EA**, **Karl DM**. 2000. Phosphate depletion in the Western North Atlantic Ocean. Science (80- ) **289**:759–762.

55. **Bradley DE**. 1980. A function of Pseudomonas aeruginosa PAO polar pili: Twitching motility. Can J Microbiol **26**:146–154.

56. **Whitchurch CB**, **Hobbs M**, **Livingston SP**, **Krishnapillai V**, **Mattick JS**. 1991. Characterisation of a Pseudomonas aeruginosa twitching motility gene and evidence for a specialised protein export system widespread in eubacteria. Gene **101**:33–44.

57. **Wolfgang M**, **Lauer P**, **Park HS**, **Brossay L**, **Hébert J**, **Koomey M**. 1998. PilT mutations lead to simultaneous defects in competence for natural transformation and twitching motility in piliated Neisseria gonorrhoeae. Mol Microbiol **29**:321–330.

58. **Chiang P**, **Burrows LL**. 2003. Biofilm formation by hyperpiliated mutants of Pseudomonas aeruginosa. J Bacteriol **185**:2374–2378.

# Chapter 3

A low pH microenvironment surrounds *Mariprofundus ferrooxydans* PV-1 cells: implications for biomineralization

**Abstract**

Diverse microorganisms, from photosynthetic cyanobacteria to deep sea sulfur-oxidizing bacteria, are known to influence mineral dissolution and precipitation by altering the pH around them. With respect to stalk-forming iron oxidizing bacteria (FeOB), this has been postulated as one mechanism that could aid in directing the mineralization of their stalks. However, key questions remain as to whether and how FeOB could localize such pH alterations, and whether it can be correlated to stalk formation. Here we measured the "pH landscapes" surrounding cells of the model marine FeOB *Mariprofundus ferrooxydans* PV-1 using pH sensitive fluorescent dyes and confocal microscopy in a series of experimental treatments aimed at testing the efficacy of site-specific extracellular pH manipulation. We confirmed for the first time that *M. ferrooxydans* PV-1 cells do indeed establish low pH microenvironments around themselves and that these microenvironments are, in part, actively mediated by cellular activity. We then used geochemical modeling to examine the effect these pH microenvironments would have on iron oxidation energetics, dissolved inorganic carbon (DIC) speciation, and $Fe^{3+}$ solubility. We found only modest decreases in energetic yield for iron oxidation of 4.3 ± 1.7%, though significantly more DIC was found to be present as carbon dioxide around the cell, potentially allowing for greater passive diffusion of DIC instead of active transport. We also showed that solubility of $Fe^{3+}$ increases by 32.5 ± 15.8% in the area immediately surrounding the cell, likely aiding the cell in directing iron precipitation towards its stalk, though future work is needed to address how the directionality of stalk formation is maintained by the organism.

## Introduction

Diverse bacteria often modulate extracellular pH, which can have effects on the solubility of various mineral phases (1, 2). For instance, heterotrophic bacteria in dental biofilms consume sugars and other organic carbon sources and produce organic acids, lowering their local pH (3, 4). This increases the solubility of hydroxyapatite, the primary mineral component of tooth enamel, causing demineralization of the area on the tooth where the biofilm has formed, eventually leading to tooth decay and dental caries (5). Autotrophic organisms can also cause shifts in extracellular pH, often making their surroundings more alkaline through the consumption of protons and $CO_2$ during carbon fixation. Cyanobacteria, for example, have been shown to create microenvironments of alkaline pH proximal to their cells (6). When large numbers of cyanobacteria form biofilms, these local alkaline conditions can influence the saturation conditions of calcium carbonate, leading to calcification even when precipitation of calcium minerals would not be predicted based on the pH of the overlying water column (7).

Extracellular pH is of particular importance to microbes that oxidize iron for energy, due to the increasing stability of $Fe^{2+}$ under oxic conditions with decreasing pH, as well as the increased solubility of $Fe^{3+}$ under more acidic conditions (8). At neutral pH, however, $Fe^{3+}$ is not stable in solution and almost entirely precipitates immediately as iron oxyhydroxides (9). This poses a problem for bacteria that oxidize iron at circumneutral pH: they must have strategies for dealing with possible encrustation by iron minerals that, if allowed to precipitate on the cell membrane, could limit diffusion of nutrients to the cell (10). Phototrophic iron oxidizing bacteria (photoferrotrophs) have been shown to avoid mineral encrustation by reducing local pH (11). This increases the solubility of $Fe^{3+}$ around the cell, allowing dissolved Fe(III) to diffuse away to a region of higher pH where it then precipitates, thereby allowing the cell to escape encrustation.

Neutrophilic microaerobic iron oxidizing bacteria (FeOB), chemotrophic organisms that catalyze the oxidation of $Fe^{2+}$ to $Fe^{3+}$ with oxygen as their electron acceptor, must also contend with iron oxide precipitation and possible encrustation. This could be an issue for FeOB perhaps to an even greater extent than photoferrotrophs due to the rapid abiotic oxidation of $Fe^{2+}$ to $Fe^{3+}$ by oxygen and subsequent precipitation (12, 13). FeOB generally live in opposing gradients of dissolved Fe(II) and oxygen, though, where abiotic oxidation rates are slow and FeOB can compete more easily – in some cases biological activity is responsible for up to 99% of iron oxidation (10, 12–15). It is thought that FeOB avoid becoming encrusted by their iron oxide waste products both by oxidizing $Fe^{2+}$ on the outer membrane of the cell, thus preventing the formation of iron minerals within the cell itself, and by the production of structures from these mineral waste products (16–20). FeOB-produced structures include twisted iron stalks, sheaths, and "dreads," though amorphous oxides are also produced by some species (14, 21, 22). Of these structures, twisted iron stalks have been extensively studied, but how exactly these structures form remains somewhat of a mystery.

FeOB that produce twisted iron stalks attach to a surface and then excrete acidic polysaccharides that are hypothesized to bind the $Fe^{3+}$ that results from $Fe^{2+}$ oxidation (16, 17, 20). As Fe(III) minerals precipitate in these polysaccharides, they form fibrils of iron oxides, which make up the structural component of the stalk. The cell continues to excrete polysaccharide and produce its stalk, turning as stalk formation propels it away from its point of attachment, leading to the characteristic twisted ribbon shape of the stalk. Over time the buildup of these stalks leads to the formation of flocculent iron mats, which can alter flow regimes on larger scales and so further affect chemical regimes within the mat and at its surface (14). How exactly oxidized $Fe^{3+}$ gets from the cell to the polysaccharides that bind it is unclear, however.

Localized acidification has been proposed as one mechanism that could aid in stalk formation, though it was until now unknown whether FeOB establish pH microenvironments around themselves, and indeed it was even questioned whether such a phenomenon was possible for these organisms (11, 16).

To test whether FeOB form pH microenvironments around their cells and what effect, if any, this might have on mineral solubility and thus stalk formation we studied the model FeOB *Mariprofundus ferrooxydans* PV-1, a member of the Zetaproteobacteria and an obligate iron oxidizer and chemolithoautotroph that fixes carbon via the Calvin-Benson-Bassham pathway (23). It was originally isolated from Lō'ihi Seamount, a hydrothermal system off the coast of Hawai'i characterized by low temperature (~30˚C) diffuse venting with high $Fe^{2+}$ concentrations (up to ~1 mM) (24, 25). FeOB like PV-1 thrive in these conditions and vast areas of Lō'ihi vent fields have been seen covered with the iron mats these organisms produce (26). The fluid from these vents is also lower in pH than the surrounding seawater (seawater pH = ~8.1), with values of 4.5-6.0 reported (24, 25). PV-1, like many marine FeOB isolates, grows preferentially at pH close to this range, with an optimum of 6.2-6.5 (15, 23).

In this study, we used confocal microscopy and the pH sensitive fluorescent dye seminaphtharhodafluor-4F-5-(and-6)-carboxylic acid (SNARF) to image living *M. ferrooxydans* PV-1 cells grown in gradient slides. SNARF is a single excitation, dual emission dye; it is excited with one wavelength of laser light and its emission is collected at two different wavelengths corresponding to the protonated and deprotonated forms of the dye (27). Since the protonated and deprotonated forms of the dye exist in equilibrium that is dependent on pH (SNARF $pK_a$ = 6.4), the ratio of the intensities of these emission spectra can be used to determine the pH in specific areas of the image in a process known as ratiometric imaging (3, 4,

28). This allowed us to visualize the pH landscape around each cell and examine how cells affected their environmental pH. We also used the protonophore carbonyl cyanide m-chlorophenyl hydrazone (CCCP), which neutralizes membrane potentials, to determine whether the establishment of pH microenvironments was due to cellular activity (11). Furthermore, we used geochemical modeling to assess the consequences of an acidic microenvironment for PV-1 in terms of energetics of iron oxidation and solubility of waste Fe(III). Notably, fluid from Lō'ihi vent fields is generally high in carbon dioxide (values up to 418 mM reported) as well and alteration of extracellular pH would change the equilibrium of which dissolved inorganic carbon (DIC) species are present in solution around the cell, with $CO_2$ dominating at more acidic conditions and $HCO_3^-$ at higher concentrations under more neutral conditions (29, 30). We therefore also modeled availability of DIC for PV-1 based on any pH microenvironments that were seen.

We found that PV-1 cells do have a low-pH microenvironment around themselves and that these microenvironments are at least partially actively maintained by cellular activity. Geochemical modeling revealed that the energetic cost to living at lower pH is minimal, while availability of $CO_2$ would be significantly increased. We also speculate how the increased solubility of Fe(III) due to the decreased pH in these microenvironments may aid in the direction of iron oxide precipitation for stalk formation.

## Methods

### Cultivation conditions

*Mariprofundus ferrooxydans* PV-1 was cultured in artificial seawater-ZVI plates, according to the National Center for Marine Algae and Microbiota culturing guidelines for

cultivating marine iron-oxidizing bacteria. Petri dishes were filled with 20 ml artificial seawater (ASW, pH ~6.4), with 100 mg -200 mesh zero-valent iron (ZVI) powder (Alfa Aesar Inc.), sterilized via gamma irradiation, added as an Fe(II) source. Plates were incubated in gas-tight jars with valves that allowed the jar headspace to be replaced with a gas mix of 8% $O_2$/10% $CO_2$/82% $N_2$. Jars were incubated at ambient temperature (~24˚C).

**Gradient slide construction and inoculation**

Slides were constructed to allow *M. ferrooxydans* PV-1 to grow in a gradient of $Fe^{2+}$ and $O_2$ and then be imaged *in situ*. (Figure 3.1) These slides consisted of a standard 25 x 75 mm microscope slide (VWR) with a #1.5 22 x 50 mm coverglass (Electron Microscopy Sciences) held above it using 4 1.5 x 2 mm Viton o-rings (McMaster-Carr) as spacers. Three edges of this assembly were then sealed with Epoxy Resin 105 (West System) and allowed to set overnight.

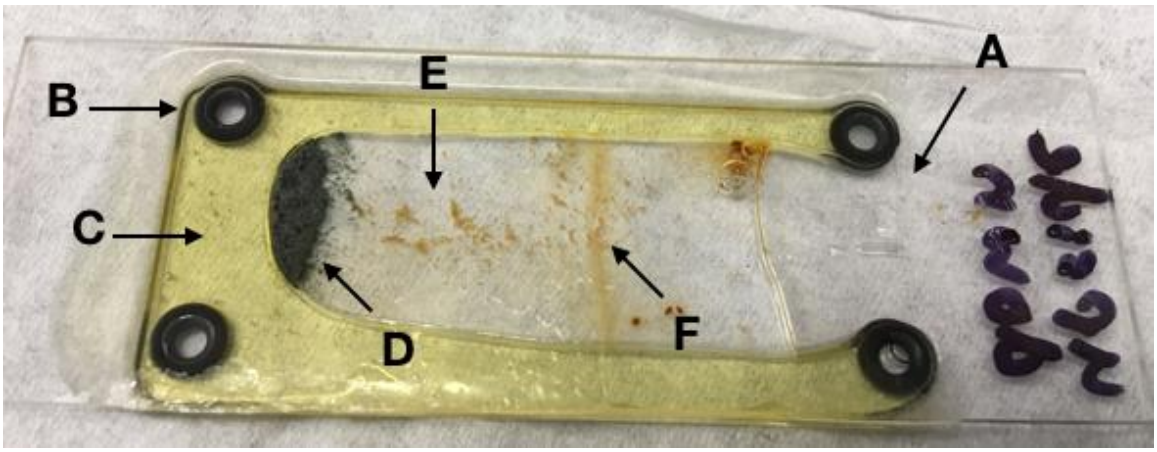


**Figure 3.10) Diagram of inoculated gradient slide.** Sample gradient slide that was inoculated with *M. ferrooxydans* PV-1 and incubated for 48 h at room temperature. Similar gradient slides were constructed with added SNARF dye and used to visualize pH landscapes around living PV-1 cells A) #1.5 coverglass, B) Viton o-rings, C) epoxy resin, D) zero-valent iron (ZVI) powder, E) iron oxides from initial inoculum, F) band of growing PV-1 cells

For growing live PV-1 cells, enough ZVI powder was added to each gradient slide to just cover the bottom of the slide. 500 µl ASW containing 20 µM SNARF-4F-5-(and-6)-carboxylic

acid (Thermo Fisher Inc.) and 10 mM PIPES pH 6.5 was then added to each slide. PV-1 cells were inoculated from late log phase cultures grown in ZVI plates by drawing cells from a ZVI plate into a syringe with attached needle, then inserting the needle to the bottom of the gradient slide and drawing it up as the plunger of the syringe was depressed. This was done to ensure cells were present at their optimal location for growth in the $Fe^{2+}/O_2$ gradient formed by ZVI dissolving at the bottom of the slide and $O_2$ diffusing from the top.

Inoculated slides were placed in petri dishes with a wet laboratory wipe (VWR) to prevent evaporation. Petri dishes were then wrapped in tin foil to protect them from light and placed in the same gas tight jar used for routine culturing. The headspace in the jar was replaced with the same gas mix used for routine culturing (8% $O_2$/10% $CO_2$/82% $N_2$) and slides were incubated at ambient temperature (24˚C).

**Construction of SNARF standard curve**

SNARF standards were prepared in a 96-well plate with a glass bottom that was equivalent in thickness to a #1.5 coverglass (Thomas Scientific). 196 µl 50 mM Bis-Tris adjusted to pH values from 5.0 to 7.5 in 0.1 pH increments were then added to wells in the plate (total of 26 standards) and 4 µl 1mM SNARF-4F-5-(and-6)-carboxylic acid was added to each well for a final SNARF concentration of 20 µM. Standards were made at the same time that gradient slides were inoculated, then incubated at ambient temperature for 48 hours prior to imaging. This was done to control for any changes the SNARF may have experienced in the gradient slides while incubating, though no differences were detected between fresh and 48-hour-old standards.

Each well was imaged on an LSM 880 confocal microscope (Zeiss) with a 63X/1.4 oil immersion objective. SNARF was excited at 488 nm and fluorescence was collected at 550-600

nm (channel 1) and 625-675 nm (channel 2). The resulting images were analyzed in FIJI using a custom macro to measure the mean intensities of each channel for each pH standard (31). The mean intensity of channel 2 was then divided by that of channel 1. The resulting ratios were plotted against their respective pH and a best-fit line was determined to use as a standard curve.

**Imaging of gradient slides**

One hour prior to imaging, slides were removed from their petri dishes and stained for imaging. All slides were stained for DNA using 0.03 mg/ml Hoechst 34580 (VWR) and iron stalks were stained using 0.04 mg/ml soybean agglutinin (SBA) conjugated Alexa Fluor 647 (Thermo Fisher Inc.) To determine whether pH microenvironments around cells were due to cellular activity, half of the gradient slides also had the protonophore carbonyl cyanide m-chlorophenyl hydrazone (CCCP) dissolved in ethanol added to a final concentration of 10 μM. CCCP disrupts proton gradients and would eliminate any pH microenvironment that cells were establishing through active transport of protons across the cell membrane (11).

Slides were also imaged on an LSM 880 confocal microscope equipped with a 63X/1.4 oil immersion objective, in addition to an Airyscan superresolution detector. SNARF was imaged as described for pH standards above. Cells were visualized using Hoechst DNA stain, which was excited at 405 nm and collected in the blue channel of the Airyscan detector. Stalks were visualized using SBA conjugated Alexa Fluor 647, which was excited at 633 nm and collected in the far-red channel of the Airyscan detector. A total of 10 cells attached to stalks were imaged each for live cells and CCCP-treated controls.

**Generation of pH maps and determination of extracellular pH**

Images of cells attached to stalks were imported into FIJI for image analysis using a custom macro. This was done by first dividing the channel 2 SNARF fluorescence intensity by the channel 1 SNARF intensity. Minimum and maximum brightness were set on the resulting image according to the highest and lowest value resulting from the standard curve. The image was then denoised using a Median filter with a 3 pixel area. A custom lookup table was then created based on the total pH range measured to display pH microenvironments in the image.

The macro also determined cell location by automatically thresholding the DNA stain channel using the Otsu method and creating a custom selection around the resulting area where each cell was located. This selection was then used to create a second selection for the area immediately around the cell, i.e,. a ring around the cell 0.1 μm in thickness. The mean intensity of this selection was measured and used to determine the average pH immediately surrounding each cell. A larger area away from any iron oxides was also selected and analyzed for average pH in each image to serve as a background.

To account for the buffering capacity of the media, the significance of the difference in pH change between live and CCCP-treated cells was determined based on the number of protons required to shift the background pH to match that of the area immediately surrounding the cells. This was done by assuming an average cell volume equal to that of a cylinder with length 1 μM and diameter 0.5 μM, which was based on measurements taken in FIJI. We then calculated the total number of protons needed to change the pH of a 0.1 μM thick envelope around each cell from the measured background pH to the measured pH immediately surrounding the cell using the Henderson-Hasselbalch equation (32). These differences between cell and background for

both live and CCCP-treated cells were then compared using Welch's t-test to determine if there was a significant difference.

**Modeling of free energy yield change based on pH**

The free energy yield (ΔG) of iron oxidation was determined over the pH range 6.0-7.0 using the Rxn module of Geochemist's Workbench 12.0 (Aqueous Solutions LLC). We assumed a starting oxygen concentration of 10 μM, as this is the oxygen concentration at which PV-1 has been shown to be responsible for >90% of iron oxidation (15). We also assumed an initial $Fe^{2+}$ concentration of 200 μM, based on a previous study using similar gradient slides, where PV-1 stalks were found in a region of the slide that contained ~200 μM $Fe^{2+}$ (33). The activity of $Fe(OH)_{3(ppt)}$ was set to 1.0 by convention.

As >99% of $Fe^{3+}$ resulting from the oxidation of $Fe^{2+}$ precipitates as oxyhydroxides, the reaction was balanced in terms of $Fe(OH)_{3(ppt)}$ with an overall reaction formula of $Fe^{2+} + 2.5\ H_2O + 0.25\ O_{2(aq)} \rightarrow Fe(OH)_{3(ppt)} + 2\ H^+$. We then varied the pH of the reaction from 6.0 to 7.0 in 0.1 pH unit increments, which encompassed the entire pH range observed using the SNARF dye. The resulting ΔG values were then plotted against pH and the equation from this line was used to determine the average difference in ΔG that would result from iron oxidation occurring at live PV-1 cell surfaces or in the bulk media.

**Modeling of dissolved inorganic carbon speciation based on pH**

Speciation of dissolved inorganic carbon (DIC) between $CO_{2(aq)}$ and $HCO_3^-$ was calculated for all live cell and live background measurements using the Henderson-Hasselbalch Equation and the $pK_a$ of 6.35 for carbon dioxide (32, 34). All conjugate acid was assumed to be present as $CO_{2(aq)}$ as the ratio $CO_{2(aq)}$:$H_2CO_3$ in solution is approximately 840 at ~20˚C (35). This was then used to determine the average difference in $CO_{2(aq)}$ concentration between the area immediately surrounding live cells and the bulk media.

**Modeling of Fe(III) solubility based on pH**

Total soluble Fe(III) ($Fe(III)_{(aq)}$) was calculated for a pH range of 6.0-7.0 in the React module of Geochemist's Workbench 12.0 after Hegler et al. 2010 (11). This was done by defining a basis within Geochemist's Workbench with the same constituents as the artificial seawater used for growing PV-1 cells and again assuming an initial oxygen concentration of 10 µM. The starting concentration of $Fe^{3+}$ was determined by assuming the complete oxidation of $Fe^{2+}$ from the previous model to $Fe^{3+}$. We thus used a starting concentration of 200 µM $Fe^{3+}$. The $Fe^{2+}/Fe^{3+}$ redox couple was then decoupled to prevent any $Fe^{3+}$ from being re-reduced.

We assumed, given the short time period for which gradient slides were incubated, that the only iron mineral to precipitate would be ferrihydrite ($(Fe^{3+})_2O_3 \bullet 0.5H_2O$). We therefore suppressed the precipitation of other iron minerals that would likely form if slides were incubated for longer (e.g., goethite (α-FeO(OH)) and hematite (α-$Fe_2O_3$)). The React module was then set to model the speciation of these constituents from pH 6.0 to 7.0 in 0.1 pH unit increments. $Fe(III)_{(aq)}$ was then plotted against pH to determine the solubility of Fe(III) at a given

pH and the resulting equation from this plot was used to determine the average solubility of Fe(III) near the surface of live cells and in the bulk media.

## Results

### Low pH microenvironments exist around live and CCCP-treated PV-1 cells

We used ratiometric imaging with SNARF dye to observe pH landscapes around live and CCCP-treated PV-1 cells that were attached to iron stalks. These images revealed that both live and CCCP-treated cells had pH microenvironments localized around the entire circumference of each cell, as shown in a representative image in Figure 3.2. These microenvironments were significantly lower in pH than the background for both live and CCCP-treated cells. (Figure 3.3)

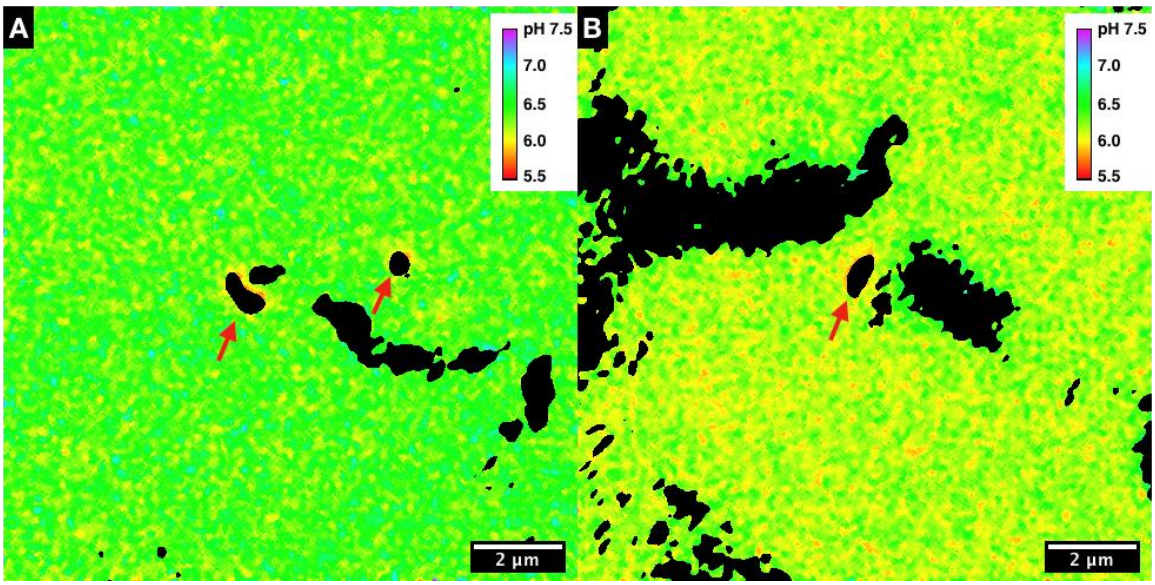


**Figure 3.11) pH landscapes of PV-1 cells attached to iron stalks.** False color has been added to show the pH microenvironments surrounding A) living PV-1 cells and B) CCCP-treated cells. Warmer colors indicate decreasing pH, which is generally located proximal to cells. Note that background pH is lower in frame B due to the addition of CCCP dissolved in ethanol. Cells are indicated with arrows, while other black patches are biogenic iron oxide identified by binding of rhodamine-conjugated *Ricinus communis* agglutinin.

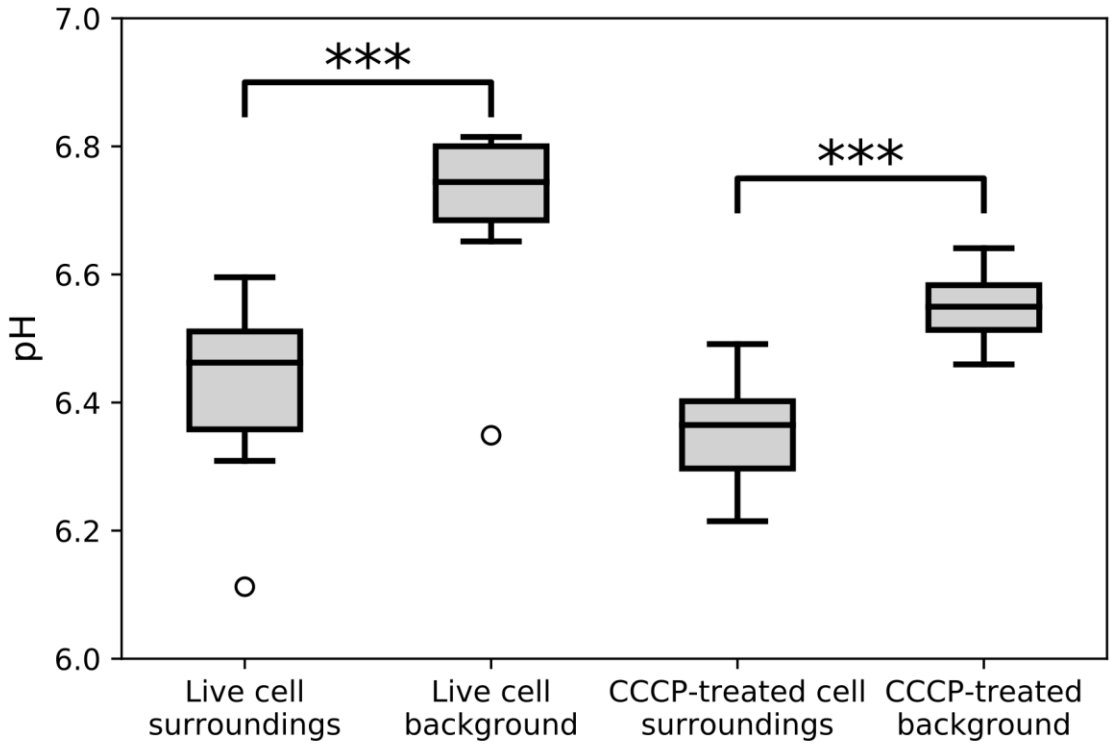


**Figure 12.3) pH of cell surroundings and background for live and CCCP-treated slides.** Background pH was determined by measuring an area away from cells and oxides in each of 10 images, while cell surroundings were measured in a 0.1 μm ring around each cell for the same 10 images. Cell surroundings were each significantly lower than the respective background pH. (*** = P<0.001) Note that CCCP-treated background pH is lower due to the addition of ethanol used to dissolve CCCP.

We then sought to determine whether the establishment of these pH microenvironments was mediated by cellular activity. Because the media these cells were grown in was well buffered, we determined the total number of protons that would be necessary to shift the pH around each cell to tell if live cells were having a greater effect on pH than CCCP-treated cells. Living cells did require the addition of significantly more protons proximal to the cell to shift the pH of their bulk media to the measured pH immediately surrounding them. (Figure 3.4)

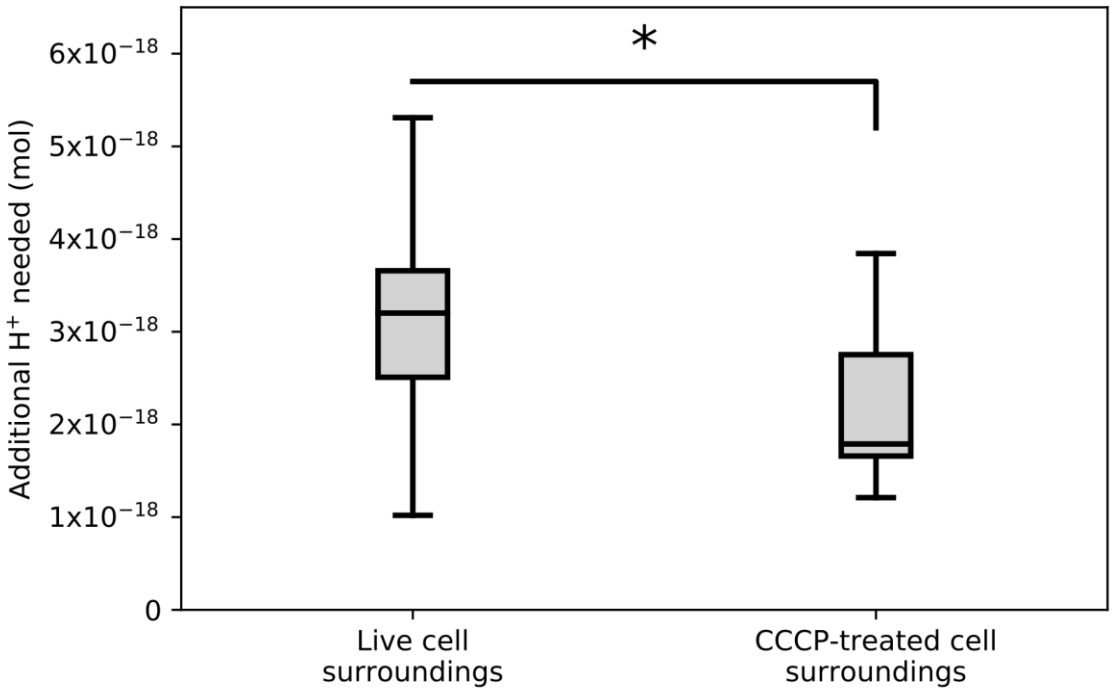


**Figure 3.13) Number of $H^+$ ions needed to decrease the pH immediately surrounding live and CCCP-treated cells.** Live cells required significantly more $H^+$ ions to decrease the pH of their surroundings. (* = P<0.05)

## Free energy yield in low pH microenvironments around live PV-1 cells decreases slightly compared to bulk media

The $Fe^{2+}/Fe^{3+}$ redox couple changes with pH, as does the solubility and stability of both Fe(II) and Fe(III) (36), so it was likely that actively metabolizing PV-1 cells would experience a change in the energetic yield of iron oxidation. We used geochemical modeling to demonstrate that the ΔG of iron oxidation increases (i.e. its energy yield decreases) with decreasing pH PV-1 cells establishing a low pH microenvironment would therefore actually be losing some energy per reaction compared to if they were oxidizing iron at the pH of the bulk media. (Figure 3.5) This energy loss was relatively small, however, with living cells obtaining a calculated average of -70.45 ± 1.59 $kJ•mol^{-1}$ of Fe(II) oxidized while iron oxidation in the bulk media would yield an average of -73.62 ± 1.56 $kJ•mol^{-1}$. The average reduction in free energy yield for live cells

compared to the bulk media is thus approximately 3.17 kJ•mol$^{-1}$ ± 1.26 kJ•mol$^{-1}$ or about 4.3 ± 1.7%.

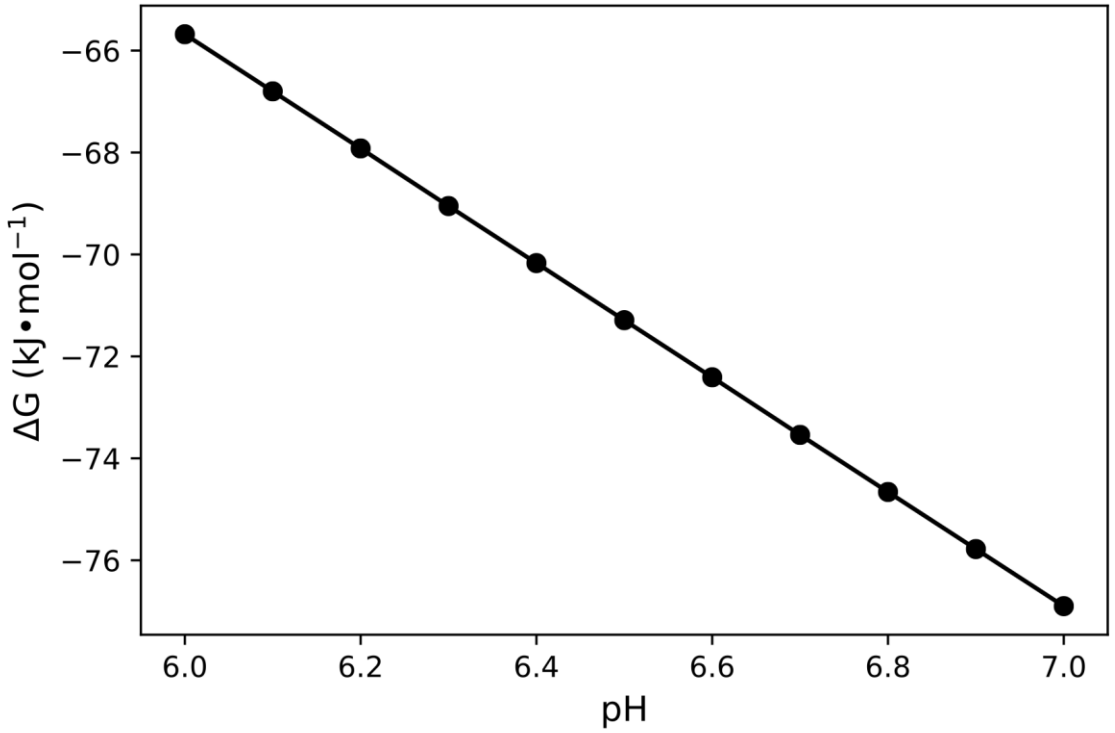


**Figure 3.14) Change in free energy yield of the oxidation of $Fe^{2+}$ to $Fe(OH)_3$ as a function of pH.** Free energy yield increases linearly with increasing pH. Total change in ΔG over the pH range 6.0 to 7.0 is modest, however.

**More DIC is present as $CO_{2(aq)}$ in the pH microenvironment surrounding live cells than in bulk media**

Changing pH also changes the $CO_{2(aq)} \rightleftharpoons HCO_3^-$ equilibrium of seawater, which could affect how much $CO_2$ is available for PV-1 via passive diffusion versus the active transport of $HCO_3^-$. Given that the pH around each cell was lower than the bulk media and this pH was around the $pK_a$ of $CO_{2(aq)} \rightleftharpoons HCO_3^-$ ($pK_a$ = 6.35)(34), we expected there to be a large increase in the amount of $CO_{2(aq)}$ present. We used the Henderson-Hasselbalch equation to model the shift in

this equilibrium and determine whether there was actually more $CO_{2(aq)}$ present in solution. Though $CO_{2(aq)}$ exists in equilibrium with $H_2CO_3$ in water, the ratio $CO_{2(aq)}$:$H_2CO_3$ in solution is approximately 840 at the temperatures PV-1 thrives at, so all conjugate acid was assumed to be $CO_{2(aq)}$ for the purposes of this model. We determined that significantly more DIC would be present as $CO_{2(aq)}$ in the low pH microenvironment surrounding live PV-1 cells than in the bulk media. (Figure 3.6)

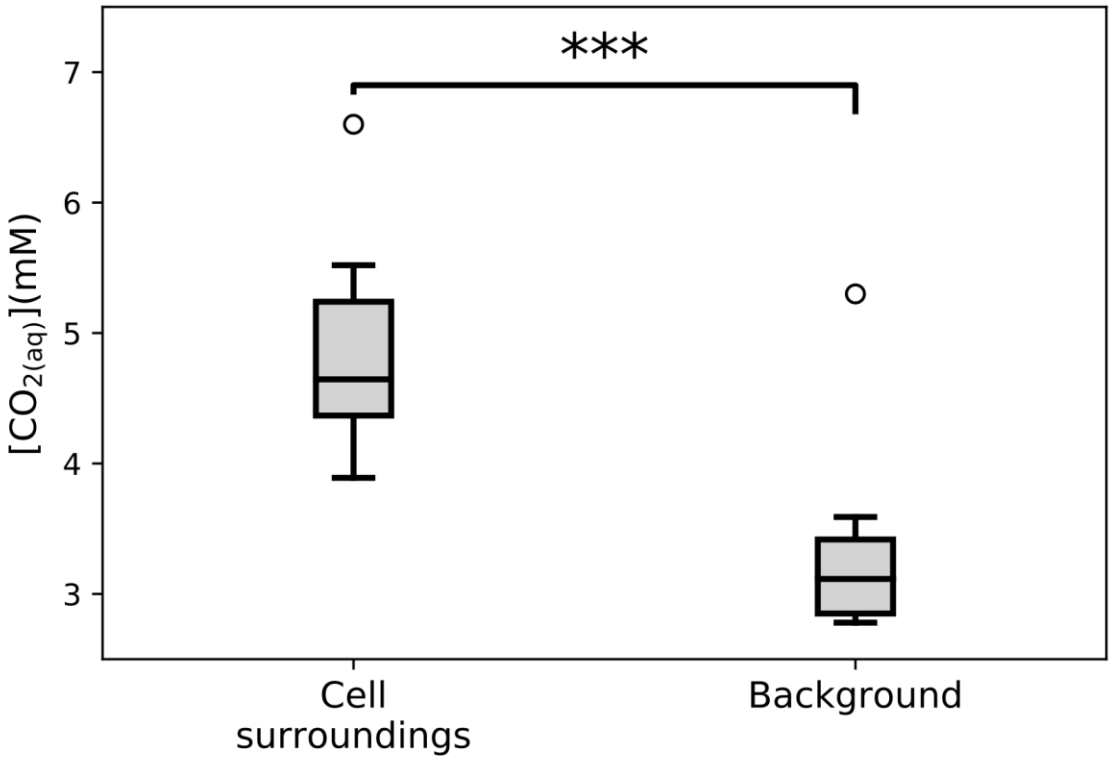


**Figure 3.15) Amount of dissolved inorganic carbon present as $CO_{2(aq)}$ in pH microenvironment immediately surrounding live cells and at their background pH.** Live cells have a significantly greater concentration of DIC present as $CO_{2(aq)}$ than the background. (*** = P<0.001)

**Solubility of Fe(III) is greater in low pH microenvironments surrounding live PV-1 cells compared to bulk media**

It is well known that Fe(III) is more soluble at lower pH, which would in turn affect how quickly it would precipitate as iron oxides (11). We used geochemical modeling to determine how much more soluble Fe(III) would be in the microenvironment surrounding PV-1 cells compared to in the bulk media. Our model, assuming an initial Fe(III) concentration of 200 μM and an initial oxygen concentration of 10 μM, shows that $Fe(III)_{(aq)}$ does indeed increase as pH decreases, i.e. Fe(III) is more soluble at lower pH. (Figure 3.7) The media in the microenvironment around live PV-1 cells would, according to this model, have an average $Fe(III)_{(aq)}$ concentration $1.71 \bullet 10^{-7} \pm 4.39 \bullet 10^{-8}$ mol•$L^{-1}$, while the bulk media would have only $1.14 \bullet 10^{-7} \pm 2.67 \bullet 10^{-8}$ mol•$L^{-1}$ $Fe(III)_{(aq)}$. Live cells therefore have $5.65 \bullet 10^{-8} \pm 2.70 \bullet 10^{-8}$ mol•$L^{-1}$ more $Fe(III)_{(aq)}$ surrounding them compared to the bulk media, a difference of approximately $32.5 \pm 15.8\%$.

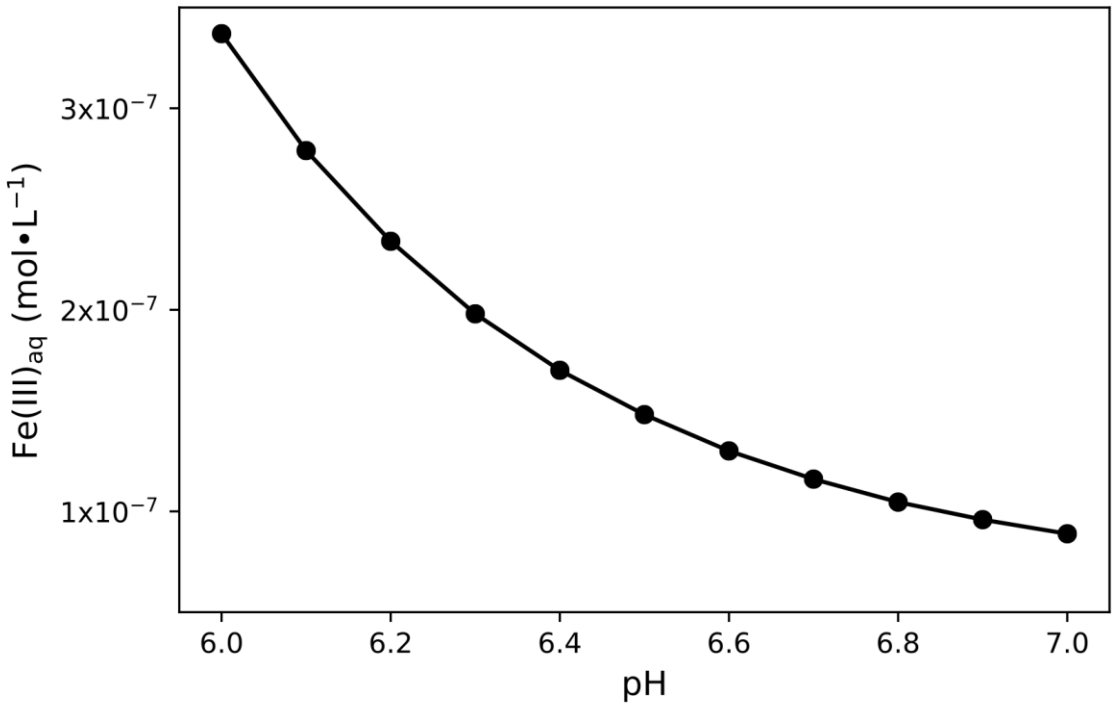


**Figure 3.16) Change in solubility of Fe(III) species as a function of pH.** Increasing pH leads to lower solubility for Fe(III), with >3 fold more dissolved Fe(III) in solution at pH 6.0 compared to pH 7.0.

**Discussion**

Regulation of pH is important for all cells for a number of reasons, including energy conservation and maintenance of proper protein folding (37). Bacteria have been shown to be capable of modulating their intracellular pH to maintain a proton-motive force, where a difference in pH across a membrane promotes the movement of protons through ATP synthase, allowing the cell to store energy (38, 39). Many cells have been shown to have an effect on the pH of their surroundings as well, usually as a consequence of their metabolism. Heterotrophic bacteria are known to acidify their surroundings, creating low pH microenvironments around themselves and in biofilms, mostly through production of organic acids (3, 4). Cyanobacteria have also been shown to establish microenvironments of pH around their cells, though these microenvironments are often higher in pH due to the consumption of protons and $CO_2$ by Calvin-

Benson-Bassham Cycle autotrophy (6, 7). In contrast to this, photoautotrophic iron oxidizing bacteria also establish pH microenvironments, though in this case the cells acidify their surroundings although they are also photoautotrophic (11). It was until now, however, unknown how neutrophilic microaerobic FeOB affect the extracellular pH proximal to their cells. It has even in the past been doubted that FeOB would form localized pH microenvironments, given the fact that iron oxidation is a low energy metabolism and microaerophilic FeOB are unable to rely on light energy to pump protons (11).

Through ratiometric confocal imaging using the pH sensitive fluorescent dye SNARF-4F-5-(and-6)-carboxylic acid we have confirmed for the first time that *Mariprofundus ferrooxydans* PV-1 does indeed establish an acidic microenvironment around the entirety of the cell. Additionally, the magnitude of the difference in pH between the area immediately surrounding the cell and the bulk media is decreased when PV-1 is treated with the protonophore carbonyl cyanide m-chlorophenyl hydrazone (CCCP), which disrupts the cell's membrane potential, indicating that the ΔpH these cells create is in part an active process. Cells that were treated with CCCP still had microenvironments around them that were significantly more acidic than the background, however. This is in contrast to what is known about phototrophic iron oxidizers, where CCCP completely eliminated any ΔpH between cells and their environment (11). We hypothesize that PV-1 may use passive processes to circumvent its energy limitations, not needing to expend energy for part of this ΔpH, perhaps relying on the hydrolysis of water by $Fe^{3+}$ to a greater extent than phototrophic iron oxidizers. The mechanism by which it does this was not determined as part of this study, however, and presents an interesting avenue for further research.

These acidic microenvironments present a number of consequences for PV-1, the first of which is the energetics of iron oxidation. As pH decreases, the redox potential of the $Fe^{2+}/Fe^{3+}$ couple increases and, in addition, the solubility of $Fe^{3+}$ ions in solution increases, causing the buildup of one of the endproducts of PV-1's metabolism that would otherwise precipitate and be removed solution, thus decreasing the favorability of iron oxidation (36). It is possible that this would pose an issue for PV-1, as the energetic yield of iron oxidation is low compared to other lithtrophic metabolisms (10). Our modeling shows that PV-1 would experience a modest decrease in energy yield as a result of living at the pH levels we measured. In spite of this energy loss, however, PV-1 still actively mediates the production of a ΔpH. Thus, although decreasing local pH incurs a cost beyond only the energy expended to establish these microenvironments, the detrimental effects must be outweighed by the benefits conferred to an organism that makes a living by oxidizing iron.

One possible benefit is an increased proportion of dissolved inorganic carbon being present as carbon dioxide. In carbonate buffered systems like seawater, dissolved carbon dioxide exists at equilibrium with bicarbonate, with the bicarbonate form dominant in seawater at a pH of close to 8.0 (34). PV-1, however, was isolated from regions of diffuse hydrothermal venting at Lō'ihi Seamount that are lower in pH, generally between 6.0 and 7.0, and has a pH optimum of 6.2-6.5 (15, 23, 40).

This range includes the $pK_a$ of carbon dioxide ($pK_a = 6.35$), around which small changes in pH would result in large shifts in the $CO_{2(aq)} \rightleftharpoons HCO_3^-$ equilibrium (34, 41). This is relevant to PV-1 because uncharged $CO_{2(aq)}$ can passively diffuse across the cell membrane, while charged $HCO_3^-$ must be actively transported, though PV-1 does possess genes for bicarbonate uptake (42). It may be that by changing the pH around its cells PV-1 increases the concentration of

available $CO_{2(aq)}$ that can then diffuse into the cell in addition to the bicarbonate it actively transports. This could be particularly important because PV-1 does not produce carboxysomes or other carbon concentrating mechanisms, nor does it have the genetic potential to do so (42). Carboxysomes are found in many bacteria that use RubisCO to fix carbon, functioning to reduce respiratory loss from RubisCO binding to oxygen instead of carbon dioxide by increasing local concentrations of carbon dioxide (43). Vent fluid at Lō'ihi is highly enriched in carbon dioxide (up to 418 mM), however, and PV-1 allowing a greater proportion of $CO_{2(aq)}$ to diffuse into its cells could function as an analogue to carbon concentration mechanisms found in other microaerobic chemoautotrophs that rely on the Calvin-Benson-Bassham pathway for carbon fixation (30, 44). PV-1 may therefore be able to circumvent the need for carboxysomes to maintain high [$CO_2$] around RubisCO despite its metabolic requirement for oxygen.

Uniquely, microbes that oxidize iron at circumneutral pH must contend with precipitation of their waste $Fe^{3+}$ as iron oxyhydroxides. Iron oxidation is therefore carried out on the extracellular membrane to prevent precipitation inside the cell, but there is still the issue of encrustation by iron oxides that could eventually lead to entombment. It has long been postulated that stalk-forming FeOB like PV-1 construct their stalks in part to avoid encrustation, and localized acidification has been implicated as a possible aid in this as well (16). Indeed, though the exact mechanisms of stalk formation remain somewhat of a mystery, the acidic microenvironments established by PV-1 cells may help explain how FeOB direct iron oxide precipitation at the site of stalk formation because of the aforementioned increased solubility of $Fe^{3+}$ ions at lower pH. By increasing the solubility of $Fe^{3+}$, PV-1 would inhibit the precipitation of Fe(III) minerals relative to its environment. It is also known that PV-1 produces iron-binding acidic extracellular polysaccharides that coordinate oxide precipitation for stalk formation (16,

17, 20). We hypothesize that these polysaccharides act as a "trap" for iron oxidation, presenting conditions that are more conducive to iron oxide precipitation than the rest of the cell surroundings. Iron oxide precipitation would then decrease the relative concentration of $Fe^{3+}$ surrounding the stalk, causing more $Fe^{3+}$ to diffuse towards the stalk, which would then precipitate driving the process further.

Thus a combination of low pH and site-specific nucleation may be an effective method of directing precipitation in a manner that is advantageous to the cell. The data presented here, as well as the observation that PV-1 cells do not encrust in iron minerals neither confirm nor refute this hypothesis but they are consistent with it. Additionally, it would help explain why the only precipitation around cells that is seen is in the form of iron stalks. We would expect to see precipitation in other areas nearby PV-1 cells if, similar to phototrophic iron oxidizers, the low pH microenvironment simply allowed $Fe^{3+}$ to diffuse away from the cell before precipitating. Instead, the only region near the cell where we see precipitation is at the site of stalk formation which is within the low pH microenvironment, the opposite of what would be expected based purely on our thermodynamic model of differences in $Fe^{3+}$ solubility due to pH.

It should also be noted that, to our knowledge, iron oxide precipitation is not seen near PV-1 cells except for in the stalk. This may mean that PV-1 only metabolizes iron at the site of stalk formation. If instead PV-1 could oxidize iron at any point on its surface we would expect to see more iron oxides surrounding its cells, which would form after $Fe^{3+}$ diffuses away into regions away from the cell that have much lower $Fe^{3+}$ concentrations due to greater precipitation resulting from higher pH. What we do see, however, is the precipitation of iron oxides proximal to the cell but only in the stalk, where we would also expect higher $Fe^{3+}$ concentrations. This implies that $Fe^{3+}$ is only produced in the site of stalk formation. Having the low pH

microenvironment all around its cells would still likely be beneficial to PV-1, however, as this would prevent any abiotic oxidation from encrusting the cell.

## Conclusion

The establishment of a low pH microenvironment around its cells presents a number of possible advantages for *M. ferrooxydans* PV-1 for relatively little cost. The loss in energetic yield of iron oxidation is small, the ΔpH that we have seen seems to only partially be dependent on cellular activity, and the actively produced portion could simply be a byproduct of iron oxidation due to hydrolysis from $Fe^{3+}$ waste products. In return, PV-1 may be able to increase the concentration of carbon dioxide inside its cells, allowing for increased efficiency of carbon fixation through reducing the likelihood that RubisCO binds oxygen instead of carbon dioxide.

In addition, the demonstration that these microenvironments exist may provide new insights into the formation of twisted iron stalks. It is still unknown how exactly stalk-forming FeOB control the mineralization of their stalks, but modulating local pH may aid them in directing precipitation towards the EPS they produce, preventing haphazard precipitation and encrustation. Further, we think that iron oxide precipitation occurring only in the stalk despite the existence of these microenvironments surrounding the entire cell supports the hypothesis that PV-1 only oxidizes iron at the site of stalk formation. This would mean that the cell is possibly losing out on the potential to metabolize a greater amount of iron by using its entire surface area in addition to the likely high energy expenditure necessary to make a highly ordered structure such as an iron stalk. Taken together, this could make stalk production a significant energy sink for PV-1, yet it still makes a stalk, underscoring its importance to an iron-oxidizing lifestyle.

## References


1. **Barker WW**, **Welch SA**, **Chu S**, **Banfield JF**. 1998. Experimental.observations of the effects of bacteria on aluminosilicate weathering. Am Mineral **83**:1551–1563.

2. **De Los Ríos A**, **Wierzchos J**, **Sancho LG**, **Ascaso C**. 2003. Acid microenvironments in microbial biofilms of antarctic endolithic microecosystems. Environ Microbiol **5**:231–237.

3. **Schlafer S**, **Raarup MK**, **Meyer RL**, **Sutherland DS**, **Dige I**, **Nyengaard JR**, **Nyvad B**. 2011. pH landscapes in a novel five-species model of early dental biofilm. PLoS One **6**:1–11.

4. **Schlafer S**, **Garcia JE**, **Greve M**, **Raarup MK**, **Nyvad B**, **Dige I**. 2015. Ratiometric imaging of extracellular pH in bacterial biofilms with C-SNARF-4. Appl Environ Microbiol **81**:1267–1273.

5. **Marquis R**. 1995. Oxygen metabolism, oxidative stress and acid-base physiology of dental plaque biofilms. J Ind Microbiol **15**:198–207.

6. **Richardson LL**, **Stolzenbach KD**. 1995. Phytoplankton cell size and the development of microenvironments. FEMS Microbiol Ecol **16**:185–191.

7. **Bissett A**, **Reimer A**, **De Beer D**, **Shiraishi F**, **Arp G**. 2008. Metabolic microenvironmental control by photosynthetic biofilms under changing macroenvironmental temperature and pH conditions. Appl Environ Microbiol **74**:6306–6312.

8. **Bird LJ**, **Bonnefoy V**, **Newman DK**. 2011. Bioenergetic challenges of microbial iron metabolisms. Trends Microbiol **19**:330–340.

9. **Hallbeck L**, **Pedersen K**. 1990. Culture parameters regulating stalk formation and growth rate of Gallionella ferruginea. J Gen Microbiol **136**:1675–1680.

10. **Emerson D**, **Fleming EJ**, **McBeth JM**. 2010. Iron-oxidizing bacteria: an environmental and genomic perspective. Annu Rev Microbiol **64**:561–583.

11. **Hegler F**, **Schmidt C**, **Schwarz H**, **Kappler A**. 2010. Does a low-pH microenvironment around phototrophic FeII-oxidizing bacteria prevent cell encrustation by FeIII minerals? FEMS Microbiol Ecol **74**:592–600.

12. **Emerson D**, **Moyer C**. 1997. Isolation and characterization of novel iron-oxidizing bacteria that grow at circumneutral pH. Appl Environ Microbiol **63**:4784–4792.

13. **Emerson D**, **Floyd MM**. 2005. Enrichment and isolation of iron-oxidizing bacteria at neutral pH. Methods Enzymol **397**:112–123.

14. **Chan CS**, **McAllister SM**, **Leavitt AH**, **Glazer BT**, **Krepski ST**, **Emerson D**. 2016. The architecture of iron microbial mats reflects the adaptation of chemolithotrophic iron oxidation in freshwater and marine environments. Front Microbiol **7**.

15. **McAllister SM**, **Moore RM**, **Gartman A**, **Luther GW**, **Emerson D**, **Chan CS**. 2019. The Fe(II)-oxidizing Zetaproteobacteria: historical, ecological and genomic perspectives. FEMS Microbiol Ecol **95**:1–18.

16. **Chan CS**, **Fakra SC**, **Emerson D**, **Fleming EJ**, **Edwards KJ**. 2011. Lithotrophic iron-oxidizing bacteria produce organic stalks to control mineral growth: implications for biosignature formation. ISME J **5**:717–727.

17. **Chan CS**, **Fakra SC**, **Edwards DC**, **Emerson D**, **Banfield JF**. 2009. Iron oxyhydroxide mineralization on microbial extracellular polysaccharides. Geochim Cosmochim Acta **73**:3807–3818.

18. **Barco RA**, **Emerson D**, **Sylvan JB**, **Orcutt BN**, **Jacobson Meyers ME**, **Ramírez GA**, **Zhong JD**, **Edwards KJ**. 2015. New Insight into Microbial Iron Oxidation as Revealed by the Proteomic Profile of an Obligate Iron-Oxidizing Chemolithoautotroph. Appl Environ Microbiol **81**:5927–5937.

19. **Chan CS**, **McAllister SM**, **Garber A**, **Hallahan BJ**, **Rozovsky S**. 2018. Fe oxidation by a fused cytochrome-porin common to diverse Fe-oxidizing bacteria. bioRxiv 228056.

20. **Comolli LR**, **Luef B**, **Chan CS**. 2011. High-resolution 2D and 3D cryo-TEM reveals structural adaptations of two stalk-forming bacteria to an Fe-oxidizing lifestyle. Environ Microbiol **13**:2915–2929.

21. **Chiu BK**, **Kato S**, **McAllister SM**, **Field EK**, **Chan CS**. 2017. Novel pelagic iron-oxidizing Zetaproteobacteria from the Chesapeake Bay oxic-anoxic transition zone. Front Microbiol **8**:1–16.

22. **Mori JF**, **Scott JJ**, **Hager KW**, **Moyer CL**, **Küsel K**, **Emerson D**. 2017. Physiological and ecological implications of an iron- or hydrogen-oxidizing member of the Zetaproteobacteria, Ghiorsea bivora, gen. nov., sp. Nov. ISME J **11**:2624–2636.

23. **Emerson D**, **Rentz JA**, **Lilburn TG**, **Davis RE**, **Aldrich H**, **Chan C**, **Moyer CL**. 2007. A novel lineage of proteobacteria involved in formation of marine Fe-oxidizing microbial mat communities. PLoS One **2**.

24. **Karl DM**, **McMurtry GM**, **Malahoff A**, **Garcia MO**. 1988. Loihi Seamount, Hawaii: A mid-plate volcano with a distinctive hydrothermal system. Nature **335**:532–535.

25. **Glazer BT**, **Rouxel OJ**. 2009. Redox speciation and distribution within diverse Iron-dominated microbial habitats at Loihi Seamount. Geomicrobiol J **26**:606–622.

26. **Rassa AC**, **McAllister SM**, **Safran SA**, **Moyer CL**. 2009. Zeta-proteobacteria dominate the colonization and formation of microbial mats in low-temperature hydrothermal vents

at loihi seamount, hawaii. Geomicrobiol J **26**:623–638.

27. **Whitaker JE**, **Haugland RP**, **Prendergast FG**. 1991. Spectral and photophysical studies of benzo[c]xanthene dyes: Dual emission pH sensors. Anal Biochem **194**:330–344.

28. **Hunter RC**, **Beveridge TJ**. 2005. Application of a pH-sensitive fluoroprobe (C-SNARF-4) for pH microenvironment analysis in Pseudomonas aeruginosa biofilms. Appl Environ Microbiol **71**:2501–2510.

29. **Karl DM**, **McMurtry GM**, **Malahoff A**, **Garcia MO**. 1988. Loihi Seamount, Hawaii: a mid-plate volcano with a distinctive hydrothermal system. Nature.

30. **Sedwick P.**, **McMurtry G.**, **Macdougall J.** 1992. Chemistry of hydrothermal solutions from Pele's Vents, Loihi Seamount, Hawaii. Geochim Cosmochim Acta **56**:3643–3667.

31. **Schindelin J**, **Arganda-Carreras I**, **Frise E**, **Kaynig V**, **Longair M**, **Pietzsch T**, **Preibisch S**, **Rueden C**, **Saalfeld S**, **Schmid B**, **Tinevez JY**, **White DJ**, **Hartenstein V**, **Eliceiri K**, **Tomancak P**, **Cardona A**. 2012. Fiji: An open-source platform for biological-image analysis. Nat Methods **9**:676–682.

32. **Hills AG**. 1973. pH and the Henderson-Hasselbalch equation. Am J Med **55**:131–133.

33. **Krepski ST**, **Emerson D**, **Hredzak-Showalter PL**, **Luther GW**, **Chan CS**. 2013. Morphology of biogenic iron oxides records microbial physiology and environmental conditions: Toward interpreting iron microfossils. Geobiology **11**:457–471.

34. **Stumm W**, **Morgan JJ**. 1996. Aquatic Chemistry. John Wiley & Sons, Inc., New York, NY.

35. **Soli AL**, **Byrne RH**. 2002. CO2 system hydration and dehydration kinetics and the equilibrium CO2/H2CO3 ratio in aqueous NaCl solution. Mar Chem **78**:65–73.

36. **Ilbert M**, **Bonnefoy V**. 2013. Insight into the evolution of the iron oxidation pathways. Biochim Biophys Acta - Bioenerg **1827**:161–175.

37. **Krulwich TA**, **Sachs G**, **Padan E**. 2011. Molecular aspects of bacterial pH sensing and homeostasis. Nat Rev Microbiol **9**:330–343.

38. **Morimoto Y V.**, **Kami-Ike N**, **Miyata T**, **Kawamoto A**, **Kato T**, **Namba K**, **Minamino T**. 2016. High-resolution pH imaging of living bacterial cells to detect local pH differences. MBio **7**:1–8.

39. **Kashket ER**. 1985. The Proton Motive Force in Bacteria : a Critical Assessment of Methods. Annu Rev Microbiol **39**:219–242.

40. **Glazer BT**, **Rouxel OJ**. 2009. Redox speciation and distribution within diverse Iron-dominated microbial habitats at Loihi Seamount. Geomicrobiol J **26**:606–622.

41. **Lodish H**, **Berk A**, **Kaiser CA**, **Krieger M**, **Bretscher A**, **Ploegh H**, **Amon A**, **Scott MP**. 2013. Molecular Cell Biology. Macmillan Higher Education, New York, NY.

42. **Singer E**, **Emerson D**, **Webb EA**, **Barco RA**, **Kuenen JG**, **Nelson WC**, **Chan CS**, **Comolli LR**, **Ferriera S**, **Johnson J**, **Heidelberg JF**, **Edwards KJ**. 2011. Mariprofundus ferrooxydans PV-1 the first genome of a marine Fe(II) oxidizing Zetaproteobacterium. PLoS One **6**.

43. **Yeates TO**, **Kerfeld CA**, **Heinhorst S**, **Cannon GC**, **Shively JM**. 2008. Protein-based organelles in bacteria: Carboxysomes and related microcompartments. Nat Rev Microbiol **6**:681–691.

44. **Dobrinski KP**, **Longo DL**, **Scott KM**. 2005. The carbon-concentrating mechanism of the hydrothermal vent chemolithoautotroph Thiomicrospira crunogena. J Bacteriol **187**:5761–5766.